Structures and Materials Research
Department of Civil Engineering

Report No. UCSESM 70-12

THE ANALYSIS OF MODERATELY THICK TO THIN SHELLS BY THE FINITE ELEMENT METHOD

by

Stuart F. Pawsey

Faculty Investigator: Ray W. Clough

Report to

U.S. Army Corps of Engineers
Walla Walla District

Structural Engineering Laboratory
University of California, Berkeley, California

August 1970

ABSTRACT

A three-dimensional finite element is adapted to represent a curved shell element, of arbitrary geometry, with the conventional five degrees of freedom per node. The numerical integration of the strain energy is performed separately for each strain energy component, resulting in an efficient shell element for either moderately thick or thin shells.

Four variational principles, applying to the linear theory of elasticity, are given. Using two of these principles, an examination of the efficiency of one class of mixed model is made.

Using the displacement method, the performance of a shell element, derived from a three-dimensional element, is discussed. The determination is made of the numerical integration required to guarantee correct convergence of the solution, as the finite element mesh is refined. A numerical integration scheme is developed, satisfying the convergence criteria, which allows the element to represent certain higher order bending and in-plane deformation modes more efficiently. The element is used in a finite element program and a number of static and dynamic problems, involving both thick and thin shells, are solved. Comparisons of these solutions are made with solutions by full three-dimensional finite elements and thin shell finite elements.

ACKNOWLEDGEMENT

The research reported herein was performed under contract DACW 68-67-C-0004, Three-Dimensional Finite Element Analysis.

The author wishes to express his deepest appreciation to Professor Ray W. Clough for his patient guidance of this research; to Professors Edward L. Wilson, and Beresford Parlett, for reviewing the manuscript; to the U.S. Army Corps of Engineers for their financial assistance; to the University of California Computer Center for the use of computer facilities; to Mrs. Shirley Edwards for typing the manuscript, and to his wife, Glenda, for patience beyond the call of duty.

It is the profound hope of the author, that, in these disturbing times, any uses to which this research may be put will be for the benefit of mankind and not for the destruction of men, women or children in any land.

TABLE OF CONTENTS

Page

PREFACE

Until quite recently, the analysis of shell structures presented a formidable task, capable of solution for only the simplest of shapes and loadings. Simplifying approximations were made at all stages of the analysis in order to be able to obtain any solution at all. Approximations were made at the outset regarding the stress and displacement fields. These approximations enabled the setting up of a set of differential equations, that described the shell's behavior. Many different approximations were then made on these equations themselves in order to obtain a solution.

The increasing availability of digital computers and the rapid increase in efficiency of both computer hardware and analysis techniques now have allowed many of the simplifying assumptions of classical shell theory to be discarded, and a virtually unlimited range of geometrical shapes to be analyzed. Indeed, using three dimensional analysis, a structure with any geometry and loads could be analyzed, subject only to restrictions of computer space and time. At the present time, however, these restrictions are very real and three dimensional analysis is a prohibitively expensive way to analyze most structures.

The analysis of many structures can be simplified by recognizing certain characteristics of these structures and by making justifiable kinematic or stress assumptions. This research is an attempt to develop a shell element for use in the finite element method, which, being derived from general three-dimensional elements, is capable of analyzing shells whose geometries are such that classical thin shell assumptions are not applicable, yet which is efficient enough to be able to be used on classical thin shells also, if desired.

I. FINITE ELEMENT METHOD

I.1 Description

In linear structural mechanics we seek to solve the boundary value problem characterized by

$$\mathcal{L}u = f \tag{I-1}$$

and an appropriate set of boundary conditions. $\mathcal{L}$ is a linear differential operator, operating on the variable u in a region R.

An alternative way of posing the problem is by the use of a variational formulation. We seek an extremum of a functional $I(u)$ (associated with the operator $\mathcal{L}$) over a range of admissible functions u. This latter statement of the problem is the form generally used in the finite element method. The admissible functions are those functions that satisfy certain constraints on the boundary or interior of R, and satisfy certain continuity conditions. The functional is such that its variation with respect to the variables u yields an extremum for those values of u given by the differential equation $\mathcal{L}u = f$. This is known as the Euler equation of the functional.

In the theory of elasticity, the variable u represents some or all of the stresses (τ_{ij}), strains (ϵ_{ij}) and displacements (u_i) of the system, and the Euler equation represents the field equations of the theory of elasticity.

In a finite element formulation the region R is considered as subdivided into subregions known as finite elements. Within each element, the variables represented by u are approximated by a function v. The functions v are defined by interpolation functions

within the element, associated with generalized coordinates v_i which are the values of v at points called nodes within the element or on its boundary. The interpolation functions p are usually taken as polynomial expressions in the global coordinates x_j, or in a local system of axes. Thus the variables are approximated by

$$v = \langle p_1\ p_2\ p_3 \cdots p_n \rangle \begin{Bmatrix} v_1 \\ v_2 \\ \vdots \\ v_n \end{Bmatrix} \equiv \langle p \rangle \{ \underset{\sim}{v} \} \qquad \text{(I-2)}$$

When the variable is expressed this way the functional $I(v)$ can be determined as a function of the nodal values v_j. The solution of the variational problem in the discrete variables v_j then yields a set of linear equations to be solved for the v_j.

$$[K]\ \{v\} = \{R\}$$

Using the values of v_j found from this set of equations, and the interpolation functions p, the complete spatial solution for v is recovered, which approximates the true solution u.

Provided that v satisfies certain requirements to be discussed later, the systematic subdivision of the region into finer meshes results in v converging to u.

I.2 Some Variational Principles

In elasticity problems, any or all of the stress, strain, or displacement variables may be used as independent parameters defining the functional.

All stress, strain and displacement components are used in a variational principle quoted by Fraejis de Veubecke, in an excellent article on this subject (6). In this form, all components of stress (τ_{ij}), strain (ϵ_{ij}), and displacement (u_i) are totally independent, and are not related, a priori, by any of the field equations of the theory of elasticity. Using indicial notation, the functional can be defined by:

$$I = \iiint_R W(\epsilon_{ij})\, dv - \iiint_R \bar{f}_i u_i\, dv - \iint_{\Sigma_\tau} \bar{t}_i u_i\, ds \qquad \text{(I-3)}$$

$$+ \iiint_R \tau_{ij}\left(\frac{u_{i,j} - u_{j,i}}{2} - \epsilon_{ij}\right) dv + \iint_{\Sigma_u} t_i\left(\bar{u}_i - u_i\right) ds$$

In this and the following variational principles, the following definition apply:

$\iiint_R dv$ represents the volume integral over the body R.

$\iint_\Sigma ds$ represents the surface integral over the surface, Σ.

Σ_τ represents that part of the surface over which stresses are defined.

Σ_u represents that part of the surface over which displacements are defined.

Σ represents the entire surface of the body R.

$\bar{f}_i$ represents body forces per unit volume.

t_i represents surface tractions.

$\bar{t}_i$ represents the prescribed surface tractions on Σ_τ

$\bar{u}_i$ represents the prescribed surface displacements on Σ_u

$W(\epsilon_{ij})$ represents the strain energy density, calculated from the strain field, ϵ_{ij}

Taking the variation of the functional with respect to each variable results in an extremum for those values of the variables that satisfy all the field equations:

$$\epsilon_{ij} = (u_{i,j} + u_{j,i})/2$$
$$\tau_{ij,j} + \bar{f}_i = 0$$
$$\tau_{ij} = c_{ijkl}\,\epsilon_{kl}$$

and boundary conditions:

$$t_i = \bar{t}_i \quad \text{on } \Sigma_\tau$$
$$u_i = \bar{u}_i \quad \text{on } \Sigma_u$$

The previous general variational form can be simplified to involve only one, or two of the three basic parameters, (τ_{ij}, ϵ_{ij}, u_i), of the functional.

If we satisfy, a priori, the constitutive relation

$$\tau_{ij} = c_{ijkl}\,\epsilon_{kl}$$

we get a functional involving only displacements and stresses or only displacements and strains. These two are actually fully equivalent forms and may be converted from one to the other through the constitutive relations. This functional, involving stresses is known as the Hellinger Reissner Principle (21) and can be written:

$$I \equiv \iiint_R W(\tau_{ij})\,dv + \iiint_R \bar{f}_i u_i\,dv + \iint_{\Sigma_\tau} \bar{t}_i u_i\,ds \qquad \text{(I-4)}$$
$$- \iiint_R \tau_{ij} \times \tfrac{1}{2}(u_{i,j} + u_{j,i})\,dv - \iint_{\Sigma_u} t_i(\bar{u}_i - u_i)\,ds$$

For completeness, another form of the same functional, derived by use of the divergence theorem in vector field algebra, will be presented here:

$$I = \iiint_R W(\tau_{ij})\, dv + \iiint_R u_i (\tau_{ij,j} + \bar{f}_i)\, dv - \iint_{\Sigma_u} t_i \bar{u}_i\, ds + \iint_{\Sigma_T} (\bar{t}_i - t_i) u_i\, ds \tag{I-5}$$

A detailed discussion, with numerical examples, of the application of these two principles will be given in Chapter II.

If, further, the strain-displacement relations are satisfied a priori, and the displacements are constrained to satisfy displacement boundary conditions on Σ_u, only displacements are left as independent parameters, and we are left with a functional that represents the potential energy, and the variational principle is known as the minimum potential energy theorem. The functional becomes:

$$I = \iiint_R W(u_i)\, dv - \iiint_R \bar{f}_i u_i\, dv - \iint_{\Sigma_T} \bar{t}_i u_i\, ds \tag{I-6}$$

Further details of this principle, to be used in the main section of this research will be given in Chapter I.4.

For completeness, one more functional will be presented, also derived from the two-field Hellinger Reissner Principle. If the stresses are assumed, a priori, to satisfy the equilibrium equations, and to provide equilibrium on the stress boundary Σ_T, then the functional reduces to:

$$I = \iiint_R W(\tau_{ij})\, dv - \iint_{\Sigma_u} t_i \bar{u}_i\, ds \tag{I-7}$$

This formulation is the basis of the equilibrium method of finite element analysis (19), (20).

I.3 Convergence Requirements

In order to be confident of the accuracy of a solution by the finite element method, it is necessary that the solution should converge to the exact solution as the finite element mesh is repeatedly subdivided into finer and finer meshes. The nature of the functions p_j chosen for each element determines whether this convergence will be attained.

The requirements for convergence fall into two categories. The first requirement is completeness of the expansion. The second is inter-element continuity.

First we will examine the completeness requirement. This is simply a requirement that ensures that the energy represented by the functional includes the possibility of a constant energy state in each element. If this is provided, then the true energy state of the whole body can be represented, in the limit, as the mesh layout is refined, by a series of step functions of infinitesimal width. Mathematically, this requires that in each element, all uniform states of the variable v must be included up to the highest derivative occurring in the functional. In the displacement method, for example, the highest derivatives of displacements occurring in the functional are the first derivatives. Thus completeness requires that at least linear expansions must be provided for displacements. This results in the familiar requirement that "constant strain" and "rigid body" states must be satisfied.

The second requirement is that of continuity between adjacent elements. In order to avoid introducing singularities in the energy integral occurring at the inter-element boundaries, it has been considered necessary to provide continuity of any variable v of one order lower than the order of that variable's highest derivative in the functional. Thus in the displacement method, again, continuity of order C° was required, resulting in the requirement of full inter-element compatibility. Success of certain non-compatible elements have however led to a re-evaluation of this requirement. The weaker condition, first stated by Zienkiewicz, (25) demands that continuity of the above order be maintained only for the states of constant energy in the region R.

A rigorous examination of the above requirements is contained in the doctoral dissertation by K. Willam (31) and nothing further will be presented here.

I.4 Displacement Method

With the exception of Chapter II, the research described in the following chapters is concerned with the displacement method only. A brief summary of the displacement method of the finite element method will now be given. Many references are available on this basic material (25, 26) and only the briefest outline is included here.

The variational principle (I-6) given in Chapter I.2 involves the functional:

$$I = \iiint_R W(u_i)\, dv - \iiint_R \bar{f}_i u_i \, dv - \iint_{S_T} \bar{t}_i u_i \, ds$$

If $\{\epsilon\} \equiv \begin{Bmatrix} \epsilon_{11} \\ \epsilon_{22} \\ \epsilon_{33} \\ \gamma_{12} \\ \gamma_{23} \\ \gamma_{31} \end{Bmatrix}$, $\{\sigma\} \quad \begin{Bmatrix} \tau_{11} \\ \tau_{22} \\ \tau_{33} \\ \tau_{12} \\ \tau_{23} \\ \tau_{31} \end{Bmatrix}$

and the constitutive relation is:

$$\{\tau\} = [E]\{\epsilon\} \tag{I-8}$$

The functional can be written, for three dimensional elasticity

$$I = \frac{1}{2}\iiint_R \langle \epsilon^T \rangle [E] \{\epsilon\} \, dv - \iiint_R \langle u\ v\ w \rangle \begin{Bmatrix} \bar{f}_1 \\ \bar{f}_2 \\ \bar{f}_3 \end{Bmatrix} dv - \iint_{S_T} \langle u\ v\ w \rangle \begin{Bmatrix} \bar{t}_1 \\ \bar{t}_2 \\ \bar{t}_3 \end{Bmatrix} ds \tag{I-9}$$

The displacements at any point are defined in terms of the nodal values within the element or on its boundary (I-2), by means of interpolation functions

$$\begin{Bmatrix} u \\ v \\ w \end{Bmatrix} = \begin{bmatrix} \langle p \rangle & & \\ & \langle p \rangle & \\ & & \langle p \rangle \end{bmatrix} \begin{Bmatrix} \underline{u} \\ \underline{v} \\ \underline{w} \end{Bmatrix}$$

or

$$\begin{Bmatrix} u \\ v \\ w \end{Bmatrix} = \begin{bmatrix} p \end{bmatrix} \begin{Bmatrix} \underline{u} \\ \underline{v} \\ \underline{w} \end{Bmatrix} \tag{I-10}$$

By use of the strain-displacement relations

$$\epsilon_{ij} = \frac{1}{2}\left(u_{i,j} + u_{j,i}\right)$$

we can write $\{\epsilon\}$ in terms of the nodal displacements as

$$\{\epsilon\} = [T]\begin{Bmatrix}\underline{u}\\ \underline{v}\\ \underline{w}\end{Bmatrix} \qquad \text{(I-11)}$$

Where [T] is obtained from [P] by appropriate differentiation.

Using the above relations we get the contribution to the total potential energy from each element:

$$I_{elt.} = \frac{1}{2}\langle \underline{u}^T \underline{v}^T \underline{w}^T \rangle \iiint_{elt.} [T^T][E][T]\, dv \begin{Bmatrix}\underline{u}\\ \underline{v}\\ \underline{w}\end{Bmatrix}$$

$$- \langle \underline{u}^T \underline{v}^T \underline{w}^T \rangle \iiint_{elt.} [P^T]\, ds \begin{Bmatrix}\bar{f}_1\\ \bar{f}_2\\ \bar{f}_3\end{Bmatrix}$$

$$- \langle \underline{u}^T \underline{v}^T \underline{w}^T \rangle \iint_{elt.} [P^T]\, ds \begin{Bmatrix}\bar{t}_1\\ \bar{t}_2\\ \bar{t}_3\end{Bmatrix}$$

and the total energy $I = \sum I_{elt.}$ (I-12)

We will now re-interpret $\underline{u}$, $\underline{v}$, $\underline{w}$ as nodal displacements for for the whole structure, and [P], [T] as being "patch" functions for any node which are defined by the interpolation functions p for elements connected to that node and are zero otherwise. Using these new

definitions, the previous equation for the energy of one element applies for the total energy, the integrations now being performed over the whole region R.

Taking the variation of U with respect to u, v, and w and setting $\Delta U = 0$

we obtain

$$\iiint_R [T^T][E][T]\, dv \begin{Bmatrix} \underline{u} \\ \underline{v} \\ \underline{w} \end{Bmatrix} = \iiint_R [p^T] \begin{Bmatrix} \bar{f}_1 \\ \bar{f}_2 \\ \bar{f}_3 \end{Bmatrix} dv + \iint_{S_T} [p^T] \begin{Bmatrix} \bar{t}_1 \\ \bar{t}_2 \\ \bar{t}_3 \end{Bmatrix} \tag{I-13}$$

or writing

$$\{v\} = \begin{Bmatrix} \underline{u} \\ \underline{v} \\ \underline{w} \end{Bmatrix}$$

$$[K] = \iiint_R [T^T][E][T]\, dv$$

and

$$\{R\} = \iiint_R [p^T] \begin{Bmatrix} \bar{f}_1 \\ \bar{f}_2 \\ \bar{f}_3 \end{Bmatrix} + \iint_{S_T} [p^T] \begin{Bmatrix} \bar{t}_1 \\ \bar{t}_2 \\ \bar{t}_3 \end{Bmatrix} ds$$

then

$$[K]\{v\} = \{R\} \tag{I-14}$$

In a finite element computer program the integrations are performed element by element, and added successively to the stiffness matrix [K] and the nodal force vector {R} defined for the entire structure .

Since a term in [K] is non-zero only if the two nodes associated with this term are connected to the same element, the matrix [K] is very sparse. The non-zero terms may be arranged in band form, if the equations are placed in the appropriate order. Further, the equations associated with nodes that are connected to only one element involve only those degrees of freedom associated with that element and may therefore be eliminated from the stiffness of that element before assembly of the whole stiffness matrix [K]. This process of eliminating internal degrees of freedom is known as static condensation and decreases both the bandwidth and the total number of equations in the whole system. The stiffness matrix [K] is both symmetric and positive definite, allowing the simplest equation-solving algorithm to be used.

Once the nodal displacements are found by solving the equations, the displacements, strains and stresses within each element may be found by use of equations (I-10), (I-11), (I-8). This completes the formal solution by the displacement method.

II. ONE CLASS OF MIXED MODEL

II.1 General Comments

In an attempt to improve the efficiency of analysing thick shells, a general examination of one class of mixed model was undertaken.

In the displacement method, displacements are the primary variables and the stress field is computed from the displacements by differentiation. The stress field is thus of lower order accuracy than the displacement field. Yet it is the stress field which is usually sought for the purpose of design. It seemed likely, therefore, that if the stress field were a primary variable, it would give better accuracy for a given finite element mesh. It was decided to develop a three-dimensional finite element, using both stresses and displacements as primary variables, defined by values at the element nodes. This of course results in considerable more computational effort than using displacements alone. However it was hoped to take advantage of the stress boundary conditions at the nodes on each surface of the shell, thus eliminating these components of stress from the variational problem altogether.

While this research was progressing, Dunham (39) was working on similar research in two dimensions, reporting some success.

II.2 Variational Formulation

The functional to be used was presented in Chapter I and is given by:

$$I = -\int_V \tau_{ij} \frac{(u_{i,j} + u_{j,i})}{2} \, dv + \int_V W(\tau) \, dv + \int_V \bar{f}_i u_i \, dv + \int_{\Sigma_T} \bar{t}_i u_i \, ds - \int_{\Sigma_u} t_i (\bar{u}_i - u_i) \, ds \tag{II-1}$$

In this formulation, the stress field and the displacement field are totally independent. Further, the displacements are not required to satisfy boundary conditions on Σ_u and the stresses need not satisfy equilibrium either within the body or on the stress boundary Σ_T . If we choose, instead, to satisfy equilibrium on the stress boundary Σ_T , a priori, no change in the functional results. If we choose to satisfy the displacement boundary conditions, a priori, (with or without satisfying stress boundary conditions) the functional reduces to:

$$I = -\int_V \tau_{ij} \frac{u_{i,j} + u_{j,i}}{2} \, dv + \int_V W(\tau) \, dv + \int_V \bar{f}_i u_i \, dv + \int_{\Sigma_T} \bar{t}_i u_i \, ds \tag{II-2}$$

The continuity requirements stated in Chapter I required at least a complete linear expansion in displacements and full continuity of displacements between elements for states of constant energy at least. Only constant stress capability is required within each element, and no stress continuity between elements is necessary.

A different expression for the same functional (II-1) can be derived easily, by use of the divergence theorem in vector field algebra. The details will not be given here, but the alternative form of the functional is given by:

$$I = \int_V W(\tau) \, dv + \int_V u_i (\tau_{ij,j} + \bar{f}_i) \, dv - \int_{\Sigma_u} t_i \bar{u}_i \, ds + \int_{\Sigma_T} (\bar{t}_i - t_i) u_i \, ds \tag{II-3}$$

If displacement boundary conditions on S_u are satisfied, a priori, there is no change in the form of the functional, but if stress boundary conditions on S_τ are satisfield a priori, (with or without satisfying displacement boundary conditions) the functional simplifies to:

$$I = \int_V W(\tau)\, dv + \int_V u_i(\tau_{ij,j} + \bar{f}_i)\, dv - \int_{S_u} t_i \bar{u}_i\, ds \qquad \text{(II-4)}$$

In the following, we will discuss, this mixed model in two-dimensional plane stress problems, in order to evaluate its performance.

To apply the finite element method, the displacements u, v within each element are assumed to be related to the nodal values by

$$\begin{Bmatrix} u \\ v \end{Bmatrix} = \begin{bmatrix} \langle q^T \rangle & \\ & \langle q^T \rangle \end{bmatrix} \{\underset{\sim}{u}\}$$

where $\{\underset{\sim}{u}\}$ represents the vector of nodal displacements in both directions.

Similarly, the stresses within each element are related to the nodal stresses $\{\underset{\sim}{\tau}\}$, by the expression:

$$\begin{Bmatrix} \tau_{11} \\ \tau_{22} \\ \tau_{12} \end{Bmatrix} = \begin{bmatrix} \langle p^T \rangle & & \\ & \langle p^T \rangle & \\ & & \langle p^T \rangle \end{bmatrix} \{\underset{\sim}{\tau}\}$$

For simplicity, we will assume that all stress boundaries are parallel to the global x or y directions. (If this is not the case, as in the numerical examples following, a rotation of axes is required for the stress boundary integral given in the following functional).

We will also assume for simplicity that the prescribed displacements and stresses on the boundaries S_u , S_T respectively, are related to the prescribed values at the nodes by the respective interpolation functions q, p. Further, we will assume the body forces $\bar{f}_i$ to be zero.

Then, if ν_1 , ν_2 represent the direction cosines of the normal to a boundary S , and if p, q are re-defined as patch functions for the whole body, as described in Chapter I, we get the following discretized version of the functional (II-1):

$$
\begin{aligned}
I = \tfrac{1}{2}\langle \underline{\tau}^T \rangle \left[K_{pcp} \right] \{ \underline{\tau} \} \\
- \langle \underline{\tau}^T \rangle \left[K_{pq_1} \right] \{ \underline{u} \} \\
+ \langle \bar{\underline{\tau}}^T \rangle \left[{}_{S_T}K_{pq} \right] \{ \underline{u} \} \\
- \langle \underline{\tau}^T \rangle \left[{}_{S_u}K_{pq} \right] \{ \bar{\underline{u}} \} \\
+ \langle \underline{\tau}^T \rangle \left[{}_{S_u}K_{pq} \right] \{ \underline{u} \}
\end{aligned}
$$

where

$$
\left[K_{pcp} \right] = \iiint_V \begin{bmatrix} \{p\} & & \\ & \{p\} & \\ & & \{p\} \end{bmatrix} \left[E \right] \begin{bmatrix} \langle p^T \rangle & & \\ & \langle p^T \rangle & \\ & & \langle p^T \rangle \end{bmatrix} dv
$$

$$
\left[K_{pq_1} \right] = \iiint_V \begin{bmatrix} \{p\} & & \\ & \{p\} & \\ & & \{p\} \end{bmatrix} \begin{bmatrix} \langle q_{,1}^T \rangle & 0 \\ 0 & \langle q_{,2}^T \rangle \\ \langle q_{,2}^T \rangle & \langle q_{,1}^T \rangle \end{bmatrix} dv
$$

$$
\left[{}_{S}K_{pq} \right] = \iint_S \begin{bmatrix} \{p\} & & \\ & \{p\} & \\ & & \{p\} \end{bmatrix} \begin{bmatrix} \nu_1 \langle q \rangle & 0 \\ 0 & \nu_2 \langle q^T \rangle \\ \nu_2 \langle q^T \rangle & \nu_1 \langle q^T \rangle \end{bmatrix} ds
$$

The functional I is stationary with respect to the variables $\{\underline{\tau}\}, \{\underline{u}\}$ when:

$$\begin{bmatrix} K_{pcp} & -K_{pq,} + \varepsilon_u K_{pq} \\ -K_{pq,}^T + \varepsilon_u K_{pq}^T & 0 \end{bmatrix} \begin{Bmatrix} \underline{\tau} \\ \underline{u} \end{Bmatrix} = \begin{bmatrix} 0 & \varepsilon_u K_{pq} \\ -\varepsilon_\tau K_{pq}^T & 0 \end{bmatrix} \begin{Bmatrix} \bar{\underline{\tau}} \\ \bar{\underline{u}} \end{Bmatrix} \qquad \text{(II-5)}$$

This is the set of equations to be solved for stresses and displacements.

The alternative form II-3, results in the following set of equations:

$$\begin{bmatrix} K_{pcp} & K_{pq} - \varepsilon_\tau K_{pq} \\ K_{pq}^T - \varepsilon_\tau K_{pq}^T & 0 \end{bmatrix} \begin{Bmatrix} \underline{\tau} \\ \underline{u} \end{Bmatrix} \quad \begin{bmatrix} 0 & \varepsilon_u K_{pq} \\ -\varepsilon_\tau K_{pq}^T & 0 \end{bmatrix} \begin{Bmatrix} \bar{\underline{\tau}} \\ \bar{\underline{u}} \end{Bmatrix} \qquad \text{(II-6)}$$

where

$$K_{pq} = \iiint_V \begin{bmatrix} \{P_{,1}\} & \{0\} \\ \{0\} & \{P_{,2}\} \\ \{P_{,2}\} & \{P_{,1}\} \end{bmatrix} \begin{bmatrix} \langle q^T \rangle & 0 \\ 0 & \langle q^T \rangle \end{bmatrix} dv$$

In both these formulations, stresses and displacements at all nodes, even on stress or displacement boundaries, are unknowns, and, when the equations are solved, due to the discretization assumptions these unknowns will in general not equal the prescribed boundary values exactly.

If we choose to adopt forms II-2 or II-4 we get the following discretized forms.

$$\begin{bmatrix} K_{pcp} & -K_{pq} \\ -K_{pq}^T & 0 \end{bmatrix} \begin{Bmatrix} \underset{\sim}{\sigma} \\ \underset{\sim}{u} \end{Bmatrix} = \begin{bmatrix} 0 & 0 \\ -K_{pq}^T & 0 \end{bmatrix} \begin{Bmatrix} \underset{\sim}{\bar{\sigma}} \\ \underset{\sim}{\bar{u}} \end{Bmatrix} \qquad \text{(II-7)}$$

$$\begin{bmatrix} K_{pcp} & K_{pq} \\ K_{pq}^T & 0 \end{bmatrix} \begin{Bmatrix} \underset{\sim}{\sigma} \\ \underset{\sim}{u} \end{Bmatrix} \qquad \begin{bmatrix} 0 & \Sigma_u K_{pq} \\ 0 & 0 \end{bmatrix} \begin{Bmatrix} \underset{\sim}{\bar{\sigma}} \\ \underset{\sim}{\bar{u}} \end{Bmatrix} \qquad \text{(II-8)}$$

In this case, those stresses or displacements, that are on boundaries along which the boundary conditions are satisfied, a priori, are set equal to the prescribed values. Further, the equations resulting from the variation of these boundary unknowns are struck from the set of equations.

Since the two forms II-1 and II-3 are mathematically identical and only the actual numerical computations differ, we will consider only the first form II-1, from now on.

II.3 Solution Difficulties

When ordered appropriately, the discretized sets of equations II-5, II-7 are banded, as in the displacement method. However the subset of equations derived from variations of displacements contains zeroes on the diagonal of the matrix. If stress variables precede displacement

variables for each node, the solution process usually over-writes the zero before that term is used for pivoting. However, if this is not the case, an equation-solving algorithm developed by Professor Leonard Herrmann at University of California, Davis, can be used, which does not increase the bandwidth.

However a serious problem arises due to the block of zeroes associated with the displacement variations. If the number of unknown displacements n_u exceeds the number of unknown stresses n_τ, the set of n_u equations involving n_τ stresses will be of rank less than n_u. The set of equations is then singular, and redundant or contradictory equations will arise. This is a most undesirable characteristic. For two dimensional problems this situation can frequently occur if we constrain boundary stresses to satisfy stress boundary conditions. If we leave stresses on Σ_τ free to be determined by the set of equations, this problem will not arise, since there will then be always three stress components and two or less displacements, at each node. Thus $n_u < n_\tau$

As an example consider the arch divided into elements as shown in Fig. II.1

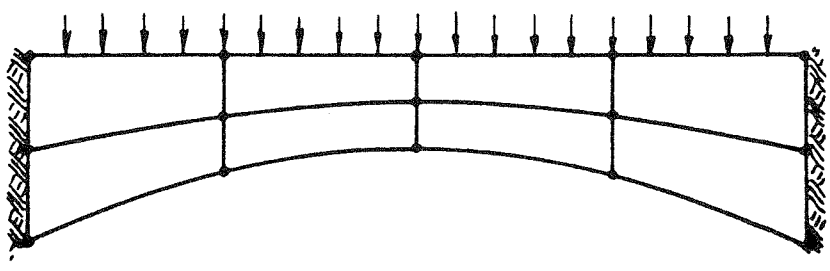

Fig. II.1

If all τ , u are unknowns,

$$n_\tau = 15 \times 3 = 45$$

$$n_u = 15 \times 2 = 30$$

and as, $n_u < n_\tau$ no singularities occur.

If, however, we satisfy stress boundary conditions, a priori, two stress components are eliminated from each node on the faces of the arch leaving

$$n_\tau = 45 - 10 \times 2 = 25$$

and $n_u = 30$ as before

So $n_u < n_\tau$ and the resulting set of 55 equations will be singular.

To compare the efficiency of mixed models using full stress continuity, with displacement models, we will choose the easiest way of avoiding this singularity problem. We will use only those forms of the functional that treat all stress components as unknowns, at all nodes. Using plane stress examples we will compare solutions with displacements on S_u both free and constrained to the prescribed boundary values. These results will be referred to as "U_f" and "U_c" respectively, and they will be compared with results from a displacement model referred to as ZI4, in which stresses at the nodes are averaged from all adjacent elements. In each case, quadrilateral elements will be used with bilinear interpolation functions within each element, and a node on each of the four corners. The interpolation functions are as described in Chapter V, for isoparametric elements.

II.4 Numerical Examples

The first example is to examine the effect of the stress concentration at a hole in a rectangular plate in tension. Using symmetry, a quarter of the plate was analysed. The dimensions are shown in Fig. II.2. A coarse mesh for the mixed model, and a finer mesh for the displacement model were adopted to give approximately the same total computer time.

Displacements in the x directions along the horizontal line of symmetry and stresses τ_{xx} on the vertical and horizontal lines of symmetry are shown in Figs. II.4, 5, 6. The reference curves are as given by Howland (40).

Examining these graphs, we see that the displacements for the displacement model ZI4 are very much superior to those of the mixed models U_f, U_c. Similarly the stresses for ZI4 are closer to the correct values than either mixed model. The stresses for U_f and U_c appear to give a reasonable solution considering the coarseness of the grid used, crossing the true solution, in each case. However with a grid so much coarser than that for ZI4, the stresses from the mixed models are unable to follow the changes of stress as accurately as the solution by ZI4 with the finer mesh.

The second example to be shown, consists of a circular disc loaded with diametrically opposite concentrated forces. The solution is given by Timoshenko (39). Again, using symmetry, only a quarter of the disc is analysed.

The displacement u and the two stresses τ_{yy} and τ_{xx} along the horizontal line of symmetry are shown in Figs. II.7, 8, 9. The stress component τ_{yy} along the vertical edge is shown in Fig. II.10.

The displacement of ZI4 shown in Fig. II.7 are graphically indistinguishable from the exact values. However, those from the mixed models show considerable departure from the reference curve. The stresses calculated by ZI4 are in each case, once again, considerably more accurate than those from both U_f and U_c, the latter two giving stresses that oscillate severely about the reference curves.

These results and other examples not recorded here, indicate that the mixed model, that maintains continuity of stress, is inferior to the displacement model with the same interpolation functions within the element, when equal computation time is used as the basis for comparison. Dunham (38) reported that the mixed model gave improved results over the displacement model. However, in his comparisons he used identical meshes for each model and no account was taken of the greater amount of computation required for the mixed models. When a finer mesh is used for the displacement model, to give the same computation time, the stresses and displacements of the displacement model are markedly superior to those of the mixed model.

As a result of these investigations, it was decided to abandon this line of research and to attempt to improve the performance of three-dimensional displacement elements.

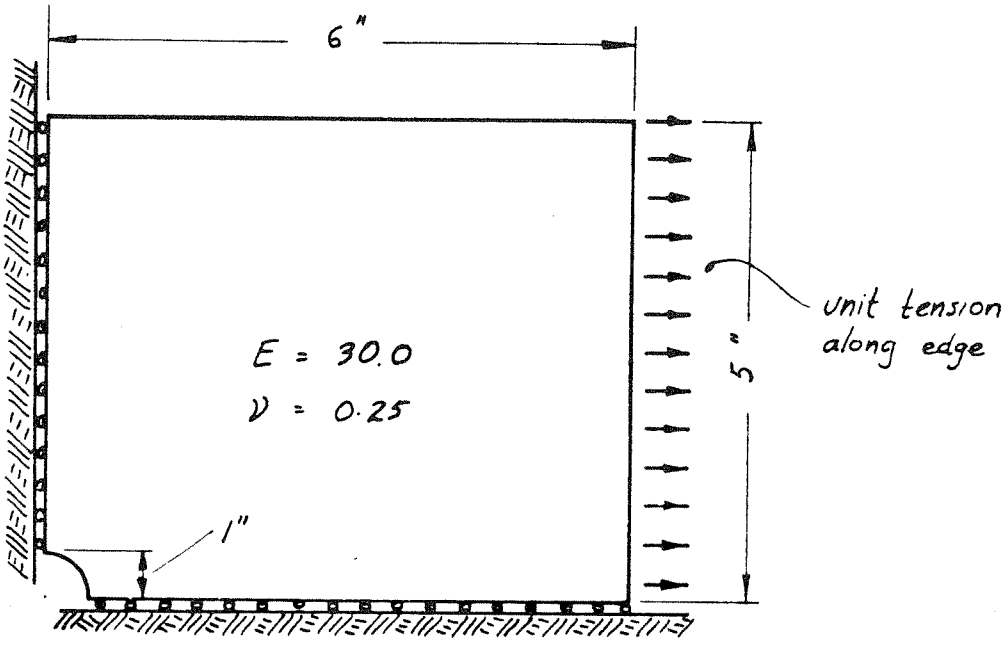

fig II.2 Plate with Circular Hole

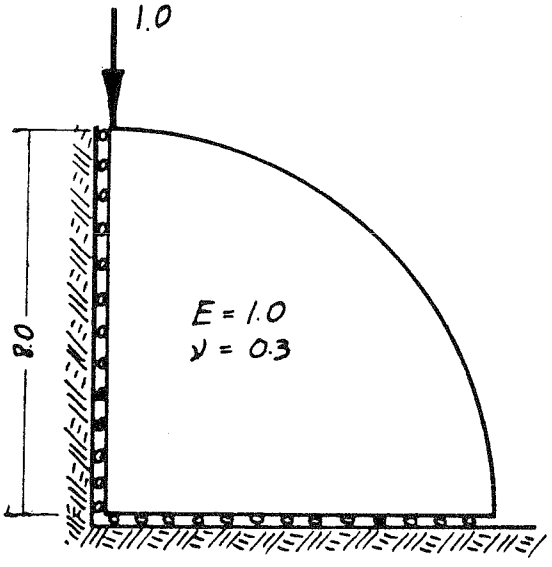

fig II.3 Disc with Diametrically Opposite Loads

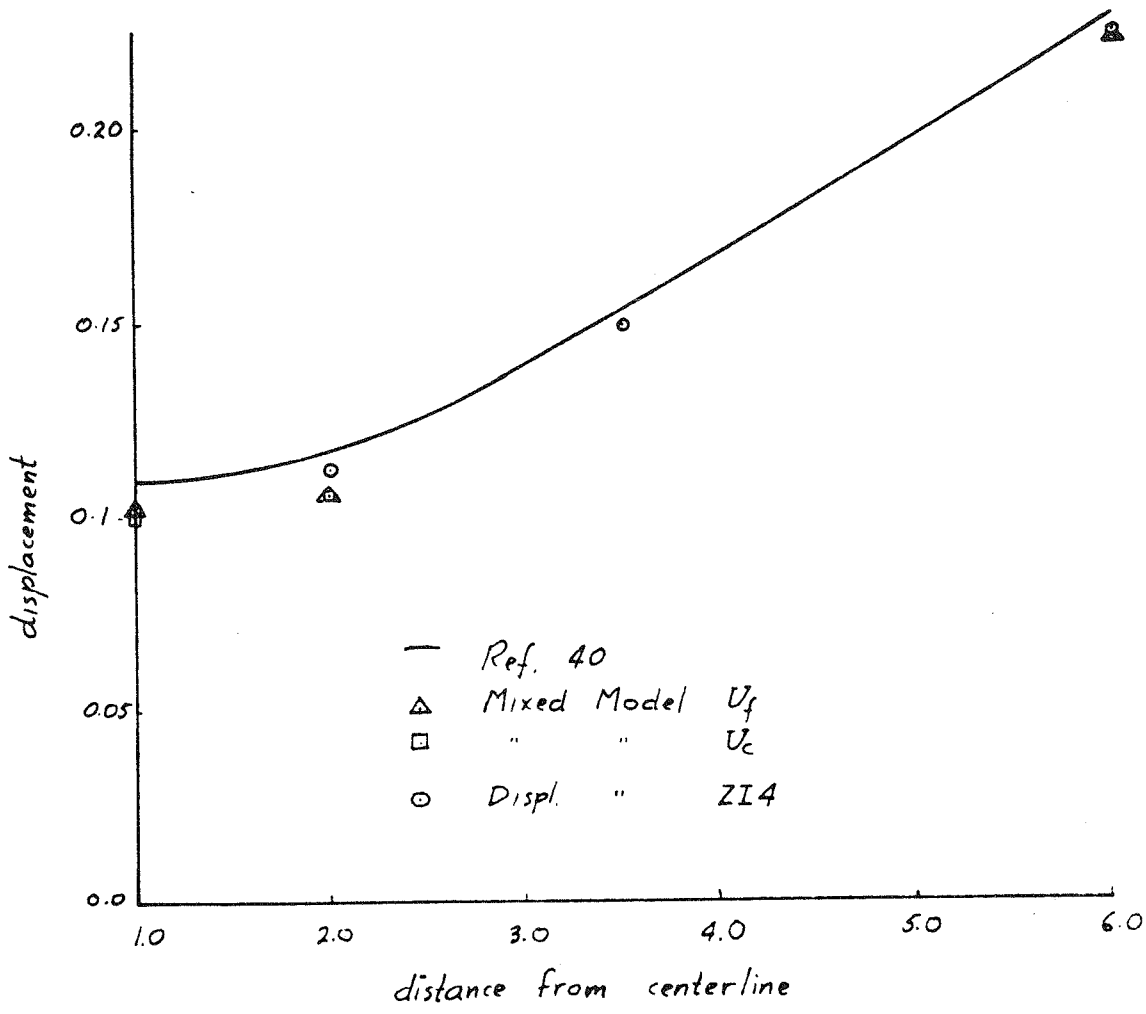

fig II.4 Plate with Circular Hole

Horizontal Displacement on Horizontal Centerline

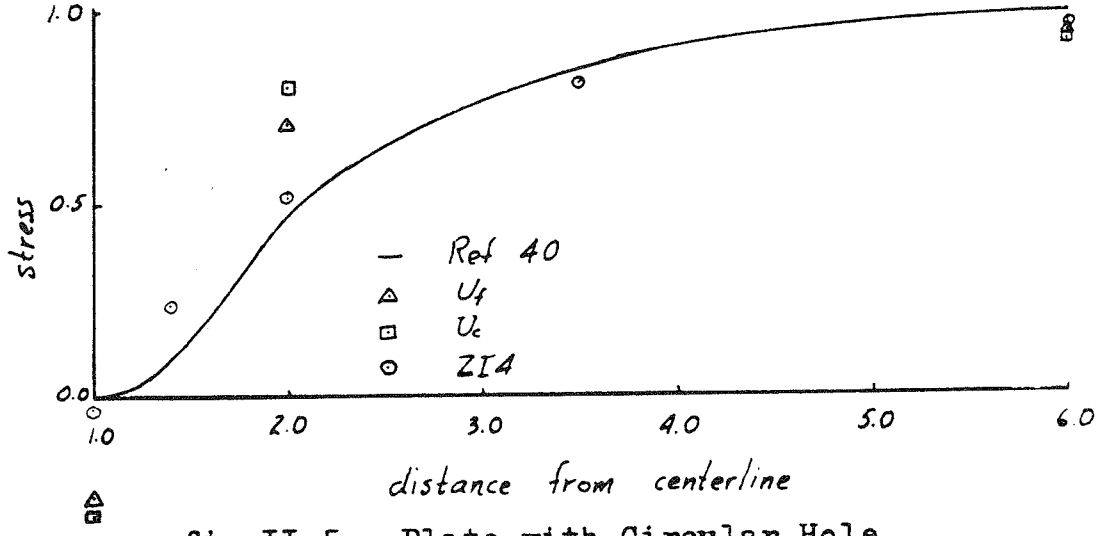

fig II.5 Plate with Circular Hole

σ_{xx} on Horizontal Centerline

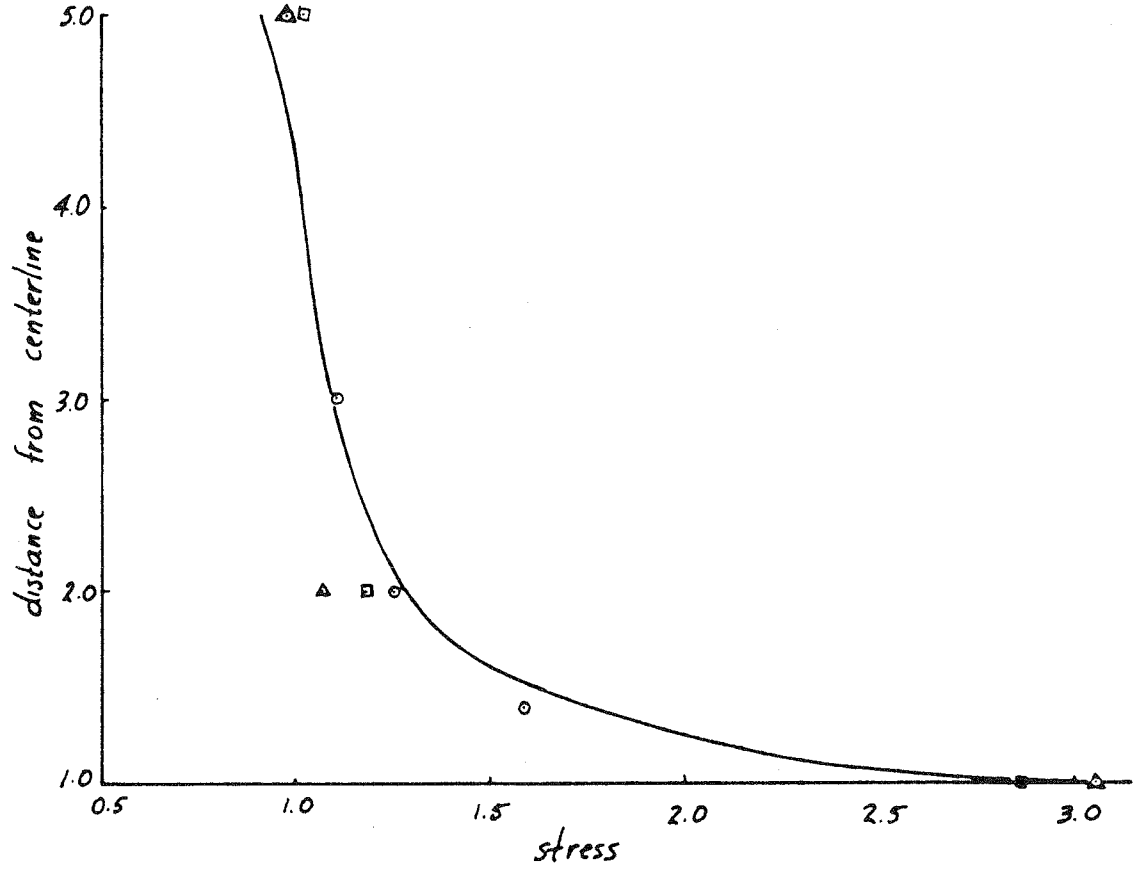

fig II.6 Plate with Circular Hole

τ_{xx} on Vertical Centerline

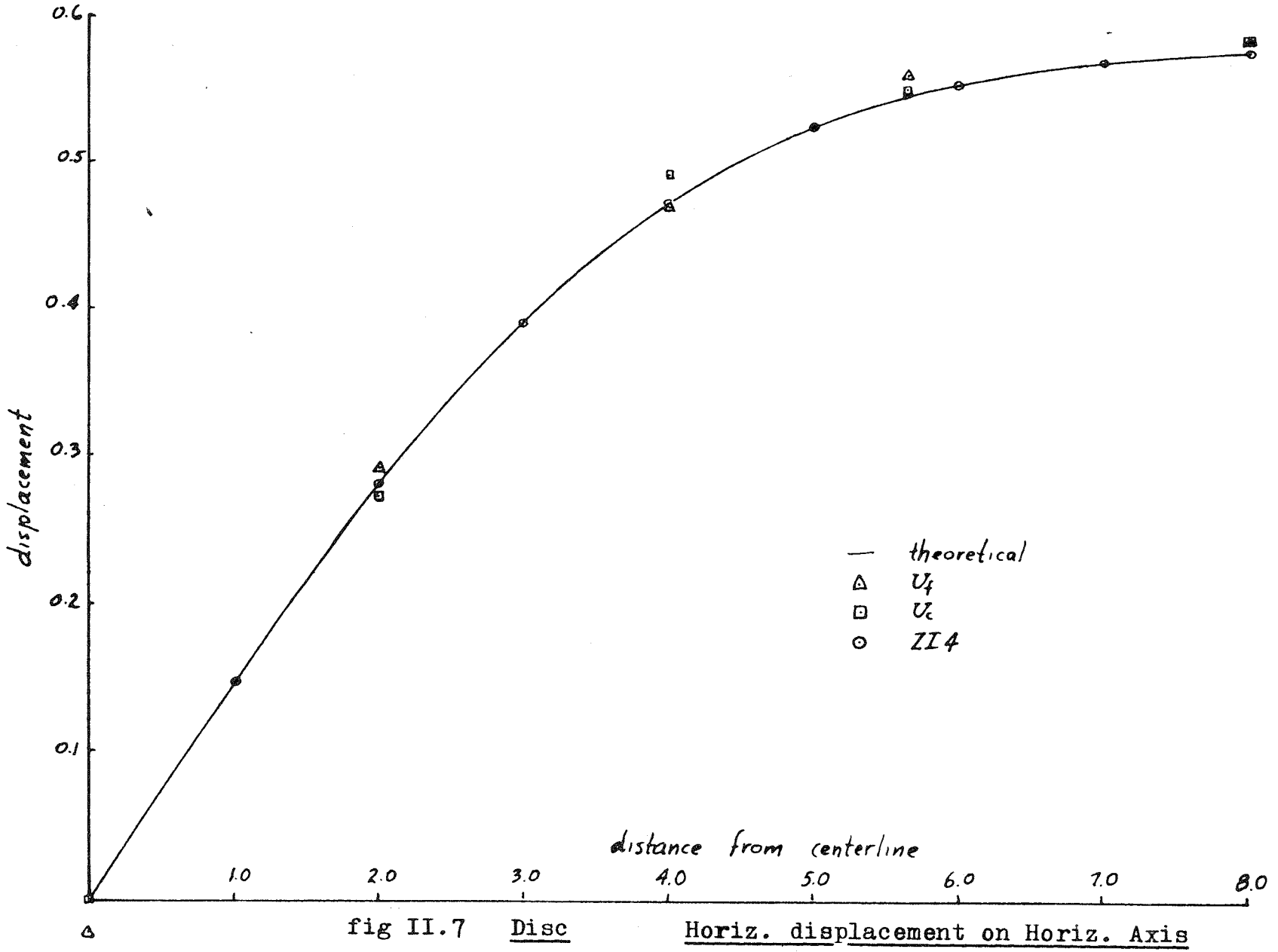

fig II.7 Disc Horiz. displacement on Horiz. Axis

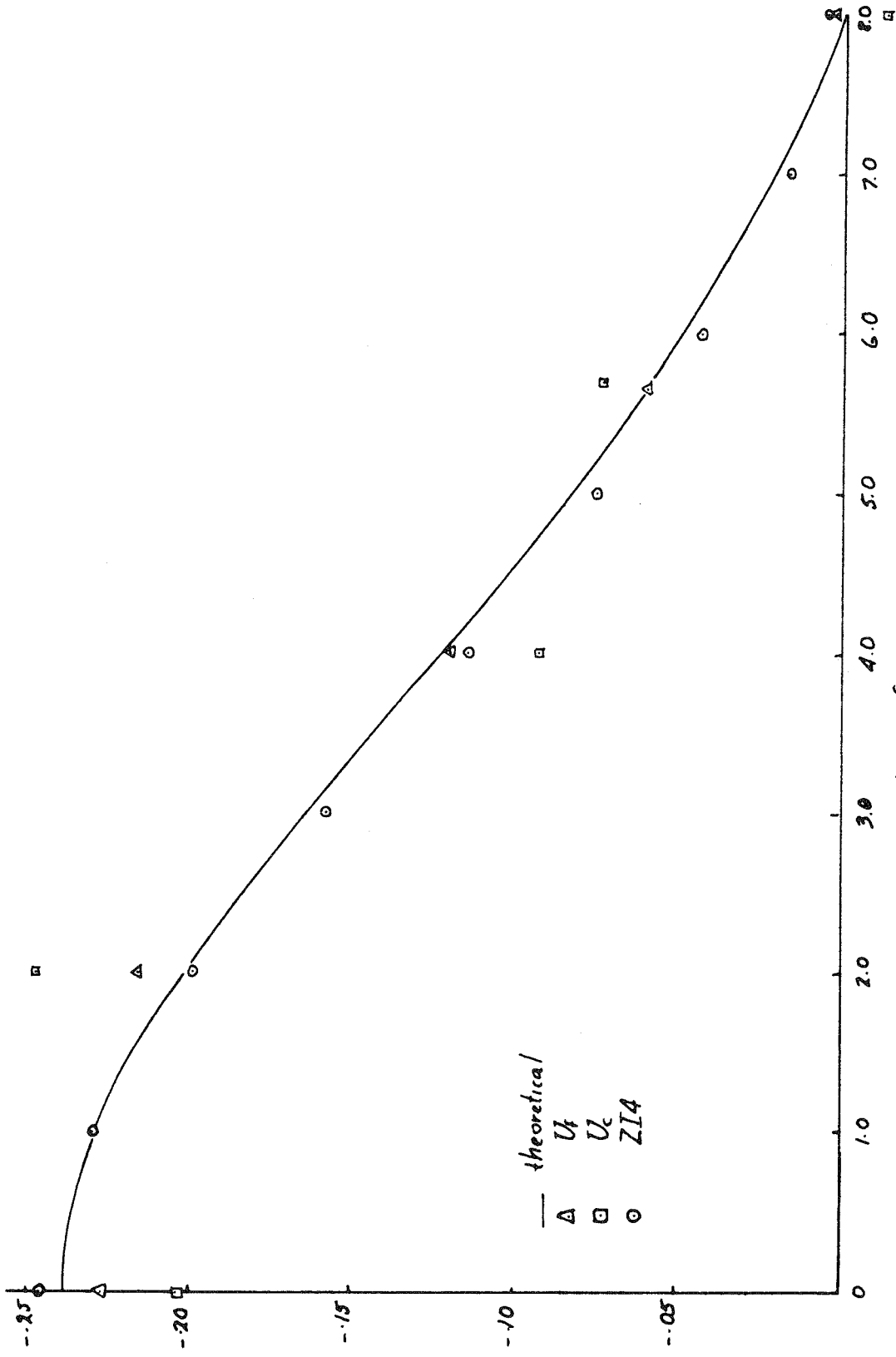

fig II.8 Disc τ_{xy} on Horizontal Axis

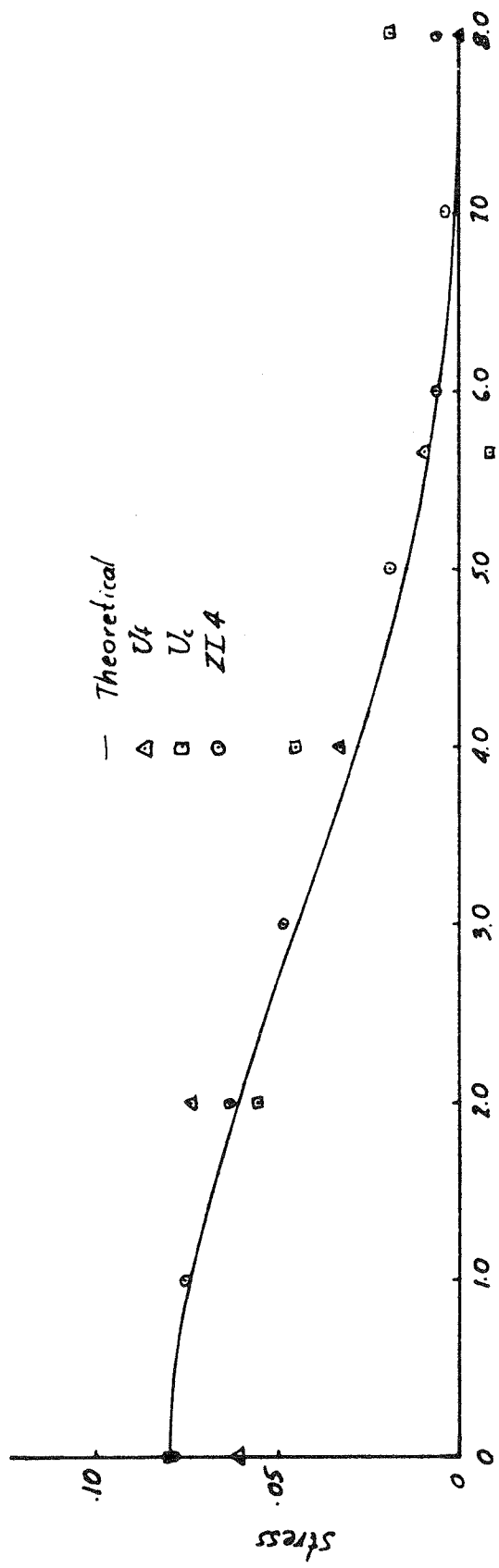

fig II.9 Disc

γ_{xx} on Horiz. Axis

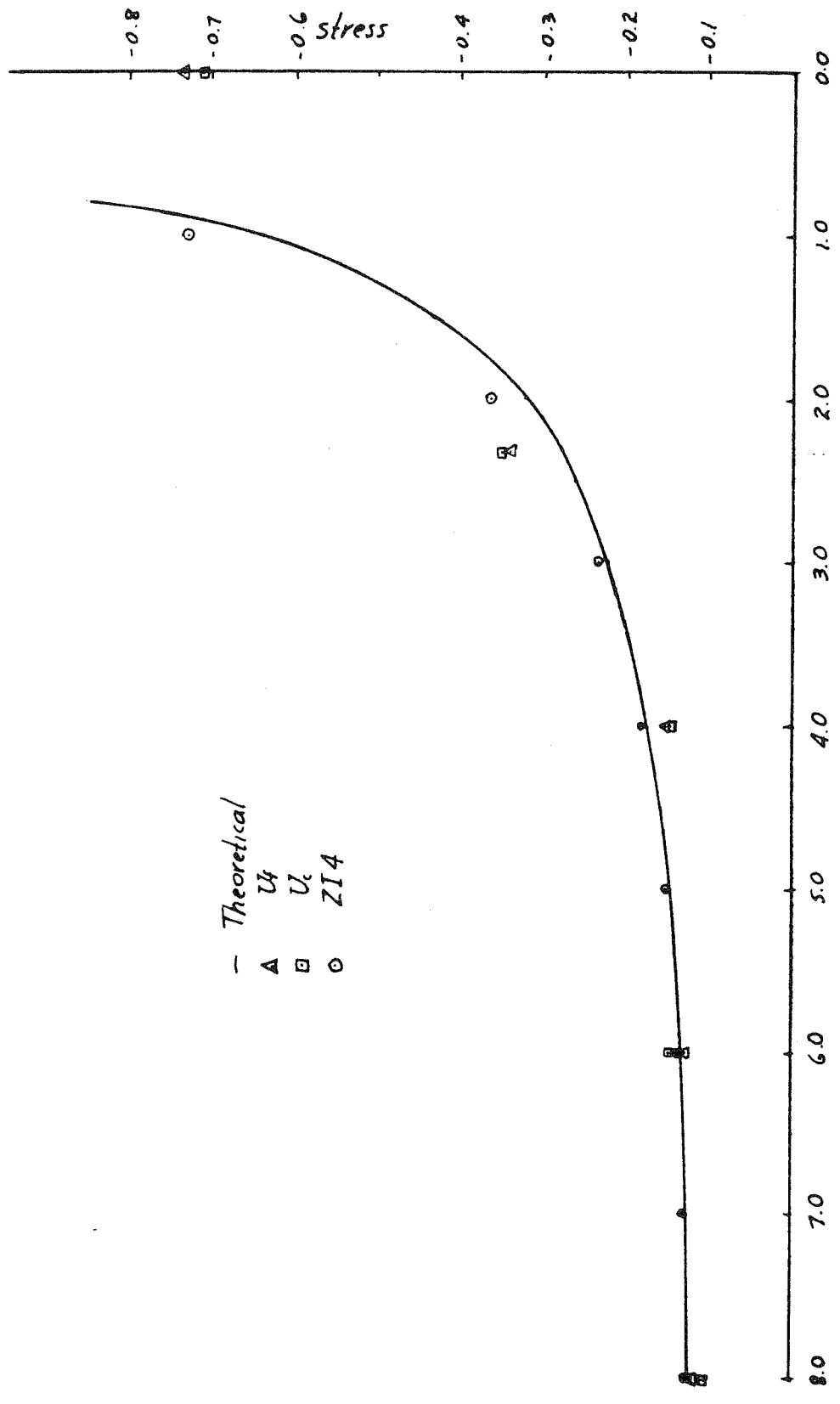

fig II.10 Disc

τ_{yx} on Vertical Axis

III. ANALYSIS OF SHELLS

For the purposes of this discussion we can define a shell as a structural component, whose geometrical properties can be conveniently described by reference to two curvilinear coordinate axes described on a reference surface in space. The shape of the reference surface, the actual definition of material geometry with reference to that surface, and the loading pattern determine the class of shell.

The simplest class of shell is the degenerate shell defined by a plane reference surface. This is referred to as a plate. Displacements in the plane of the plate result in membrane action, those perpendicular to the plate result in bending. In the linear theory of small deflections, these is no coupling between these two types of behavior of a plate.

However, if the reference surface is curved, in general, deformations in the tangential plane and perpendicular to it are coupled.

If the thickness of the shell is small compared with the radii of curvature of the reference surface (or mid surface as it is usually called) the shell will be referred to as a geometrically thin shell. If the largest total transverse shear force per unit width acting on a shell is small enough so that transverse shear deflections are insignificant, then it will be referred to as a structurally thin shell. This latter concept can be of special importance in dynamic analysis. Certain simplifications can be made for thin shells, that will be outlined below.

Other classifications, of importance to closed form methods of analysis are concerned with the form of the mid-surface. Thus we can

refer to shallow shells, shells of revolution, shells of translation, cylindrical shells, etc. These categories all fall within the general curved shell analysis to be presented here, and hence need not be considered as special cases. It should perhaps be remarked that certain of the following work could easily be applied to the solution of axisymmetric shells formulated by an axi-symmetric solution method, but this approach has not been pursued in the present work.

We will be concerned with the limited case of small deflections and linear elastic, isotropic material properties in the following, although using standard techniques now available the range of applicability could be expanded into the nonlinear range.

We will now consider the various assumptions usually applied to thin and moderately thick plates and shells.

Consider an element of a shell as shown in Fig. (III. 1).

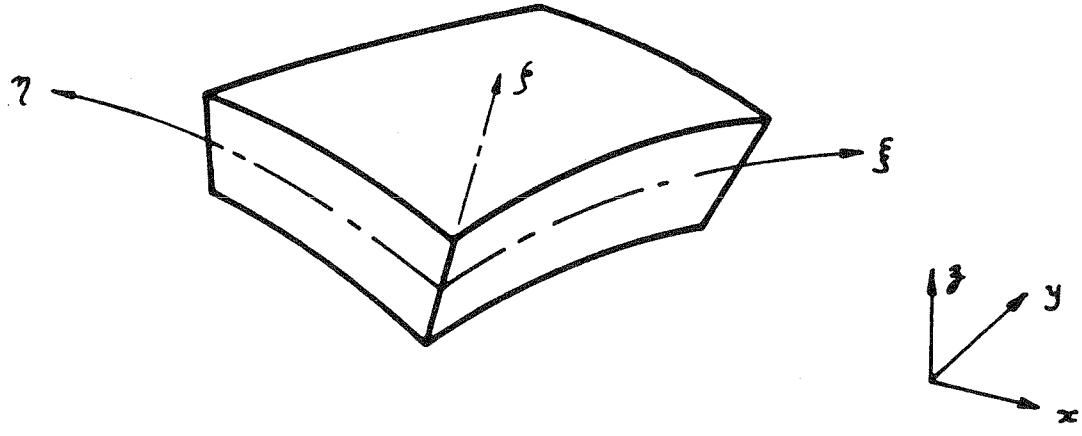

fig III.1 Shell Coordinates

Any point in the shell can be referred to the global coordinate system (x, y, z) or to a curvilinear coordinate system (ξ, η, ζ) where ξ, η are coordinates on the mid-surface, and ζ is a coordinate perpendicular to the mid-surface.

In order to reduce the three-dimensional problem to a problem in the two shell coordinates, we must specify the deformed state of the shell uniquely by the displacements of the mid-surface.

We will describe now the kinematic and geometric assumptions usually made for shells that are thin both geometrically and structurally.

It is assumed that as the shell deforms and the mid surface stretches and bends, the fibers of the shell initially straight and normal to the mid surface remain straight and normal to the mid surface. (See Fig. III. 2) this assumption is identical to the usual assumption introduced in simple beam theory, and is referred to as Kirchhoff's Hypothesis.

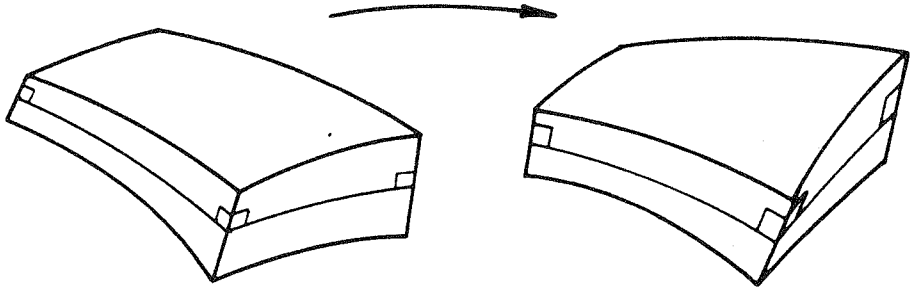

Initial Position **Deformed Position**

fig III.2 Kirchhoff's Hypothesis

Using this assumption, from any assumed deformed shape of the mid surface, we can (at least in theory) calculate the strains at all points in the shell and hence find the stresses, which must satisfy equilibrium. The above kinematic assumptions, however, are not sufficient to determine the

strain in the normal direction ζ and a further assumption must be made. The simplest assumption, requiring the normal to displace by simple translational and rotational displacements, without change of length, enforces a zero strain in the normal direction. This results in membrane stresses in the shell that are $1/(1-\nu^2)$ too great. Instead, the assumption is made that the normal <u>stress</u> is zero, resulting in the desirable membrane stresses. This assumption is reasonable since in-plane stresses are usually far greater than the normal stresses caused by the surface loading or the shell curvature.

In computing strains from the displacements of curved shells a simplifying assumption is usually made. Due to the fact that the initial length of the fibers at any surface, such as ab in Fig. III. 3, depends on the radial distance r, a displacement of the normal, undeformed, results in a non-linear strain distribution across the thickness. In this case, lack of linearity depends on the ratio of the thickness of the beam to the radius of curvature of the middle surface. For thin shells, i.e.

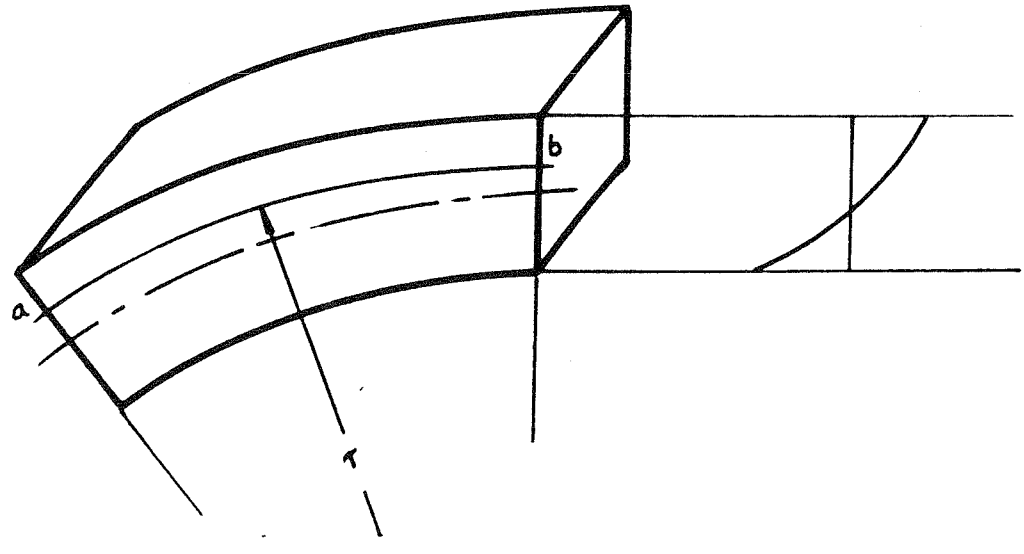

fig III.3 Tangential Strain Variation for Thick Shell

if t/R is small enough, we can ignore this effect, using the initial length of the mid surface as the initial length of all fibers. This results in a linear strain distribution across the thickness of the shell.

In order to be able to describe the stresses acting on the cross section of a shell by two coordinates ξ and η only, it is necessary to eliminate their dependence on ζ, the normal coordinate. This is done as in elementary beam theory by integrating the stresses across the thickness, resulting in moments and in-plane forces as the variables used in the formulation. As we see in Fig. III. 4, this integral

$$\int \sigma \, dA = \int \sigma \cdot bc \cdot dr$$

involves elemental areas which depend on the width b-c, which is a function of the radius r.

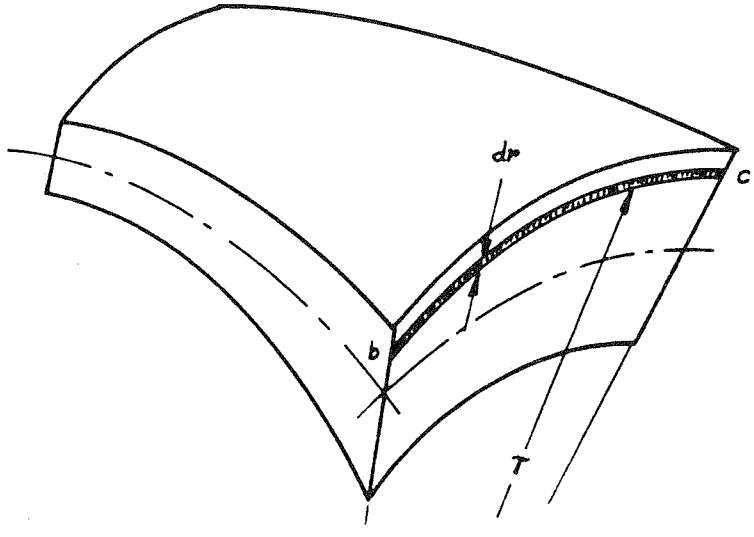

fig III.4 Integration Area for Stress Resultants

For geometrically thin shells, we usually ignore this effect, and integrate using a constant width equal to that at the mid surface.

With the preceding kinematic assumptions we can relate the strains in the shell with the displacements of the mid surface. Hence we can compute the stresses and hence moments and in-plane forces, which must satisfy a set of equilibrium conditions. This procedure looks deceptively simple. The resultant differential equations represent:

(i) Equilibrium conditions

(ii) Equations relating moments and in-plane forces with extensions and changes in curvature of the mid surface

(iii) Equations relating extension and curvature changes of the mid-surface with displacements.

This set of equations is, in fact, quite difficult to solve except for the simplest geometry and loadings. In most realistic situations, the solutions become almost intractable. In order to get some sort of solution for these differential equations we must resort to simplifications of the differential equations themselves. The art and science of the theory of thin shells relies largely on judicious approximations to, and deletions of, various terms of the differential equations.

Numerical methods may be employed to solve these differential equations, or we can circumvent the elaborate mathematical treatment by the finite element method, to be described in later chapters.

When the shell is thick enough compared with the radii of curvature, various of the above thin shell assumptions may be invalid. We may find that the assumption of the linear strain distribution across the thickness and the simplified integration on the cross section introduce unacceptable errors and more exact relationships should be used. This of course results in a far more complicated set of shell

equations. Further, the kinematic assumptions adopted to enable a two dimensional theory to be used, may be too restrictive. This may come about by significant bending of the normal, rapid change of thickness of the shell, or by the interaction between the inplane stresses and the normal stresses due to extreme curvature. In these situations the analysis become at least partly three dimensional, and two dimensional shell equations may be unsuitable.

Even if the shell is geometrically thin enough that none of the preceding assumptions are invalid, another condition may arise that will render classical thin shell theory inadmissible. If the transverse shear stresses are significant compared with the in-plane stresses, then all the thin shell assumptions may be acceptable except for the Kirchhoff Hypothesis, which restrains the normal to remain perpendicular to the middle surface. This type of deformation will be typical of what we have referred to here as "structurally thick" shells.

Theoretically, transverse shear deformation results in a cubic deformation of the normal as shown in Fig. III. 5, preserving zero shear strain at the surfaces of the plate. (27)

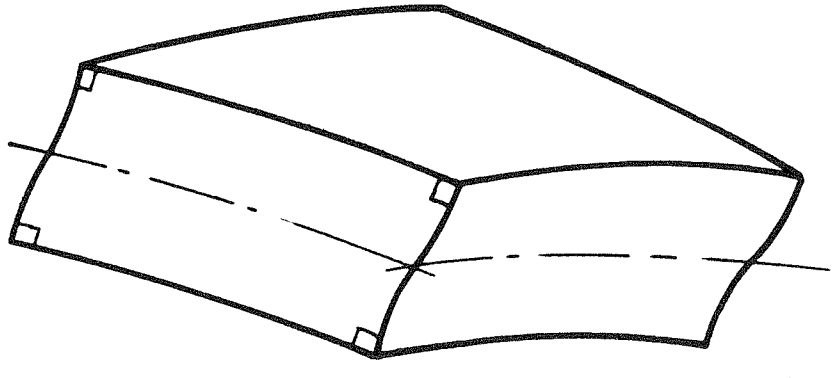

fig III.5 Shear Deformation of Normal

However since this shear effect is normally quite small, and since a linear deformation of the normal is therefore quite close to the true deformation, we can obtain good results by forcing the normal to remain straight, but allowing rotation of the normal with respect to the middle surface. This procedure was adopted by Reissner (21) in his classic paper on plate deflections.

Large transverse shear stresses can occur in situations where the shell's thickness is significant compared with its other dimensions, or even for thin shells when the loading is such as to cause many lines of bending contraflexure in the shell. One example where this might be important is the dynamic behavior of shells or plates subject to high frequency excitation. The static behavior might be well within the class of structurally and geometrically thin shells or plates. However, the high frequency vibrations, which result in sinusoidal - like displacement patterns with wavelengths of the same order of magnitude as the thickness, may require assumptions appropriate to a structurally thick shell.

Many situations arise in practice, where the shell over all or part of its structure cannot be considered a thin shell, and hence a solution based on thin shell approximations is invalid. For instance, an arch dam may be quite thick compared to its radius of curvature and span especially at the base, and even low frequencies of vibration can very easily have wavelengths comparable to the thickness over parts of the structure. A full three dimensional analysis is quite time-consuming and an analysis providing refinement between this and thin shell theory is called for.

In the totally different class of structures represented by a steel I-beam, we can examine another case where more than a thin shell theory is required, but less than a three dimensional solution is needed. Let us suppose we are interested in reproducing local buckling of the flanges and web. The buckling may occur with wavelengths only a few times the flange or web thickness, so we would not expect very good agreement with a theory based on thin plates connected together. A thick plate solution would be required to represent this accurately and efficiently.

The research described in the following pages concerns the development of an efficient shell element for moderately thick shells, that is based on the assumption of undeformed normals and zero normal stresses, but makes no other geometrical or kinematic assumptions described in this Chapter.

IV. REVIEW OF SHELL ELEMENTS

IV.1 Flat Elements, from Bending and Membrane Elements

The earliest attempts at constructing suitable shell elements were based on combining membrane elements with plate-bending elements that enforced Kirchhoff's Hypothesis. This process resulted in elements with uncoupled membrane and bending actions and hence were restricted to flat elements. Assembly of these elements into a many-faceted surface gave a geometry which approximated the true shell surface. This class of shell element has proven to have good convergence characteristics and is widely used at the moment for the analysis of thin shells (29).

The development of shell elements of this type closely paralleled the development of good plate-bending elements, from which they are derived. Until 1965-66, considerable difficulty had been experienced in forming a plate-bending element of arbitrary geometry that satisfied the requirements of continuity, rigid body displacements and constant strain states. Clough and Tocher (1) presented a triangular element satisfying the above criteria, which has been quite successful in its applications. This element is constructed from three triangular sub-elements with corner nodes and mid-side nodes between the sub-elements. A more recent paper by Clough and Felippa (4) gives details of a quadrilateral element formed similarly.

IV.2 Relaxation of Kirchhoff's Hypothesis and Compatibility

Until 1966, most research effort had been put into the search for elements for which there was full continuity of displacements and slopes and for which the Kirchhoff's Hypothesis, appropriate to thin plates and shells, was maintained. The former assumption was considered a necessary

condition for convergence, while the latter was considered a "simplifying" assumption as in classical shell theory.

Two papers presented at the same conference, the first by Bazely, Cheung, Irons and Zienkiewicz (3) and the second by Melosh (2), suggested the weakening of one or more of these conditions.

Bazely et al. recognized that the requirement of slope compatibility between elements was unnecessarily strict. They restated the compatibility condition as requiring continuity of slope, only for the condition of constant curvature. This, with rigid body displacements exactly satisfied, they pointed out, is sufficient to guarantee convergence. They illustrated the weaker condition with some examples of non-conforming and conforming elements. This weaker compatibility requirement has since been shown more rigorously by Oliveira (22).

Irons and Draper (23) had pointed out in 1965 the difficulties that the Kirchhoff Hypothesis caused in defining an element with corner nodes. Melosh (2) abandoned this requirement, allowing independent transverse displacements and rotations of the normal. He adopted a triangle with corner nodes and assumed linear expansions for the transverse displacement and each rotation of the normal. This element automatically included the effects of transverse shear deformations, thus allowing a wider class of shells to be analyzed than previously possible.

The effect of shear was also considered by Clough and Felippa (4) in the quadrilateral version of their conforming element, by allowing a shear rotation of the normal, relative to the mid-surface, that varied linearly within the element. The inclusion of these shearing angles as nodal parameters leads to a stiffness including both actual rotations of

the normals and shearing angles. Since the shearing angles don't affect compatibility, they are eliminated from consideration by static condensation.

When elements similar to that discussed by Melosh were used in actual problems, a problem of inefficiency was encountered. When the nodes of a plate element of this type are given displacements corresponding to some bending deformation, the transverse shear energy is usually large compared with the correct value. This results in a high stiffness for the element. As the size of the element decreases, with refining of the mesh, this discrepancy in shear energy decreases and the solution to the problem converges to the correct solution, but at a rather slow rate.

A paper by Wempner, Oden and Kross (17) explained how, by suitable choice of the displacement variables, constraints could be imposed pointwise at the nodes to enforce the Kirchhoff Hypothesis at these discrete points only. Thus the overall degrees of freedom are reduced, and the convergence to the thin shell solution is speeded up.

A similar paper by Stricklin, Haisler, Tisdale and Gunderson (10) gave the details of a triangular plate element in which a similar discrete version of the Kirchhoff Hypothesis was used to give an element with 9 plate-bending degrees of freedom.

IV.3 Some Curved Shell Elements

Curved elements, based on exact or approximate shapes of shells began to appear in 1967.

Bogner, Fox and Schmit (12) describe a cylindrical shell element, which used interpolation functions defined in shell coordinates. Nodal values involved the three displacements and various derivatives, with

respect to the local coordinates, of these displacements. This resulted in a stiffness with twelve degrees of freedom for each of the four nodes in an element.

Utku (11) expanded on the work of Melosh, previously described, and widened the use of the triangular element to include shallow curved triangular shell elements. Using three displacements and two rotations at each node, by use of thin shallow shell equations, he defined the internal strains from an assumption of linear variation of the displacement quantities within the triangular element.

IV.4 Equilibrium and Mixed Models

While much work was going into the foregoing displacement models, a number of researchers were seeking solutions to plate and shell problems by the use of finite elements based on other variational principles (see Chapter I.2). Three more or less distinct classes of element resulted, which will be described briefly.

Following the initial presentation of the basis for the equilibrium element (6), de Veubecke followed his first paper on plane stress elements with a plate-bending element (19), (20) in which moments are the primary variables and the stress field resulting from the assumed interpolation functions satisfy stress equilibrium, or in the case of a plate, moment equilibrium, point-wise over the whole element. The complementary energy variational principle is used to determine the actual stress field.

The second class of element, being simultaneously developed, was the so-called mixed model, based on a variational principle including both displacements and stresses (or moments) as primary

variables. One principle, first enunciated by Reissner (21) was discretized by Herrmann (5) to give a model with both moments and displacements varying linearly within a triangle. A later paper by Herrmann (7) improved considerably on the first element by slight changes in the definition of the element.

An interesting mixed model, generally referred to as a "hybrid" element, was developed by Pian (8). He used nodal displacements as the primary variables, from which the displacements along the inter-element boundaries are defined. However the displacement field is not defined within the element at all, and instead, a stress field depending on certain parameters is defined, in such a way that the stress field is in equilibrium at all points within the element. The complementary energy principle is used for each element to determine the stress parameters, and from these the stiffness of the element with respect to its nodal displacements can be determined by a matrix inversion.

This method has been used by Dungar, Severn and Taylor (9) to construct a triangular element for shell analysis.

IV.5 Three-Dimensional Elements in Shell Analysis

While the foregoing shell elements were being developed, work was continuing on the wider class of solids that could only be represented by fully three-dimensional elements. Their development by Argyris (24) and Zienkiewicz and Irons (18) made possible the representation of a shell as a three-dimensional solid, with no special shell assumptions being made.

Zienkiewicz and his group popularized the highly successful isoparametric series of elements described by Irons (13). The displacement functions for these elements, defined in a local curvilinear

coordinate system, are the same as the functions defining the global coordinates of points within the element, in that local coordinate system.

The logical extension of this work was the development by Ahmad, Irons and Zienkiewicz of a shell element, derived from three-dimensional elements, but specialized to be represented by the usual 5 degrees of freedom per node and modified to take advantage of certain shell properties. It is a refinement of this class of shell elements with which this research is concerned.

V. AHMAD-IRONS SHELL ELEMENTS

V.1 Isoparametric Elements

This versatile class of finite elements was first described by Irons (13). It has since been used widely for two and three dimensional analyses and provides efficient and easily programmed elements. A brief outline of the underlying assumptions and the stiffness formation will be given in this section. For further details, refer to any one of a number of papers by Zienkiewicz and his group at Swansea (14), or Zienkiewicz' excellent book (25).

We will consider here only three-dimensional elements. We subdivide the body being analyzed into a finite number of elements in a more or less regular way, forming six-sided hexahedra (or "bricks" as some like to call them) of regular or irregular shapes.

For simplicity we will consider for our example the simplest element, consisting of eight nodes joined by straight lines. (See Fig. V.1.)

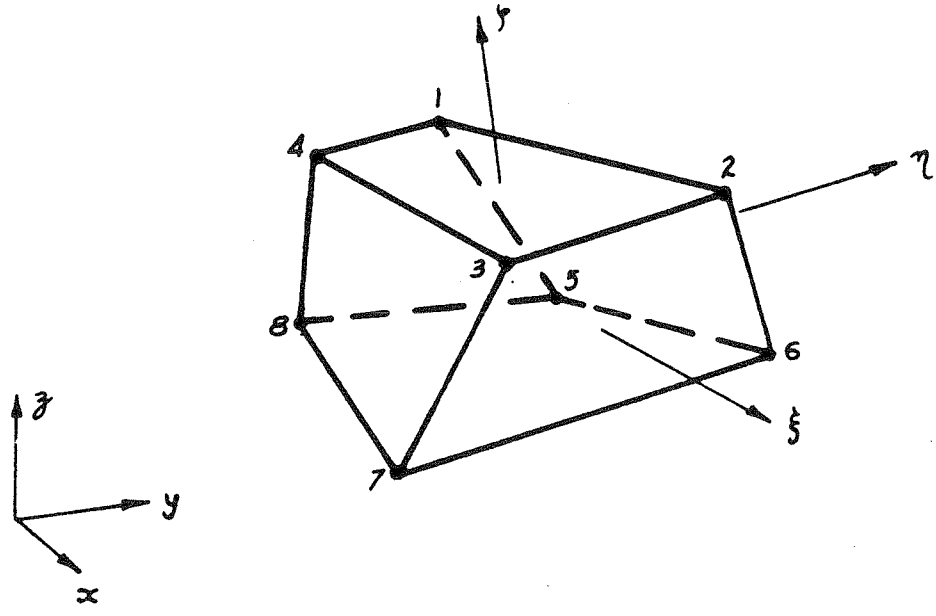

fig V.1 Three-dimensional Isoparametric Element

Each node has three degrees of freedom, one in each global direction, u, v, w. We now define a coordinate system ξ , η , ζ local to this element, such that x, y, z are products of linear interpolation functions in ξ , η , ζ , and such that ξ , η , ζ are ± 1 on the faces of the element.

We define an interpolation function for each node i (i = 1 - 8), as follows.

$$P_i = \frac{1}{8}(1+\xi_i\xi)(1+\eta_i\eta)(1+\zeta_i\zeta)$$

where ξ_i , η_i , ζ_i are the ξ , η , ζ coordinates of node i and are as follows.

i =	1	2	3	4	5	6	7	8
ξ_i	-1	+1	+1	-1	-1	+1	+1	-1
η_i	+1	+1	-1	-1	+1	+1	-1	-1
ζ_i	+1	+1	+1	+1	-1	-1	-1	-1

Explicitly this gives

$$\begin{aligned}
P_1 &= \tfrac{1}{8}(1-\xi)(1+\eta)(1+\zeta) \\
P_2 &= \tfrac{1}{8}(1+\xi)(1+\eta)(1+\zeta) \\
P_3 &= \tfrac{1}{8}(1+\xi)(1-\eta)(1+\zeta) \\
P_4 &= \tfrac{1}{8}(1-\xi)(1-\eta)(1+\zeta) \\
P_5 &= \tfrac{1}{8}(1-\xi)(1+\eta)(1-\zeta) \\
P_6 &= \tfrac{1}{8}(1+\xi)(1+\eta)(1-\zeta) \\
P_7 &= \tfrac{1}{8}(1+\xi)(1-\eta)(1-\zeta) \\
P_8 &= \tfrac{1}{8}(1-\xi)(1-\eta)(1-\zeta)
\end{aligned} \qquad \text{(V-1)}$$

We define $\langle P^T \rangle = \langle P_1 \; P_2 \; P_3 \cdots P_8 \rangle$

Using these functions we now define the coordinate transformation:

$$\langle x \; y \; z \rangle = \langle P^T \rangle \left[\underset{\sim}{x} \; \underset{\sim}{y} \; \underset{\sim}{z} \right] \qquad \text{(V-2)}$$

where $\underset{\sim}{x}$, $\underset{\sim}{y}$, $\underset{\sim}{z}$ are vectors of the global coordinates of the nodes.

We note, in passing that

$$\Sigma P_i = 1$$

We next define for any nodal displacement (u_i, v_i, w_i) at node i the displacements within the element, by reference to the local ξ , η , ζ coordinate system

$$\langle u \; v \; w \rangle = \langle P^T \rangle \left[\underset{\sim}{u} \; \underset{\sim}{v} \; \underset{\sim}{w} \right] \qquad \text{(V-3)}$$

where $\underset{\sim}{u}$, $\underset{\sim}{v}$, $\underset{\sim}{w}$, represent the vectors of these quantities, associated with each of the nodes 1 - 8.

We need the strain-displacement transformation next, but since the displacement field is defined in the local ξ , η , ζ system, we must first evaluate the derivatives in this sytem.

Thus

$$\begin{bmatrix} \frac{\partial u}{\partial \xi} & \frac{\partial v}{\partial \xi} & \frac{\partial w}{\partial \xi} \\ \frac{\partial u}{\partial \eta} & \frac{\partial v}{\partial \eta} & \frac{\partial w}{\partial \eta} \\ \frac{\partial u}{\partial \zeta} & \frac{\partial v}{\partial \zeta} & \frac{\partial w}{\partial \zeta} \end{bmatrix} = \begin{bmatrix} \langle \frac{\partial P^T}{\partial \xi} \rangle \\ \langle \frac{\partial P^T}{\partial \eta} \rangle \\ \langle \frac{\partial P^T}{\partial \zeta} \rangle \end{bmatrix} \left[\underset{\sim}{u} \; \underset{\sim}{v} \; \underset{\sim}{w} \right]$$

or, more simply

$$\left[u\ v\ w_{\xi\eta\zeta} \right] = \left[P_{\xi\eta\zeta} \right] \left[\underset{\sim}{u}\ \underset{\sim}{v}\ \underset{\sim}{w} \right] \qquad \text{(V-4)}$$

Now at any point

$$\begin{bmatrix} \frac{\partial u}{\partial \xi} & \frac{\partial v}{\partial \xi} & \frac{\partial w}{\partial \xi} \\ \frac{\partial u}{\partial \eta} & \frac{\partial v}{\partial \eta} & \frac{\partial w}{\partial \eta} \\ \frac{\partial u}{\partial \zeta} & \frac{\partial v}{\partial \zeta} & \frac{\partial w}{\partial \zeta} \end{bmatrix} = \begin{bmatrix} \frac{\partial x}{\partial \xi} & \frac{\partial y}{\partial \xi} & \frac{\partial z}{\partial \xi} \\ \frac{\partial x}{\partial \eta} & \frac{\partial y}{\partial \eta} & \frac{\partial z}{\partial \eta} \\ \frac{\partial x}{\partial \zeta} & \frac{\partial y}{\partial \zeta} & \frac{\partial z}{\partial \zeta} \end{bmatrix} \begin{bmatrix} \frac{\partial u}{\partial x} & \frac{\partial v}{\partial x} & \frac{\partial w}{\partial x} \\ \frac{\partial u}{\partial y} & \frac{\partial v}{\partial y} & \frac{\partial w}{\partial y} \\ \frac{\partial u}{\partial z} & \frac{\partial v}{\partial z} & \frac{\partial w}{\partial z} \end{bmatrix}$$

or

$$\left[u\ v\ w_{\xi\eta\zeta} \right] = \left[J \right] \left[u\ v\ w_{\xi\eta\zeta} \right] \qquad \text{(V-5)}$$

where $[J]$ is the jacobean of the transformation of x, y, z to ξ, η, ζ. Thus

$$\left[u\ v\ w_{xyz} \right] = \left[J^{-1} \right] \left[u\ v\ w_{\xi\eta\zeta} \right] \qquad \text{(V-6)}$$

Now, as $\left[x\ y\ z \right] = \left[P \right] \left[\underset{\sim}{x}\ \underset{\sim}{y}\ \underset{\sim}{z} \right]$

by differentiation

$$\left[J \right] = \left[P_{\xi\eta\zeta} \right] \left[\underset{\sim}{x}\ \underset{\sim}{y}\ \underset{\sim}{z} \right] \qquad \text{(V-7)}$$

So $[u\ v\ w_{xyz}]$ can be determined as a function of nodal displacements, at any point, by reference to equations (V-4), (V-6) and (V-7).

Now the strains ϵ_{ij} are various combinations of

$$\frac{\partial u}{\partial x}, \frac{\partial v}{\partial x}, \frac{\partial w}{\partial x}, \frac{\partial u}{\partial y}, \frac{\partial v}{\partial y}, \frac{\partial w}{\partial y}, \frac{\partial u}{\partial z}, \frac{\partial v}{\partial z}, \frac{\partial w}{\partial z}$$

and can be picked out of the matrix $[u\ v\ w_{xyz}]$, term by term.

This results in a strain dispalcement matrix [T], defined by

$$\{\epsilon\} = [T]\begin{Bmatrix} \underline{u} \\ \underline{v} \\ \underline{w} \end{Bmatrix} \qquad \text{(V-8)}$$

where ϵ^T represents $\langle \epsilon_{11} \ \epsilon_{22} \ \epsilon_{33} \ \gamma_{12} \ \gamma_{23} \ \gamma_{31} \rangle$

The element stiffness matrix, as outlined in Chapter I.4, is formed by the integration of

$$\iiint_{\text{element volume}} [T^T][E][T] \, dx \, dy \, dz \qquad \text{(V-9)}$$

where [E] is the matrix defining the constitutive relation defined by

$$\{\tau\} = [E]\{\epsilon\} \qquad \text{(V-10)}$$

$\{\tau\}$ being the stresses corresponding with the strains, $\{\epsilon\}$.

Since we are using local coordinates ξ, η, ζ we need to transform the integration over the volume of the element to an integration in the ξ, η, ζ system.

This is done by considering an infinitesimal element of volume enclosed by vectors along each local coordinate direction, at the point where the elemental volume is being considered.

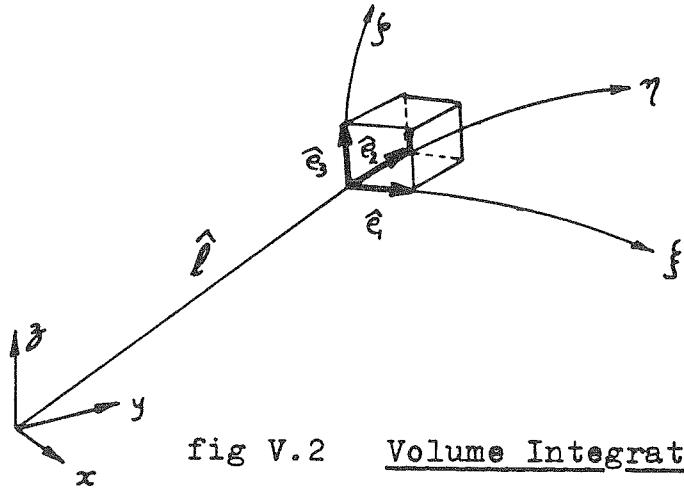

fig V.2 Volume Integration Transformation

This element of volume is equal to the scalar triple product of the three vectors $\hat{e}_1$, $\hat{e}_2$, $\hat{e}_3$.

$$dv = (\hat{e}_1 . \hat{e}_2) \times \hat{e}_3 \qquad \hat{e}_1 \cdot (\hat{e}_2 \times \hat{e}_3)$$

but

$$\hat{\ell} = x\hat{\imath} + y\hat{\jmath} + z\hat{k}$$

so

$$\left.\begin{aligned} \hat{e}_1 &= \left(\frac{\partial x}{\partial \xi}\hat{\imath} + \frac{\partial y}{\partial \xi}\hat{\jmath} + \frac{\partial z}{\partial \xi}\hat{k}\right) d\xi \\ \text{and} \\ \hat{e}_2 &= \left(\frac{\partial x}{\partial \eta}\hat{\imath} + \frac{\partial y}{\partial \eta}\hat{\jmath} + \frac{\partial z}{\partial \eta}\hat{k}\right) d\eta \\ \text{and} \\ \hat{e}_3 &= \left(\frac{\partial x}{\partial \zeta}\hat{\imath} + \frac{\partial y}{\partial \zeta}\hat{\jmath} + \frac{\partial z}{\partial \zeta}\hat{k}\right) d\zeta \end{aligned}\right\} \qquad \text{(V-11)}$$

So the volume dv

$$dv = \det J \times d\xi\, d\eta\, d\zeta$$

where det J = the determinant of the jacobean Jac.

So

$$\iiint [T^T][E][T]\, dv = \iiint [T^T][E][T] \det J\, d\xi d\eta d\zeta \qquad \text{(V-12)}$$

The inversion of [J] results in polynomials in the denominator of the integrand, and so the volume integration is performed numerically.

A Gaussian scheme of integration is most convenient, resulting in the following approximate statement

$$\iiint [T^T][E][T]\, dv \approx \iiint [T^T][E][T] \det J\, d\xi\, d\eta\, d\zeta \approx \sum_i \left[[T^T][E][T] \det J\right]_i \times k_i \qquad \text{(V-13)}$$

where k_i = Gaussian weighting factor and $[\ ]_i$ = the value of $[\ ]$ at the integration point i.

Sufficient integration points are chosen in ξ , η , ζ to get the accuracy desired.

Details of the numerical integration willbe given later, but suffice to say, that, for non-prismatic elements, the greater the number of integration points in each direction ξ , η , ζ , the more accurate the integration, and further there is a minimum order of integration that will yield a satisfactory stiffness to guarantee convergence.

The numerical integration (V-13), results in an element stiffness matrix of dimensions 24 x 24 for this eight nodal point element.

Internal stresses can be computed at any desired points from nodal displacements by use of the same transformations presented above, resulting in the relation

$$\{\tau\} = [E][T] \begin{Bmatrix} \underset{\sim}{u} \\ \underset{\sim}{v} \\ \underset{\sim}{w} \end{Bmatrix} \qquad \text{(V-14)}$$

The existence of constant strain and rigid body displacement states (which must be included in the assumed displacement interpolation functions to ensure convergence) follow simply from the definitions of the displacement field and the coordinate transformation.

Consider first a rigid body displacement of the nodes

$$\{\underset{\sim}{u}\} = k_1\{I\} + k_2\{\underset{\sim}{y}\} + k_3\{\underset{\sim}{z}\}$$

where $\{J\}$ is a vector of unit elements.

Then the internal displacements, governed by

$$u = \langle p^T \rangle \{\underset{\sim}{u}\}$$

become

$$u = \langle p^T \rangle \{k_1\{I\} + k_2\{y\} + k_3\{z\}\}$$

but $\langle p^T \rangle \{I\} = \sum p_i = 1$ as we noted earlier

and $\langle p^T \rangle \{y\} = y$

$\langle p^T \rangle \{z\} = z$

So $u = k_1 + k_2 y + k_3 z$

representing correct rigid body motion. A similar proof is used for displacements v, w.

Similarly, a constant strain condition $\epsilon_{xx} = k$ requires nodal displacements $\{\underline{u}\} = k \{\underline{x}\}$. Then, internally

$$u = \langle p^T \rangle \{u\}$$
$$= k \langle p^T \rangle \{\underline{x}\} = kx$$

Again, we get the exact displacements. Similar arguments can be used for displacements in the y, z direction.

Since the deformations of an element face are determined solely by the displacement of the four adjacent nodes, full continuity of displacement is maintained.

The simplest three dimensional isoparametric element has been used above to illustrate the basic assumptions and the stiffness formation. However, this is only one of a theoretically infinite family of similar elements of increasing geometric complexity, but having identical method

of formation. These elements may in general have edges curved in space and may or may not have internal nodes and midside (or even mid-face) nodes. A number of examples are shown in Fig. V-3.

In each case, a local coordinate system ξ , η , ζ is established, which satisfies the requirement of having values of $\pm$ 1 on opposite faces for each coordinate ξ , η , ζ in turn. Then the interpolation function for each node is defined in such a way that the function is unity at that node, and zero at all others.

Thus, for example (i) in Fig. V.3 the interpolation functions are built up from

$$
\begin{aligned}
P_1 &= \tfrac{1}{8}(1-\xi)(1+\eta)(1+\zeta) - \tfrac{1}{8}(1-\xi^2)(1-\eta^2)(1-\zeta^2) \\
P_2 &= \tfrac{1}{8}(1+\xi)(1+\eta)(1+\zeta) \quad " \\
P_3 &= \tfrac{1}{8}(1+\xi)(1-\eta)(1+\zeta) \quad " \qquad \text{(V-15)} \\
P_4 &= \tfrac{1}{8}(1-\xi)(1-\eta)(1+\zeta) \quad " \\
P_5 &= \tfrac{1}{8}(1-\xi)(1+\eta)(1-\zeta) \quad " \\
P_6 &= \tfrac{1}{8}(1+\xi)(1+\eta)(1-\zeta) \quad " \\
P_7 &= \tfrac{1}{8}(1+\xi)(1-\eta)(1-\zeta) \quad " \\
P_8 &= \tfrac{1}{8}(1-\xi)(1-\eta)(1-\zeta) \quad " \\
P_9 &= \tfrac{1}{8}(1-\xi^2)(1-\eta^2)(1-\zeta^2) \quad "
\end{aligned}
$$

NISEE/COMPUTER APPLICATIONS
DAVIS HALL
UNIVERSITY OF CALIFORNIA
BERKELEY, CALIFORNIA 94720
(415) 642-5113

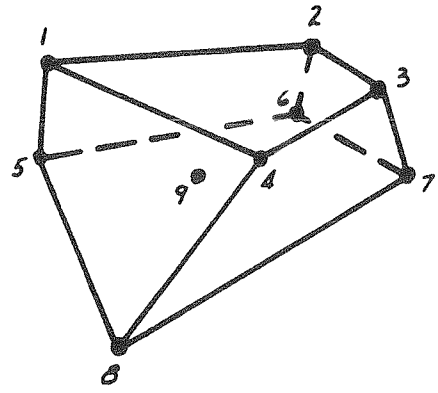

(i) Linear Element with Internal Node

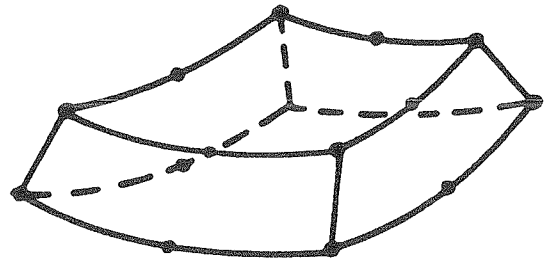

(ii) Linear x quadratic- x quadratic Element

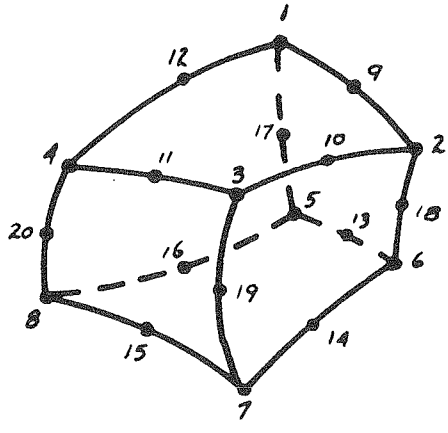

(iii) Quadratic x quadratic- x quadratic Element

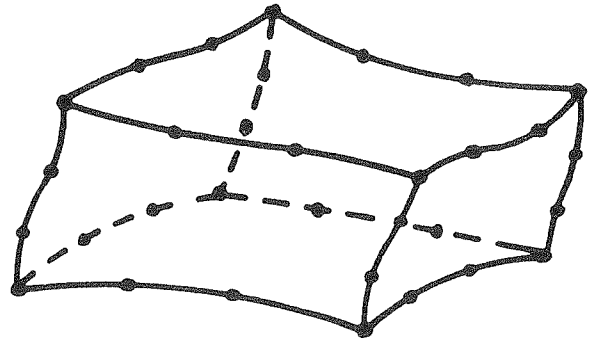

(iv) Cubic x cubic x cubic Element

fig V.3 Typical Isoparametric Elements

for example (iii) we have

$$
\begin{aligned}
P_1 &= \tfrac{1}{8}(1-\xi)(1+\eta)(1+\zeta)(-\xi+\eta+\zeta-2) \\
P_2 &= \tfrac{1}{8}(1+\xi)(1+\eta)(1+\zeta)(+\xi+\eta+\zeta-2) \\
P_3 &= \tfrac{1}{8}(1+\xi)(1-\eta)(1+\zeta)(+\xi-\eta+\zeta-2) \\
P_4 &= \tfrac{1}{8}(1-\xi)(1-\eta)(1+\zeta)(-\xi-\eta+\zeta-2) \\
P_5 &= \tfrac{1}{8}(1-\xi)(1+\eta)(1-\zeta)(-\xi+\eta-\zeta-2) \\
P_6 &= \tfrac{1}{8}(1+\xi)(1+\eta)(1-\zeta)(+\xi+\eta-\zeta-2) \\
P_7 &= \tfrac{1}{8}(1+\xi)(1-\eta)(1-\zeta)(+\xi-\eta-\zeta-2) \\
P_8 &= \tfrac{1}{8}(1-\xi)(1-\eta)(1-\zeta)(-\xi-\eta-\zeta-2) \\
P_9 &= \tfrac{1}{4}(1-\xi^2)(1+\eta)(1+\zeta) \\
P_{10} &= \tfrac{1}{4}(1+\xi)(1-\eta^2)(1+\zeta) \\
P_{11} &= \tfrac{1}{4}(1-\xi^2)(1-\eta)(1+\zeta) \\
P_{12} &= \tfrac{1}{4}(1-\xi)(1-\eta^2)(1+\zeta) \\
P_{13} &= \tfrac{1}{4}(1-\xi^2)(1+\eta)(1-\zeta) \\
P_{14} &= \tfrac{1}{4}(1+\xi)(1-\eta^2)(1-\zeta) \\
P_{15} &= \tfrac{1}{4}(1-\xi^2)(1-\eta)(1-\zeta) \\
P_{16} &= \tfrac{1}{4}(1-\xi)(1-\eta^2)(1-\zeta) \\
P_{17} &= \tfrac{1}{4}(1-\xi)(1+\eta)(1-\zeta^2) \\
P_{18} &= \tfrac{1}{4}(1+\xi)(1+\eta)(1-\zeta^2) \\
P_{19} &= \tfrac{1}{4}(1+\xi)(1-\eta)(1-\zeta^2) \\
P_{20} &= \tfrac{1}{4}(1-\xi)(1-\eta)(1-\zeta^2)
\end{aligned}
\qquad \text{(V-16)}
$$

As before

$$\langle x \; y \; z \rangle = \langle P^T \rangle [\underline{x} \; \underline{y} \; \underline{z}]$$

and

$$\langle u \; v \; w \rangle = \langle P^T \rangle [\underline{u} \; \underline{v} \; \underline{w}]$$

and all other details are identical.

It should be noted here that although we have discussed the case of the coordinate definition and the displacement definition having identical form, being defined by the functions $\langle P^T \rangle$, this is not strictly necessary. A satisfactory element may be built up with the coordinate relationship being of a lower order than the definition used for displacement. The converse, however is not, in general, true -- rigid body modes or constant strain states being violated in this case.

A simple example will illustrate this point. This example will be referred to later in the definition of a curved shell element. We will consider a quadratic x quadratic element in two dimensions with mid-side nodes, as shown in Fig. V.4. The internal node 9 will also be used to define displacements.

The geometrical relationship

$$\langle x \; y \; z \rangle = \langle P^T \rangle [\underline{x} \; \underline{y} \; \underline{z}] \qquad \text{(V-17)}$$

involves nodes 1-9 and nine interpolation functions

$$P_1 = \tfrac{1}{4}(-\xi)(1-\xi)\eta(1+\eta)$$

$$P_2 = \tfrac{1}{4}\xi(1+\xi)\eta(1+\eta) \qquad \text{(V-18)}$$

--continued...

$$
\begin{aligned}
P_3 &= \tfrac{1}{4}(+\xi)(1+\xi)(-\eta)(1-\eta) \\
P_4 &= \tfrac{1}{4}(-\xi)(1-\xi)(-\eta)(1-\eta) \\
P_5 &= \tfrac{1}{2}(1-\xi^2)(\eta)(1+\eta) \\
P_6 &= \tfrac{1}{2}(\xi)(1+\xi)(1-\eta^2) \\
P_7 &= \tfrac{1}{2}(1-\xi^2)(\eta)(1-\eta) \\
P_8 &= \tfrac{1}{2}(-\xi)(1-\xi)(1-\eta^2) \\
P_9 &= (1-\xi^2)(1-\eta^2)
\end{aligned}
$$

However, if we choose the position of node 9 suitably, the above relation degenerates to

$$\langle x \; y \; z \rangle = \langle p^{*T} \rangle [\, \underset{\sim}{x}^* \; \underset{\sim}{y}^* \; \underset{\sim}{z}^* \,] \qquad \text{(V-19)}$$

involving only the eight external nodes. In this case we find

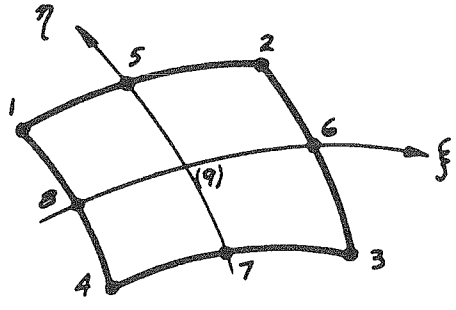

fig V.4 Plane Isoparametric Element

$$
\begin{aligned}
P_1^* &= \tfrac{1}{4}(1-\xi)(1+\eta)(-\xi+\eta-1) \\
P_2^* &= \tfrac{1}{4}(1+\xi)(1+\eta)(\xi+\eta-1) \\
P_3^* &= \tfrac{1}{4}(1+\xi)(1-\eta)(\xi-\eta-1) \\
P_4^* &= \tfrac{1}{4}(1-\xi)(1-\eta)(-\xi-\eta-1) \\
P_5^* &= \tfrac{1}{2}(1-\xi^2)(1+\eta) \\
P_6^* &= \tfrac{1}{2}(1+\xi)(1-\eta^2) \\
P_7^* &= \tfrac{1}{2}(1-\xi^2)(1-\eta) \\
P_8^* &= \tfrac{1}{2}(1-\xi)(1-\eta^2)
\end{aligned}
\qquad \text{(V-20)}
$$

Thus, if the position of the internal node is such as to satisfy this latter relation (V-20), it will also satisfy the former, (V-18).

We can therefore turn the problem around and define the geometry by the <u>eight</u> nodal point definition (V-20), and if the internal node is correctly positioned we can define the displacements by the <u>nine</u> nodes. This formulation is effectively identical to using nine nodes for both relations.

It can be easily shown however that attempts to use a higher order geometry than displacement relation, will in general fail to satisfy one or both of the constant strain or rigid body motions. Thus, for instance, we could not use an eight nodal point hexahedron with curved sides defined by 20 nodal points.

V.2 SHELL ELEMENTS BASED ON ISOPARAMETRIC ELEMENTS

The three dimensional elements described above provide a powerful tool for the solution of complex three-dimensional problems. They can, of course, be used unaltered, if desired, for shell problems.

As we refine the finite element mesh in both the surface and normal directions, the solution will converge to the correct theory of elasticity solution, since no shell assumptions have been imposed on the solution.

Clearly, this is an expensive way of modelling a shell, since various special information is known about shell behavior and some or all of the thin shell assumptions may be valid to use. Application of this knowledge should reduce the complexity of the problem.

We saw in Chapter III that there were three basic types of assumptions used in formulating any shell theory.

(i) Geometric approximations of either the shell geometry itself, or the geometric variation of strains, depending on the ratio of the thickness to the radii of curvature.

(ii) Kinematic assumptions on deformation behavior.

(iii) Assumptions on stresses themselves.

By using three-dimensional elements (or elements derived closely from them, as described in the end of this section), we are approximating the actual surface geometry, rather than the mid-surface geometry, that is used in any thin shell elements. Hence, as we refine the mesh with either curved or straight-sided elements, the actual geometry of the shell is approximated as closely as we like, and all transformations and energy integrations are based on the correct shell geometry. See Fig. V.5.

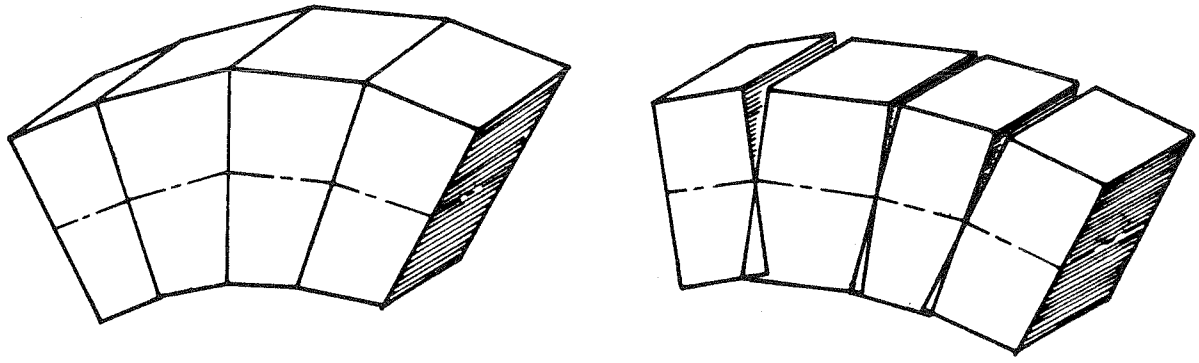

Geometry with 3-dimensional Elements

Geometry with Thin Shell Elements

fig V.5 Comparison of 3-dimensional and Thin Shell Elements

For this reason, the thickness to radii of curvature may be small or large, and no error in the converged solution will result from this cause.

The kinematic and stress assumptions, on the other hand, depend directly on the type of three-dimensional element used. It is desirable to use elements, which, when only one layer is used through the thickness, represent the kinematic deformation and stress variations that any particular class of shells requires.

If we are interested in including a particular type of deformation (e.g., transverse shear deformations) we must decide further between an element that will model this exactly, or one that will approximate this behavior.

We will now examine certain classes of shells and see what elements can be used to represent them.

For simplicity, we will examine in detail the behavior of plate elements formed from general three-dimensional elements. (Fig. V.6.)

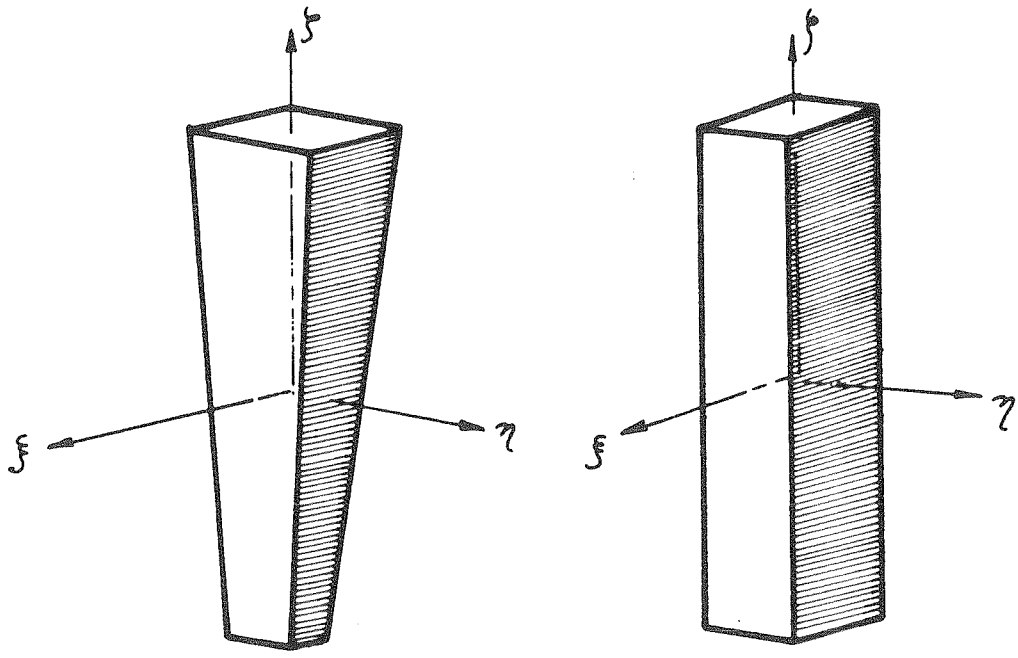

Small Element in Shell Small Element in Plate

Fig. V.6 Small Elements from Shell and Plate

The behavior of a very small element (i.e., small compared with its thickness) is similar to a small element in a shell, except for the geometrical effects discussed above. So, by requiring that a small plate element behave in a certain manner, we will be fixing the class of shell that can be represented by this element used in a shell.

We will be primarily interested in an element that can reproduce exactly (in the limit) membrane strains, and bending strains and will include, with good accuracy, deformations due to transverse shear.

Elements with this capability, formed from three dimensional elements so as to accurately reproduce geometrical relations, will be suitable elements for most thick shell applications as, for instance, arch dams. This class of element could also be used for thin shells, although

we may find that their efficiency may not be as high as elements designed for thin shells alone. This will be examined later.

We discussed previously the importance of satisfying the constant strain modes of deformation exactly, in order to get convergence to the correct solution. This necessary condition, for a shell becomes a requirement that any particular shell deformation mode can be exactly satisfied. Thus it is no longer sufficient (nor indeed relevant) that the six constant strains ϵ_{ij} are present, but that an element of small size and arbitrary shape can reproduce all constant shell deformation modes exactly.

Two characteristics of the shell element will affect this capability, namely the order of expansion for displacements in the surface coordinates ξ , η , and that in the normal coordinate ζ .

Let us first consider the simplest three dimensional isoparametric element, with 8 nodes, one at each corner, using a linear assumption on displacements.

Further, let us first examine an element with rectangular surfaces, as shown in Fig. V.7.

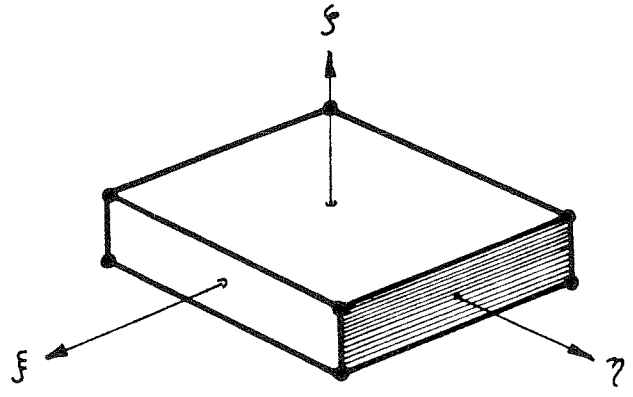

fig V.7 Rectangular 3-dimensional Element as Plate

A membrane deformation of the plane stress type will first be examined. Any membrane strain, constant in the element, can be exactly satisfied by this element, since it is one of the constant strain states that the three dimensional element must satisfy anyway.

However, this element will, in general, not satisfy a constant bending deformation precisely, for two reasons.

Under pure bending, for non-zero values of Poisson's Ratio, ν, the normal strain ϵ_{nn} in a plate varies linearly with ζ. See Fig. V.8.

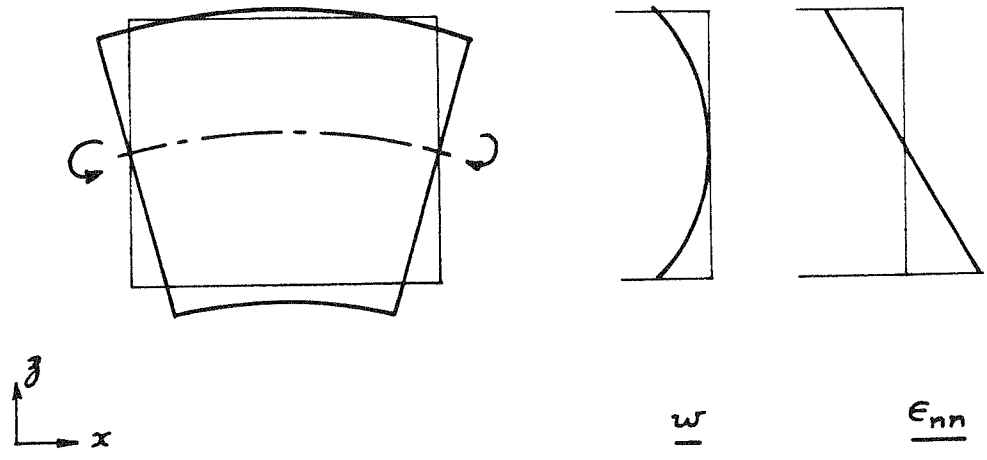

Fig. V.8 Normal Strain in Bending

This is the result of the in-plane stresses varying linearly with ζ, and the normal stress being constant and equal to zero. However, in this element the linear expansion for w in the ζ direction allows only constant ϵ_{nn}. So, as ϵ_{nn} is anti-symmetric about the mid-surface for this loading, we conclude that $\epsilon_{nn} = 0$. This causes the bending stiffness to be too large by a factor of $1/(1-\nu)^2$. No matter how small an element we examine, this failure remains, and this will cause an error of the same magnitude in

any problem involving bending. To represent this correctly, by a strictly displacement model, a quadratic variation with ζ is required for w, resulting in three nodes on the normal. See Fig. V.9.

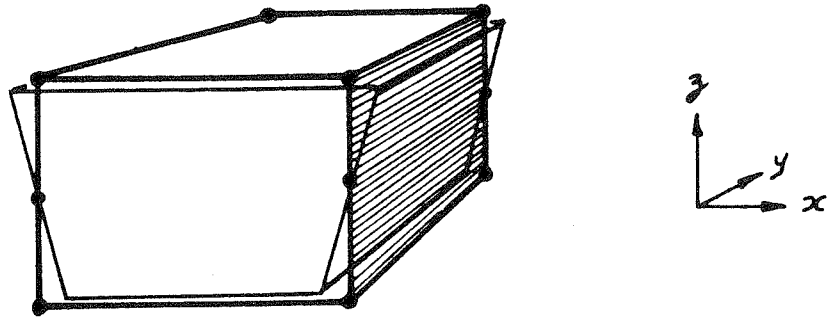

Fig. V.9 Element to Allow Quadratic Stretching of Normal

The second weakness is the result of the fact that, for pure bending, the normal displacement w of the actual shell varies quadratically with ξ and/or η . This again is impossible with the linear displacement element. See Fig. V.9 again. We see also that the transverse shear strains γ_{zx} and/or γ_{yz} are non-zero over most of the element. These two effects are the result of the same constraint. Hence, a constant moment cannot be reproduced by a finite sized element. However, as the element size is decreased, the incorrect strains caused by this constraint decrease to zero. See Fig. V.10.

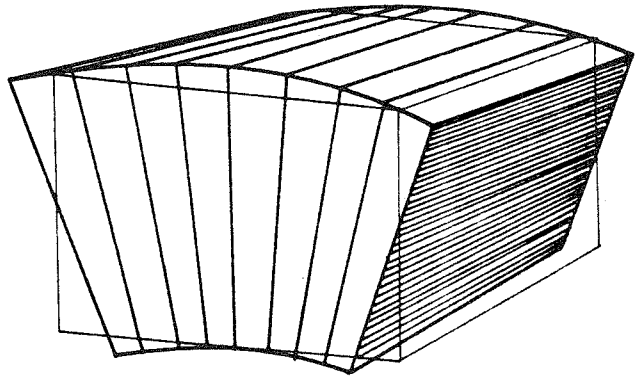

Fig. V.10 GROUP OF SMALL ELEMENTS IN BENDING

This is a necessary (although not sufficient) condition for the element to converge towards a constant moment condition. In fact we do find that this rectangular element does converge to this capability. Since an element in a fine enough mesh satisfies constant curvature as closely as we like, this element satisfies conditions for convergence of a mesh built up of these elements. So rectangular elements will converge to the exact bending solution.

However, if we consider the case of a non-rectangular plate element as shown in Fig. V. 11,

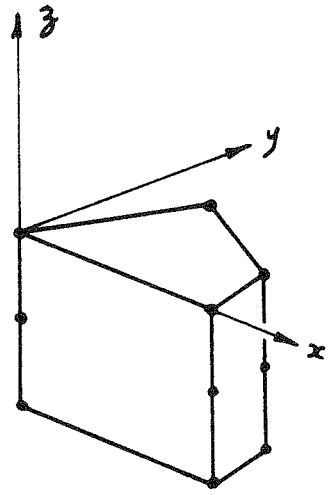

FIG. V.11 NON-RECTANGULAR PLATE ELEMENT

we are unable to show this convergence. Indeed even if we take an element that has surface dimensions very small compared with the thickness, we find that this element, when acted on by forces corresponding to a constant moment, deflects in a manner very different from the expected nodal displacements corresponding to constant curvature. Failing to satisfy the constant curvature state, even in the limit of a small element, we are unable to draw any conclusions about convergence. Since the plate element fails to satisfy conditions for convergence, no guarantee of convergence exists for a shell either.

If we now consider the next complete higher order expansion in the surface coordinates ξ and η, which is quadratic x quadratic, (Fig. V.12) we now find that even a non-rectangular element contains the constant curvature state exactly.

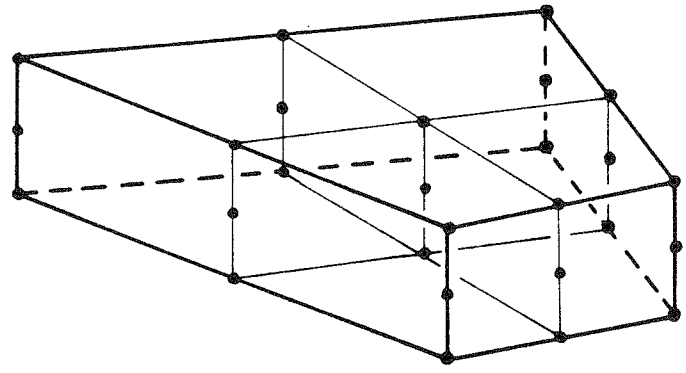

fig V.12 Full Quadratic Element

Hence this element converges to the correct bending solution. Note that the interior nodes are used to form the stiffness, since it has been generally found that in most classes of finite element the addition of interior nodes to at least the order of the expansion of the exterior nodes is beneficial to the element stiffness. This was confirmed numerically on a plate problem for this particular pair of elements.

The next constant strain mode we will examine is the transverse shear deformation. The exact solution (see for instance (39) for beams) includes a cubic term in ζ, for the in-plane displacements u, v. (Fig. III.5) The quadratic displacement variation of the element we are considering, (Fig. V.12) is not enough to represent this cubic. So this element will not exactly represent shear displacements. However the shear effects, in problems where our other assumptions are still valid,

are small, and the energy difference between the true cubic and a linear displacement that the element can reproduce is very small, and a satisfactory shear distortion mechanism results. This can, in practice, be improved somewhat by multiplying the shear energy by a factor based on the knowledge that this shear strain should be quadratic in ζ, rather than constant as imposed by this element. This is further discussed in Chapter V.

We have seen that the simplest full three-dimensional element that can represent membrane, bending and shear deformations of a shell or plate is a quadratic element in all three shell coordinates. This has 3 x 3 = 9 degrees of freedom on each normal, instead of the usual 5 (comprising two rotations and three translations) for most shell elements.

Ahmad (16) was able to adapt the full three-dimensional element to a shell element with the conventional representation by mid-surface nodes only, preserving most of the desirable characteristics of the more time-consuming three-dimensional element.

The element he started with had only a linear expansion in the normal direction ζ, representing 6 degrees of freedom for the two nodes on the normal (Fig. V.13).

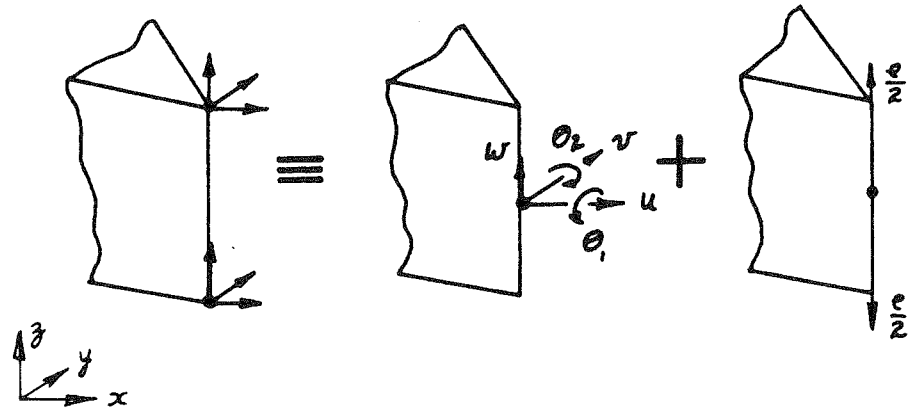

fig V.13 Transformation to Shell Degrees of Freedom

These six degrees of freedom can be transformed to six different degrees of freedom, namely three mid-point translations and two mid-point rotations about two axes perpendicular to the normal, and a change of length of the normal itself.

We saw that the three dimensional element with only two nodes on the normal yielded a stiffness too high in bending due to the fact that the normal strain $\epsilon_{nn} = 0$. However Ahmad replaced the linear variation with ζ of the normal displacement with the condition $\tau_{nn} = 0$, the usual assumption used for beam and plate theory. This assumption allows us to totally eliminate the extension of the normal from further consideration.

As we saw, a linear assumption in the ζ direction for the in-plane displacements is sufficiently good to represent membrane strain states exactly and transverse shear strains closely (but not exactly), so all desired features are now included.

The geometry of a curved shell is exactly reproduced by the elements in a fine enough mesh, since they are derived from three dimensional elements, so the resulting shell element will be applicable to shells with thickness large compared with the radii of curvature.

The final requirement for convergence is the exact representation of rigid body displacements. This requirement is exactly satisfied for any iso-parametric three dimensional element, so it will be also when the three dimensional element is used as a shell element.

So we see that a shell element based on quadratic x quadratic linear expansion in ξ, η and ζ, but with a constraint $\tau_{nn} = 0$ replacing the extensional degree of freedom of the normal, results in an acceptable element allowing considerable ratio of thickness to radius of curvature, and allowing significant transverse shear distortion.

V.3 ELEMENT STIFFNESS FORMATION

The following description of the element stiffness formation is based on the elements described by Ahmad (16), but certain details depart from the original presentation.

Consider an element with mid-surface nodes only, as discussed in the last section

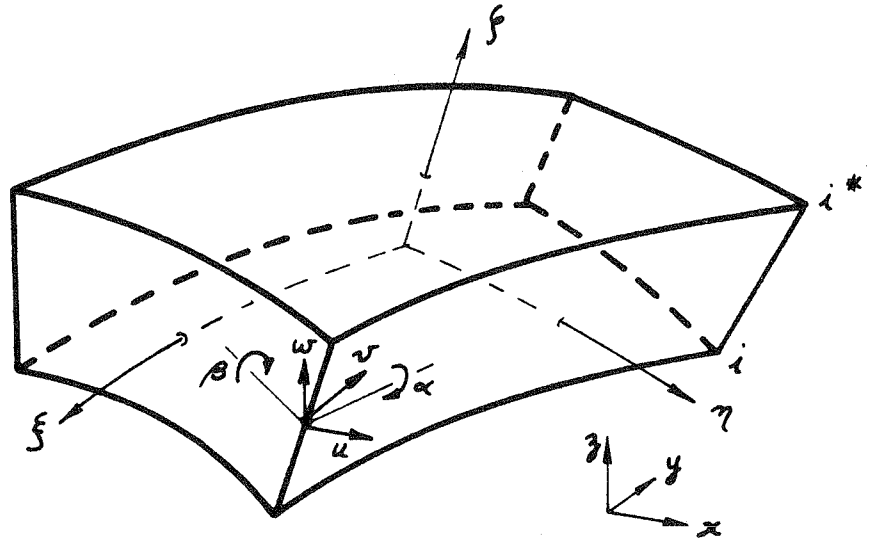

Fig. V.14 Shell Element

The global coordinate system, x, y, z has z vertically upwards. The local ξ, η, ζ system is defined by equation V.22 below. The five degrees of freedom of each node will be i) three translations u, v, w in the global x, y, z system ii) two rotations α, β about axes $\hat{a}$, $\hat{b}$. The directions of $\hat{a}$, $\hat{b}$ are defined to form a

mutually perpendicular triad with the vector $\hat{n}$, which is drawn in the direction of the ζ axis at the node (Fig. V.14). The orientation of $\hat{a}$, $\hat{b}$ is such that $\hat{a}$ is horizontal, and if both $\hat{a}$, $\hat{b}$ are horizontal, then $\hat{a}$ is in the x direction.

The local axis system ξ , η , ζ is defined in terms of x, y, z by a relation derived simply from the transformation given in Chapter V.1. (equation V.2)

We obtain

$$\langle x\ y\ z \rangle = \langle p^T \rangle \left[\underset{\sim}{x}\ \underset{\sim}{y}\ \underset{\sim}{z} \right] + \zeta \langle p^T \rangle \left[\underset{\sim}{x}^*\ \underset{\sim}{y}^*\ \underset{\sim}{z}^* \right] \qquad (V.22)$$

where $\langle p^T \rangle$ represents the vector of two-dimensional interpolation functions in ξ , η . $\underset{\sim}{x}$, $\underset{\sim}{y}$, $\underset{\sim}{z}$ are the vectors of global coordinates for the nodes. $\underset{\sim}{x}^*$, $\underset{\sim}{y}^*$, $\underset{\sim}{z}^*$ are the vectors of the global coordinates of the points (ξ_i , η_i , 1) with respect to the node (ξ_i , η_i , 0)

$$\text{i.e.} \qquad x_i^* = x_{i^*} - x_i \qquad (V.23)$$

where nodes i^*, i are shown in Fig. V.14

We now define a displacement pattern, based on the relation V.3.

$$\langle u\ v\ w \rangle = \langle p^T \rangle \left[\underset{\sim}{u}\ \underset{\sim}{v}\ \underset{\sim}{w} \right] + \zeta \langle p^T \rangle \left[\underset{\sim}{u}^*\ \underset{\sim}{v}^*\ \underset{\sim}{w}^* \right] \qquad (V.24)$$

Again $\langle p^T \rangle$ are two dimensional interpolation functions, $\underset{\sim}{u}$, $\underset{\sim}{v}$, $\underset{\sim}{w}$ are vectors of the global displacement of the nodes, and $\underset{\sim}{u}^*$, $\underset{\sim}{v}^*$, $\underset{\sim}{w}^*$ are the relative global displacements of points i* at $\zeta = 1$ with respect to those at node i at $\zeta = 0$, caused by rotations of the "normal".

We will now determine the relative displacements u*, v*, w* in terms of the rotations α, β at a node, in order to express the displacements within the element in terms of nodal displacements and rotations.

Referring back to equation V.23 we observe that x^*, y^*, z^* are the coordinates of a vector along $\hat{n}$ (see Fig. V.15).

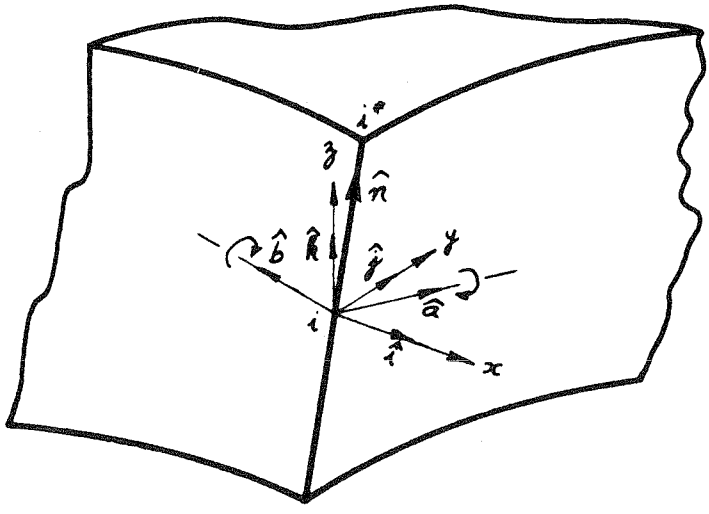

Fig. V.15 Global and Rotational Axes at Node i

From this vector $\hat{n}$ we can define a vector $\hat{a}$ perpendicular to $\hat{n}$ and also to the vertical $\hat{k}$.

Thus $$\hat{a} = \hat{k} \times \hat{n}$$

We then define $\hat{b}$ perpendicular to both $\hat{n}$ and $\hat{a}$ by

$$\hat{b} = \hat{n} \times \hat{a}$$

$$\text{So } \hat{a} = \hat{k} \times \left(x^* \hat{i} + y^* \hat{j} + z^* \hat{k} \right)$$

$$= - y^* \hat{i} + x^* \hat{j}$$

$$\text{and } \hat{b} = \left(x^* \hat{i} + y^* \hat{j} + z^* \hat{k} \right) \times \left(- y^* \hat{i} + x^* \hat{j} \right)$$

$$= - x^* z^* \hat{i} - y^* z^* \hat{j} + \left(y^* y^* + x^* x^* \right) \hat{k}$$

Note. If $x^* = y^* = 0$, define $\hat{a} = \hat{i}$

so $\hat{b} = \hat{j}$

We now normalize $\hat{a}$ and $\hat{b}$ referring from now on to the normalized vectors as $\hat{a}$, $\hat{b}$.

Consider a rotation α about axis $\hat{a}$ and β about axis $\hat{b}$.

The displacement at $\zeta = 1$, $= \frac{t}{2} \left(- \hat{b} \alpha + \hat{a} \beta \right)$

or, using the previously introduced u*, v*, w* notation

$$\langle u^* v^* w^* \rangle = - \frac{t}{2} \langle b_1 b_2 b_3 \rangle \alpha + \frac{t}{2} \langle a_1 a_2 a_3 \rangle \beta$$

Where a_i , b_i are the direction cosines of $\hat{a}$, $\hat{b}$.

The vectors of these displacements due to rotations, of all nodes, become

$$\left[\underset{\sim}{u}^* \underset{\sim}{v}^* \underset{\sim}{w}^* \right] = - \frac{1}{2} \left[\underset{\sim}{t} \right] \left[\underset{\sim}{\alpha} \right] \left[\underset{\sim}{b_1} \; \underset{\sim}{b_2} \; \underset{\sim}{b_3} \right] + \frac{1}{2} \left[\underset{\sim}{t} \right] \left[\underset{\sim}{\beta} \right] \left[\underset{\sim}{a_1} \; \underset{\sim}{a_2} \; \underset{\sim}{a_3} \right] \tag{V.25}$$

Where $\left[\underset{\sim}{t} \right]$ and $\left[\underset{\sim}{\alpha} \right]$ and $\left[\underset{\sim}{\beta} \right]$ represent the diagonal matrices of thicknesses and rotations at all nodes.

Thus the displacement definition V.24 at any point within the element becomes

$$\begin{aligned}\langle u\ v\ w\rangle \;=\; & \langle P^T\rangle \begin{bmatrix} \underset{\sim}{u} & \underset{\sim}{v} & \underset{\sim}{w} \end{bmatrix} \\ & -\tfrac{1}{2}\zeta \langle P^T\rangle \begin{bmatrix} \underset{\sim}{t} \end{bmatrix}\begin{bmatrix} \underset{\sim}{\alpha} \end{bmatrix}\begin{bmatrix} \underset{\sim}{b_1} & \underset{\sim}{b_2} & \underset{\sim}{b_3} \end{bmatrix} \\ & +\tfrac{1}{2}\zeta \langle P^T\rangle \begin{bmatrix} \underset{\sim}{t} \end{bmatrix}\begin{bmatrix} \underset{\sim}{\beta} \end{bmatrix}\begin{bmatrix} \underset{\sim}{a_1} & \underset{\sim}{a_2} & \underset{\sim}{a_3} \end{bmatrix}\end{aligned} \qquad (V.26)$$

We seek to determine the strains and, as before, we must do this by first determining the displacement derivatives with respect to local element axes.

Thus we get, since P_i are two-dimensional functions of ξ, η, ζ the relations:

$$\begin{aligned}\begin{bmatrix} u_\xi & v_\xi & w_\xi \\ u_\eta & v_\eta & w_\eta \end{bmatrix} = \begin{bmatrix} \frac{\partial u}{\partial \xi} & \frac{\partial v}{\partial \xi} & \frac{\partial w}{\partial \xi} \\ \frac{\partial u}{\partial \eta} & \frac{\partial v}{\partial \eta} & \frac{\partial w}{\partial \eta} \\ \frac{\partial u}{\partial \zeta} & \frac{\partial v}{\partial \zeta} & \frac{\partial w}{\partial \zeta} \end{bmatrix} &= \begin{bmatrix} \langle \frac{\partial P^T}{\partial \xi} \rangle \\ \langle \frac{\partial P^T}{\partial \eta} \rangle \\ 0 \end{bmatrix}\begin{bmatrix} \underset{\sim}{u} & \underset{\sim}{v} & \underset{\sim}{w} \end{bmatrix} \\ & -\tfrac{1}{2}\begin{bmatrix} \zeta\langle \frac{\partial P^T}{\partial \xi} \rangle \\ \zeta\langle \frac{\partial P^T}{\partial \eta} \rangle \\ \langle P^T \rangle \end{bmatrix}\begin{bmatrix} \underset{\sim}{t} \end{bmatrix}\begin{bmatrix} \underset{\sim}{\alpha} \end{bmatrix}\begin{bmatrix} \underset{\sim}{b_1} & \underset{\sim}{b_2} & \underset{\sim}{b_3} \end{bmatrix} \\ & +\tfrac{1}{2}\begin{bmatrix} \zeta\langle \frac{\partial P^T}{\partial \xi} \rangle \\ \zeta\langle \frac{\partial P^T}{\partial \eta} \rangle \\ \langle P^T \rangle \end{bmatrix}\begin{bmatrix} \underset{\sim}{t} \end{bmatrix}\begin{bmatrix} \underset{\sim}{\beta} \end{bmatrix}\begin{bmatrix} \underset{\sim}{a_1} & \underset{\sim}{a_2} & \underset{\sim}{a_3} \end{bmatrix}\end{aligned} \qquad (V.27)$$

As before, we need the Jacobean of the transformation of x, y, z to ξ, η, ζ to determine the global derivatives.

This is easily found from V.22

$$[J] = \begin{bmatrix} \frac{\partial x}{\partial \xi} & \frac{\partial y}{\partial \xi} & \frac{\partial z}{\partial \xi} \\ \frac{\partial x}{\partial \eta} & \frac{\partial y}{\partial \eta} & \frac{\partial z}{\partial \eta} \\ \frac{\partial x}{\partial \zeta} & \frac{\partial y}{\partial \zeta} & \frac{\partial z}{\partial \zeta} \end{bmatrix} = \begin{bmatrix} \left\langle \frac{\partial P^T}{\partial \xi} \right\rangle \\ \left\langle \frac{\partial P^T}{\partial \eta} \right\rangle \\ 0 \end{bmatrix} \begin{bmatrix} \underset{\sim}{x} & \underset{\sim}{y} & \underset{\sim}{z} \end{bmatrix} + \begin{bmatrix} \zeta \left\langle \frac{\partial P^T}{\partial \xi} \right\rangle \\ \zeta \left\langle \frac{\partial P^T}{\partial \eta} \right\rangle \\ \left\langle P^T \right\rangle \end{bmatrix} \begin{bmatrix} \underset{\sim}{x}^* & \underset{\sim}{y}^* & \underset{\sim}{z}^* \end{bmatrix} \tag{V.28}$$

and as we saw previously

$$\begin{bmatrix} u v w_{xyz} \end{bmatrix} = \begin{bmatrix} \frac{\partial u}{\partial x} & \frac{\partial v}{\partial x} & \frac{\partial w}{\partial x} \\ \frac{\partial u}{\partial y} & \frac{\partial v}{\partial y} & \frac{\partial w}{\partial y} \\ \frac{\partial u}{\partial z} & \frac{\partial v}{\partial z} & \frac{\partial w}{\partial z} \end{bmatrix} = \begin{bmatrix} J^{-1} \end{bmatrix} \begin{bmatrix} u v w_{\xi \eta \zeta} \end{bmatrix}$$

So

$$\begin{bmatrix} u v w_{xyz} \end{bmatrix} = \begin{bmatrix} J^{-1} \end{bmatrix} \begin{bmatrix} u v w_{\xi \eta \zeta} \end{bmatrix}$$

$$= \begin{bmatrix} J^{-1} \end{bmatrix} \begin{bmatrix} \left\langle \frac{\partial P^T}{\partial \xi} \right\rangle \\ \left\langle \frac{\partial P^T}{\partial \eta} \right\rangle \\ 0 \end{bmatrix} \begin{bmatrix} \underset{\sim}{u} & \underset{\sim}{v} & \underset{\sim}{w} \end{bmatrix}$$

$$- \frac{1}{2} \begin{bmatrix} J^{-1} \end{bmatrix} \begin{bmatrix} \zeta \left\langle \frac{\partial P^T}{\partial \xi} \right\rangle \\ \zeta \left\langle \frac{\partial P^T}{\partial \eta} \right\rangle \\ \left\langle P^T \right\rangle \end{bmatrix} \begin{bmatrix} \underset{\sim}{t} \end{bmatrix} \begin{bmatrix} \underset{\sim}{\alpha} \end{bmatrix} \begin{bmatrix} \underset{\sim}{b_1} & \underset{\sim}{b_2} & \underset{\sim}{b_3} \end{bmatrix} \tag{V.29}$$

$$+ \frac{1}{2} \begin{bmatrix} J^{-1} \end{bmatrix} \begin{bmatrix} \zeta \left\langle \frac{\partial P^T}{\partial \xi} \right\rangle \\ \zeta \left\langle \frac{\partial P^T}{\partial \eta} \right\rangle \\ \left\langle P^T \right\rangle \end{bmatrix} \begin{bmatrix} \underset{\sim}{t} \end{bmatrix} \begin{bmatrix} \beta \end{bmatrix} \begin{bmatrix} \underset{\sim}{a_1} & \underset{\sim}{a_2} & \underset{\sim}{a_3} \end{bmatrix}$$

From this relationship, using the strain displacement relationship

$$\epsilon_{ij} = \tfrac{1}{2}\left(u_{i,j} + u_{j,i} \right)$$

we can pick out the terms required to determine [T] in the relation

$$\{\epsilon\} = [T]\{\underset{\sim}{r}\} \tag{V.30}$$

where

$$\{\epsilon\} = \begin{Bmatrix} \epsilon_{xx} \\ \epsilon_{yy} \\ \epsilon_{zz} \\ \gamma_{xy} \\ \gamma_{yz} \\ \gamma_{zx} \end{Bmatrix} \quad \text{and} \quad \{\underset{\sim}{r}\} = \begin{Bmatrix} u_1 \\ v_1 \\ w_1 \\ \alpha_1 \\ \beta_1 \\ u_2 \\ v_2 \\ \vdots \\ \beta_n \end{Bmatrix}$$

The last step is to use the relationship $\tau_{nn} = 0$, discussed earlier. To do this we must rotate the axes from the x, y, z system to a set $\bar{x}$, $\bar{y}$, $\bar{z}$ as shown in Fig. V.16.

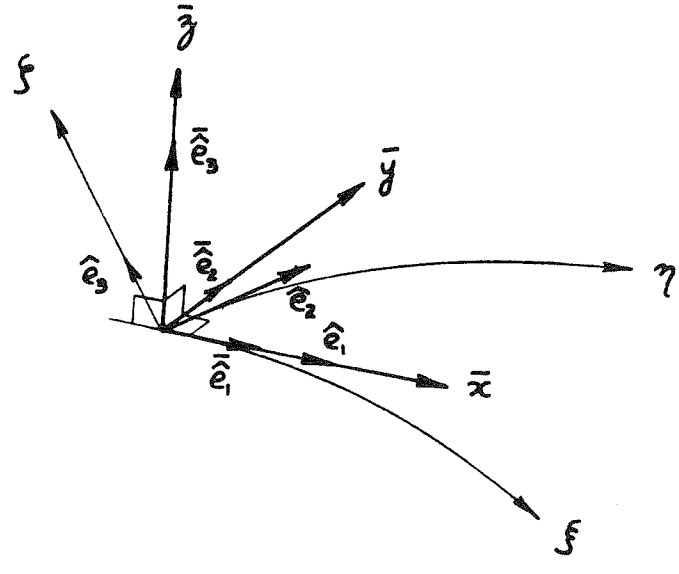

Fig. V.16 Local Axes for Strain

This is a set of mutually perpendicular axes at the point being considered. This set is determined by the local element axes ξ, η, ζ as shown in the figure. $\bar{x}$ is identical to ξ , $\bar{z}$ is perpendicular to ξ and η , $\xi, \eta, \bar{z}$ forming a right-handed set, and $\bar{y}$ is perpendicular to $\bar{x}, \bar{z}$, with, $\bar{x}, \bar{y}, \bar{z}$ forming a right handed set. The direction $\bar{z}$ will be referred to as the normal, the direction ζ as the "normal".

The rotation of coordinates to the normal axes is easily achieved using some of the previous work.

The vectors $\hat{e}_1$, $\hat{e}_2$, $\hat{e}_3$ as shown in Fig. V.16, along the local element axes, can be found by use of the relations (V.11). If $d\xi$, $d\eta$, $d\zeta$ are defined as unity

$$\begin{Bmatrix} \hat{e}_1 \\ \hat{e}_2 \\ \hat{e}_3 \end{Bmatrix} = [J] \begin{Bmatrix} \hat{\imath} \\ \hat{\jmath} \\ \hat{k} \end{Bmatrix} \qquad (V.31)$$

since the matrix of derivatives is the familiar Jacobeam, [J].

We want to define three vectors $\bar{\hat{e}}_1$, $\bar{\hat{e}}_2$, $\bar{\hat{e}}_3$, along $\bar{x}$, $\bar{y}$, $\bar{z}$, defined as we saw, by $\bar{\hat{e}}_1 = \hat{e}_1$

$\bar{\hat{e}}_3 \perp \hat{e}_1, \hat{e}_2$ $\quad$ $\hat{e}_1, \hat{e}_2, \bar{\hat{e}}_3$ forming a right hand triad

$\bar{\hat{e}}_2 \perp \bar{\hat{e}}_1, \bar{\hat{e}}_3$ $\quad$ $\bar{\hat{e}}_1, \bar{\hat{e}}_2, \bar{\hat{e}}_3$ forming a right hand triad

The direction cosines of the new normal vectors $\bar{\hat{e}}_1$, $\bar{\hat{e}}_2$, $\bar{\hat{e}}_3$, can be found from

$$\bar{\hat{e}}_3 = \hat{e}_1 \times \hat{e}_2 = \begin{aligned} &(J_{12}\, J_{23} - J_{13}\, J_{22})\,\hat{\imath} \\ &+ (J_{13}\, J_{21} - J_{11}\, J_{23})\,\hat{\jmath} \\ &+ (J_{11}\, J_{22} - J_{12}\, J_{21})\,\hat{k} \end{aligned}$$

and if we define $[\bar{J}]$ by

$$\begin{Bmatrix} \bar{\hat{e}}_1 \\ \bar{\hat{e}}_2 \\ \bar{\hat{e}}_3 \end{Bmatrix} = [\bar{J}] \begin{Bmatrix} \hat{i} \\ \hat{j} \\ \hat{k} \end{Bmatrix} \tag{V.32}$$

$$\bar{\hat{e}}_2 = \bar{\hat{e}}_3 \times \bar{\hat{e}}_1 = (\bar{J}_{32}\bar{J}_{13} - \bar{J}_{33}\bar{J}_{12})\hat{i} \; (\bar{J}_{33}\bar{J}_{11} - \bar{J}_{31}\bar{J}_{13})\hat{j} \; (\bar{J}_{31}\bar{J}_{12} - \bar{J}_{32}\bar{J}_{11})\hat{k}$$

If we now normalize the vectors $\langle \bar{J}_{11} \; \bar{J}_{12} \; \bar{J}_{13} \rangle$, $\langle \bar{J}_{21}, \; \bar{J}_{22}, \; \bar{J}_{23} \rangle$, $\langle \bar{J}_{31}, \; \bar{J}_{32}, \; \bar{J}_{33} \rangle$ we have the $[\bar{J}]$ matrix, representing direction cosines of the new axes directions, $\bar{\hat{e}}_1$, $\bar{\hat{e}}_2$, $\bar{\hat{e}}_3$.

Now the strains in the new, rotated coordinate system, are related to the global strains by

$$\bar{\epsilon}_{ns} = \bar{J}_{ni} \, \bar{J}_{sj} \, \epsilon_{ij}$$

or we can write $\{\bar{\epsilon}\} = [\theta]\{\epsilon\}$ (V.33)

Where $\{\bar{\epsilon}\}$, $\{\epsilon\}$ are the six strains (in the respective systems) written as a vector, and $[\theta]$ is constructed from $[\bar{J}]$ by appropriate multiplication.

We are now able to express the strains in the coordinate system $\bar{x}, \bar{y}, \bar{z}$ as a function of nodal displacements by

$$\{\bar{\epsilon}\} = [\theta]\{\epsilon\} = [\theta][T]\{\tau\} = [\bar{T}]\{\tau\} \tag{V.34}$$

We next consider the constitutive relation. We will consider for simplicity an isotropic linearly elastic material, for which the following holds.

$$\{\bar{\tau}\} = \frac{E}{(1+\nu)(1-2\nu)} \begin{bmatrix} 1-\nu & \nu & \nu & & & \\ \nu & 1-\nu & \nu & & & \\ \nu & \nu & 1-\nu & & & \\ & & & \frac{1-2\nu}{2} & & \\ & & & & \frac{1-2\nu}{2} & \\ & & & & & \frac{1-2\nu}{2} \end{bmatrix} \{\varepsilon\}$$

If $\tau_{\bar{z}\bar{z}} = 0$

we get the reduced relation

$$\begin{Bmatrix} \tau_{\bar{x}\bar{x}} \\ \tau_{\bar{y}\bar{y}} \\ \tau_{\bar{x}\bar{y}} \\ \tau_{\bar{y}\bar{z}} \\ \tau_{\bar{z}\bar{x}} \end{Bmatrix} = \begin{bmatrix} \frac{E}{1-\nu^2} & \frac{\nu E}{1-\nu^2} & & & \\ \frac{\nu E}{1-\nu^2} & \frac{E}{1-\nu^2} & & & \\ & & \frac{E}{2(1+\nu)} & & \\ & & & \frac{1}{k}\times\frac{E}{2(1+\nu)} & \\ & & & & \frac{1}{k}\times\frac{E}{2(1+\nu)} \end{bmatrix} \begin{Bmatrix} \epsilon_{\bar{x}\bar{x}} \\ \epsilon_{\bar{y}\bar{y}} \\ \gamma_{\bar{x}\bar{y}} \\ \gamma_{\bar{y}\bar{z}} \\ \gamma_{\bar{z}\bar{x}} \end{Bmatrix} \quad \text{(V.35)}$$

or $\{\bar{\tau}\} = [\bar{E}]\{\bar{\epsilon}\}$, with $\{\bar{\tau}\}$, $\{\bar{\epsilon}\}$ only 5 x 1 vectors now.

(Note that this differs from the relationship given by Ahmad, Irons in ref. 16, which is the relationship with the <u>strain</u> $\epsilon_{\bar{z}\bar{z}} = 0$.)

The shear modulus has been divided by a factor k for the transverse shear, to give a better representation of shear deflection

when a constant shear strain is assumed across the thickness, rather than the correct quadratic (27). The factor 6/5, applicable to a rectangular beam, will be adopted in this study.

The strain energy of the element is

$$\iiint \langle \bar{\epsilon}^T \rangle \lfloor \bar{E} \rfloor \{ \bar{\epsilon} \} \, dv = \langle \underset{\sim}{r}^T \rangle \iiint \lfloor \bar{T}^T \rfloor \lfloor \bar{E} \rfloor \lfloor \bar{T} \rfloor \, dv \, \{ \underset{\sim}{r} \}$$

So the stiffness $$[K] = \iiint [\bar{T}^T][\bar{E}][\bar{T}] \, dv$$

As for the full three dimensional element, this integral is evaluated by numerical integration with respect to the local ξ, η, ζ coordinates resulting in

$$[K] = \sum_i k_i \left[[\bar{T}^T][E][\bar{T}] \right]_i \det J \Big|_i \qquad \text{(V.36)}$$

Details of suitable numerical integration procedures will be given in Chapter VI.

The computation of nodal loads from body and surface loads follows normal procedures and will be given in detail in Chapter VI.

Finally we observe that when the element stiffnesses have been added into the full stiffness and the displacements found for the prescribed loads, we can compute the stress at any point in the shell coordinates, by use of V.35,

thus
$$\begin{aligned} \{ \bar{\tau} \} &= [\bar{E}] \{ \bar{\epsilon} \} \\ &= [\bar{E}][\bar{T}] \{ \underset{\sim}{r} \} \end{aligned} \qquad \text{(V.37)}$$

V.4 COMMENTS ON AHMAD - IRONS SHELL ELEMENTS

The family of elements described in the previous two chapters provides a useful tool for the analysis of shells falling between classical thin shells and very thick shells for which three dimensional elements are needed. Some numerical results for extreme cases of geometry are given in Chapter VIII for some simple cases. In addition a number of actual shell problems of various types are presented in Chapter VIII. These examples show that the basic assumptions are valid over a wide range of geometrical types of shell and loading conditions.

The principal weakness of the Ahmad-Irons element as described is inherent in many elements that have been derived from the relaxation of the Kirchoff hypothesis. This weakness is that, due to extraneous shear strain energy, caused by the kinematic assumptions used, the convergence is slower than desired. This effect has been noted by many authors (see Chapter IV).

We will now examine this effect as it applies to both linear (four nodal point) and quadratic (nine nodal point) elements. For simplicity we will use a one dimensional beam element to illustrate this bending behavior defect.

First, consider a linear displacement beam (Fig. V.17).

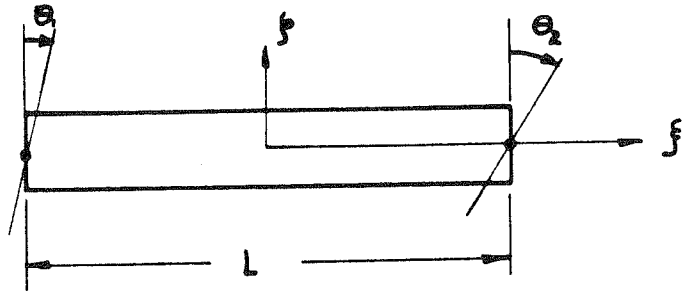

fig V.17 Linear Displacement Beam

If we exclude rigid body displacements and membrane effects from consideration, we can use the two rotations θ_1 and θ_2 at the nodes as the only degrees of freedom of the element, and we can compute the stiffness of this element, with respect to these two rotations. This can be evaluated in closed form, due to the simplicity of the element, and we obtain the stiffness K as:

$$[K] = \frac{EI}{L^2}\begin{bmatrix} L & -L \\ -L & L \end{bmatrix} + \frac{AG}{4}\begin{bmatrix} \frac{4}{3}L & \frac{2}{3}L \\ \frac{2}{3}L & \frac{4}{3}L \end{bmatrix}$$

Where EI is the bending stiffness and AG the shear stiffness.

Now consider rotations $\theta_1 = -\theta_2 = \theta$, being the correct nodal displacement for constant bending.

Then $$M_1 = \frac{EI}{L^2}(2L)\theta + \frac{AG}{4}\left(\frac{2}{3}L\right)\theta$$

$$= \frac{EI}{L}2\theta + \frac{AGL\theta}{6}$$

The first term represents the correct bending moment, the second the extraneous moment caused by the extraneous shear energy. As $L \rightarrow 0$ (with $\frac{\theta}{L}$ held constant, say)

$$M_1 \longrightarrow 2EI\frac{\theta}{L}$$ the correct value

For, say, $L = A$

$$M_1 = \frac{EA^2\theta}{6} + \frac{EA^2\theta}{12(1+\nu)}$$

representing a 50% error in moment.

The source of this error is easily seen by examining the deformation of the element. The finite element constraints imposed, result in the deformation shown in Fig. V.18, resulting in non zero shear strains as shown.

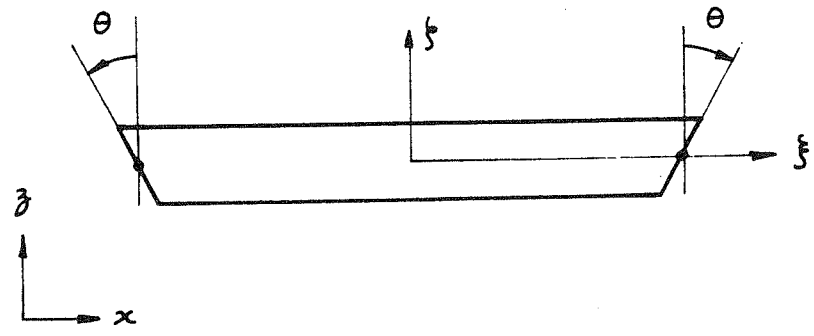

Fig. V.18 Constant Moment Nodal Rotations

We have, of course, decided against using this class of shell element, when anything other than rectangular elements are needed, but the same type of error occurs with the higher order moment condition.

Consider for simplicity a thin beam as shown in Fig. V.19.

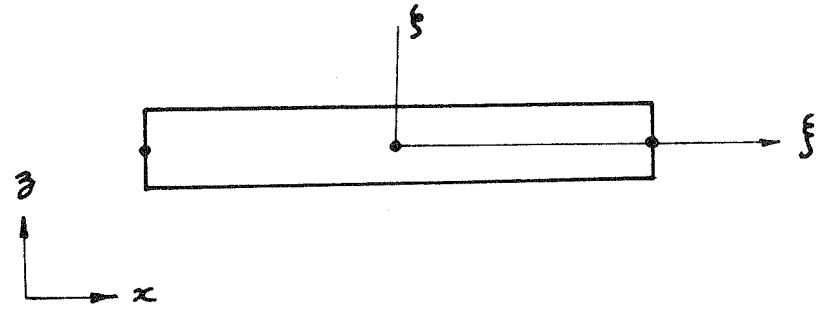

fig V.19 Quadratic Displacement Beam

This time the constant moment deformation <u>can</u> be exactly reproduced by rotations and translations of the three nodes. However, a linearly varying moment, which can be represented even by the simplest two nodal point, simple beam element, imposing Kirchhoff's Hypothesis, can't be represented by this element with three nodes. Consider nodal rotations of θ, $-\frac{\theta}{2}$, θ, as shown in Fig. V.20 which are the rotations appropriate to a linear moment condition.

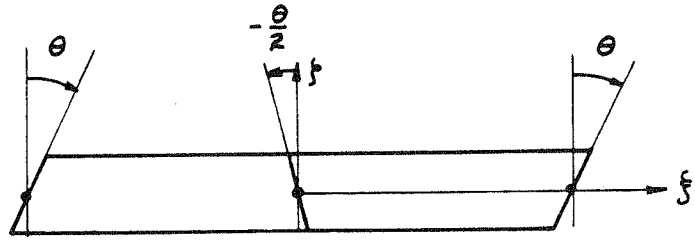

fig V.20 <u>Linear Moment Nodal Rotations (Thin Beam)</u>

The beam deforms as shown, instead of developing transverse displacements as it should. This involves shear strains which vary quadratically with x, rather than linearly, as expected for a linear moment. Once again, the excess shear energy results in a high stiffness, which slows down the convergence of the correct solution.

As an example, a cantilever beam ten times as long as its depth, gives an end displacement of 3/4 of the correct displacement, whereas a normal beam element gives the exact bending deflection.

A second weakness of the Ahmad-Irons shell element occurs when the element is curved, again resulting in a high bending stiffness

that again nevertheless converges to the correct value. Consider the quadratic element representing a thin curved beam, as shown in Fig. V.21.

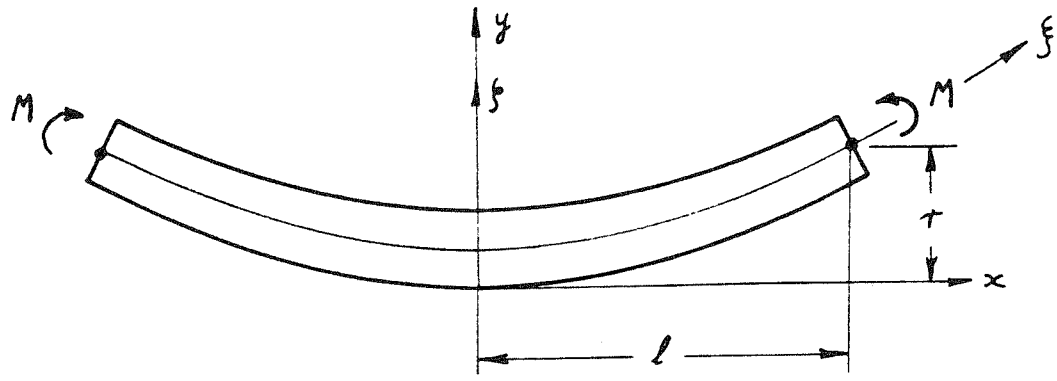

Fig. V.21 Curred Beam or Arch

We will consider a constant moment applied as shown. We will compare the displacements of the middle surface of the beam (or shell) element with that of the actual curved beam.

For simplicity, to avoid algebraic complications, we will consider a relatively flat parabola, for which we can ignore $(r/\ell)^4$ compared to 1.

We can easily show that the correct displacement pattern for the middle surface of the beam is given by:

$$u = -\frac{2M}{3EI}\frac{r}{\ell^2}x^3$$
$$v = \frac{M}{2EI}x^2 \qquad (V.38)$$

The quadratic element cannot represent the cubic power of x and hence cannot represent this simple constant moment state.

We can either appeal to mathematics or a physical argument to show that in fact this does not affect the converged solution. A more rigorous mathematical argument will be given in Chapter VI. 3, but suffice to say here, that a very small element with almost straight middle surface will not have to develop any displacement other than the normal displacement v to represent bending, and hence a curved beam formed of many such elements will satisfactorily represent constant moment in the limit.

This particular effect is far from trivial for elements of considerable curvature, giving for example a transverse deflection of less than one hundredth of the correct value, for an included angle of about 30 degrees.

VI. MODIFIED SHELL ELEMENT

VI.1 A BRIEF OUTLINE OF NUMERICAL INTEGRATION

Since this research is largely concerned with modified integration techniques for shell elements derived from isoparametric elements, a brief review of one class of numerical integration will be made at this point.

The most convenient and efficient method of integration for isoparametric elements and their related elements is the Gaussian method.

All integrations are performed with respect to each of the ξ, η, ζ coordinates between the values of -1 and +1.

We seek to find one or more points in the interval (-1, +1) for each coordinate, at which to evaluate the functions required to be integrated and, after multiplying by an appropriate weight at each point, we will add the contributions from each point to give the approximate integral. Thus if we have a function f(x,y,z) and we want to evaluate the integral over the cube bounded by x, y, z = $\pm$1 we will adopt points (x_i, y_i, z_i) called integration points and express the integral as the sum:

$$\int_{-1}^{+1}\int_{-1}^{+1}\int_{-1}^{+1} f(x,y,z)\,dx\,dy\,dz = \sum_i k_i\, f(x_i, y_i, z_i) \qquad \text{(VI-1)}$$

where k_i is the weight at point i.

We will first investigate the simpler one dimensional integral

$$\int_{-1}^{+1} f(x)\,dx = \sum_i k_i\, f(x_i) \qquad \text{(VI-2)}$$

and determine how many integration points are required for various functions f(x). We will examine only functions f(x) which are polynomials and will

express f(x) as

$$f(x) = x^j \qquad j = 0, 1, 2, \ldots$$

Thus the exact integration is given by:

$$\begin{aligned} \int_{-1}^{+1} f(x)\,dx &= \int_{-1}^{+1} x^j\,dx \\ &= \frac{x^{j+1}}{j+1}\Big|_{-1}^{+1} \\ &= \frac{2}{j+1} \quad \text{for } j \text{ even} \\ &= 0 \quad \text{for } j \text{ odd} \end{aligned} \tag{VI-3}$$

Thus for

j =	0	1	2	3	4	...
$\int_{-1}^{+1} x^j\,dx$ =	2	0	$\frac{2}{3}$	0	$\frac{2}{5}$	...

(VI-3)

Observing that the integral is zero for odd powers of x, we can immediately say that if the integration points are symmetric about x = 0 and equally weighted, then, as contributions from symmetric points cancel for odd powers of x, we achieve a zero integral as required.

Thus we may look for points as shown in Fig. VI.1 with weights k, as shown, to integrate correctly the even powers of x.

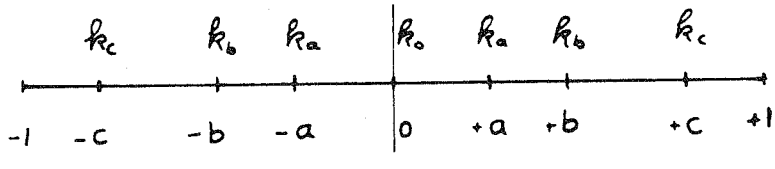

Fig. VI.1 Integration Points

Now the numerical integration of the form (VI-2) becomes

$$\int_{-1}^{+1} x^j\,dx = \sum_{i=1}^{p} k_i x_i^j$$

$$= k_0 + 2k_a + 2k_b + 2k_c + \ldots \quad \text{for } j = 0 \qquad \text{(VI-4)}$$

$$= 0 + 2k_a a^2 + 2k_b b^2 + 2k_c c^2 + \ldots \quad j = 2$$

$$= 0 + 2k_a a^4 + 2k_b b^4 + 2k_c c^4 + \ldots \quad j = 4$$

If we wish to integrate the following powers of x exactly, we must therefore satisfy, from equations (VI-3), (VI-4), the following conditions:

$$2 = k_0 + 2k_a + 2k_b + 2k_c + \ldots \quad j = 0$$

$$\frac{2}{3} = 0 + 2k_a a^2 + 2k_b b^2 + 2k_c c^2 + \ldots \quad j = 2$$

$$\frac{2}{5} = 0 + 2k_a a^4 + 2k_b b^4 + 2k_c c^4 + \ldots \quad j = 4$$

the odd powers of x, x^3, x^5 being automatically satisfied by the symmetric integration points chosen.

The numerical integration for a constant need only satisfy the first of these equations. Hence, one point, symmetrical about $x = 0$, i.e., $x = 0$ itself, and weight $k_0 = 2$, will perform the integration exactly.

If we wish to integrate x^2 <u>also</u>, we must satisfy the second equation also, the simplest way being to use two points, $x = \pm a$, and requiring as before

$$\frac{2}{3} = 2k_a a^2 \qquad \text{to integrate } x^2$$

$$2 = 2k_a \qquad \text{to integrate constant}$$

So

$$k_a = 1$$

and

$$a = \sqrt{\frac{1}{3}}$$

This is the two-point Gaussian quadrature formula.

If we wish to integrate x^4, x^2 and constant terms, we must satisfy all three equations. This can be done most simply by using three points

$$x = 0$$

$$x = \pm b$$

and we get the conditions

$$k_o + 2k_b = 2$$

$$2k_b b^2 = \frac{2}{3}$$

$$2k_b b^4 = \frac{2}{5}$$

So

$$b = \sqrt{\frac{3}{5}}$$

$$k_b = \frac{5}{9}$$

$$k_o = \frac{8}{9}$$

So the following integration schemes will integrate all powers of x up to the following powers (and trivially all odd powers)

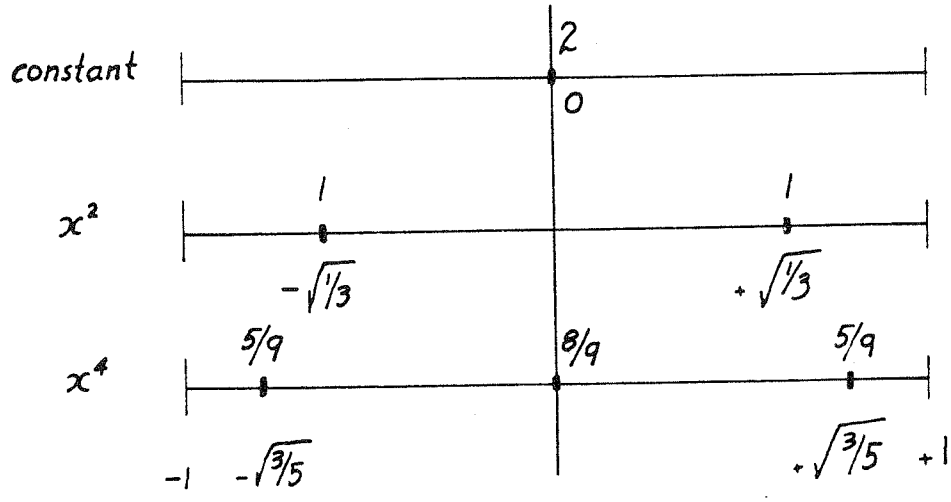

Fig. VI.2 Gaussian Quadrature Constants

We will move now to the consideration of area integrals of the type

$$\int_{-1}^{+1}\int_{-1}^{+1} f(x,y)\ dx\ dy$$

Again we will consider polynomials, now of the type $x^i y^j$

$$\int_{-1}^{+1}\int_{-1}^{+1} f(x,y)\ dx\ dy = \int_{-1}^{+1}\int_{-1}^{+1} x^i y^j\ dx\ dy$$

$$= \int_{-1}^{+1} x^i\, dx \times \int_{-1}^{+1} y^j\, dy \qquad \text{(VI-5)}$$

$$= \frac{2}{i+1} \times \frac{2}{j+1} \quad \text{for both } i,j \text{ even}$$

$$= 0 \quad \text{for either } i,j \text{ odd}$$

This separation of variables indicates that we can use separate integration schemes in each direction, multiplying the weighting factors from each direction to get the new weights. We get various integration grids, depending on the polynomials we want to integrate exactly, some examples of which are given in Fig. VI.3.

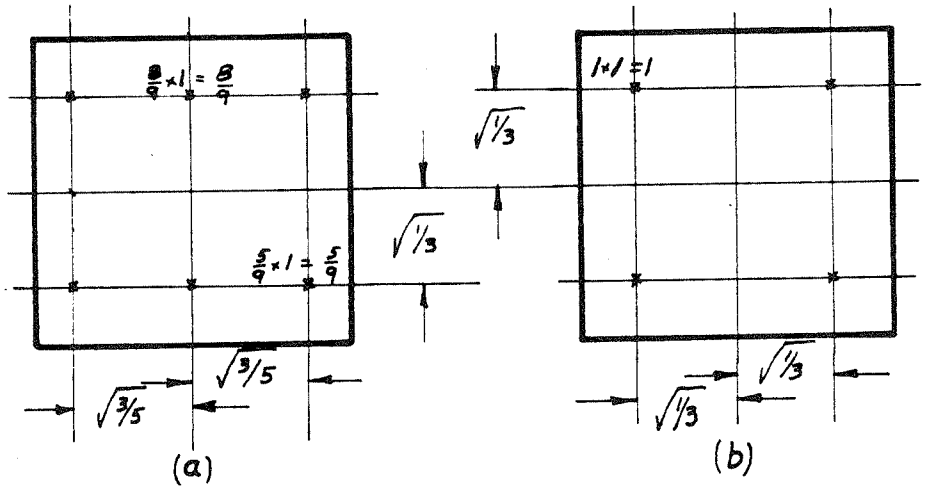

Fig. VI.3 Typical Integration Grids

From the foregoing, we see that (a) will integrate all polynomial terms up to x^4y^2 and (b) up to x^2y^2, both including all odd powers of x or y trivially.

For volume integrals of polynomials of the type

$$x^i y^j z^k$$

the integration is similarly performed with a three dimensional grid and weights that are the product of the weights from each of the three directions.

To conclude this section we will consider one last integration scheme. In a later chapter, we will wish to integrate all terms up to x^4y^4 using, not the 3 x 3 grid, but a grid composed of the points shown in Fig. VI.3(a),(b) (including the first rotated ninety degrees). This results in the grid shown in Fig. VI.4.

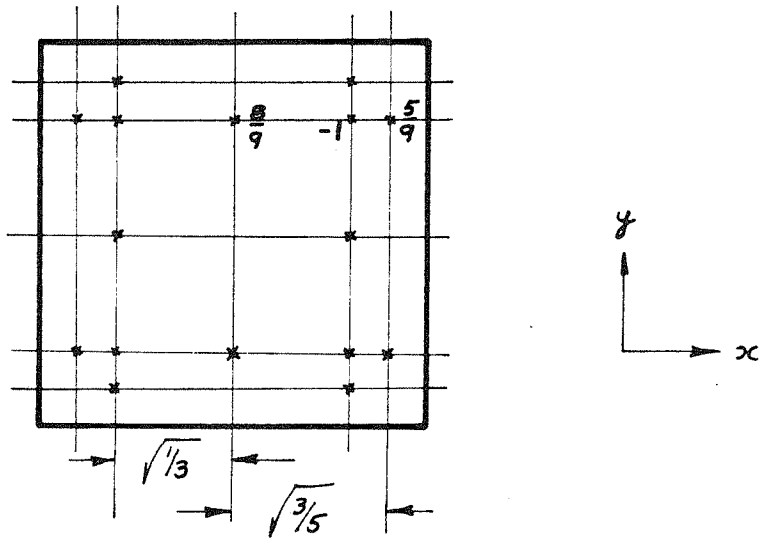

Fig. VI.4 Alternate Integration Scheme for x^4y^4

By a process similar, in two dimensions, to that already given, we can derive a set of conditions for each term x^iy^j involving the (given) positions of the points, and the (unknown) weights. We easily can show that the weights shown in Fig. VI.4 will correctly integrate all terms up to x^4y^4 as desired.

VI.2 SYMMETRIC NUMERICAL INTEGRATION FOR SHELL ELEMENTS

The formation of the stiffness of a shell (and the calculation of nodal loads from temperature, body forces, etc.) requires the volume

integration of certain functions. We will distinguish between the integration in the "normal" direction ζ, and the in-plane integration in the ξ, η coordinates.

For a flat plate element the transverse shear strains are constant through the thickness, while in-plane strains vary linearly through the thickness.

The integration used to form the stiffness is of the form:

$$\iiint \epsilon^T E \epsilon \; dx\, dy\, dz$$

so $\epsilon^T E \epsilon$ represents at most a quadratic function of the "normal" coordinate ζ. This means that a two-point integration is exact in the ζ direction.

However, a curved shell has a non-linear strain distribution across the thickness, the degree of non-linearity depending on the thickness of the shell compared with the radii of curvature. So a higher order numerical integration is needed to give exact integration. However, numerical examples on even a quite thick arch (see Chapter VIII) gave quite acceptable results, so, since the formation time for the element stiffness varies with the number of integration points, it is considered that two-point integration in the coordinate ζ is sufficient for anything except the most severe curvature, when other assumptions made may be invalid, anyway.

The rest of this chapter will be devoted to a discussion of the integration in the ξ, η directions and we will assume two-point integration in the ζ direction.

The first question to concern us is what numerical integration grid should be used to guarantee convergence of the solution to the correct solution. We will restrict our attention to the nine nodal point element described in Chapter V.2 unless noted otherwise (Fig. (VI-5).

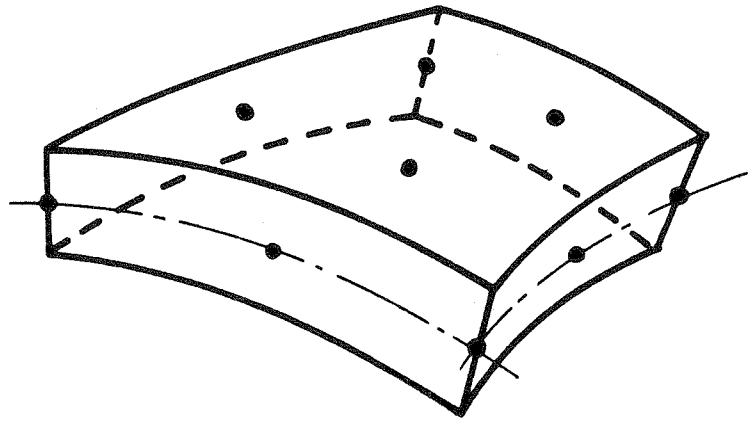

Fig. VI.5 Shell Element Adopted

We showed in Chapter V.2 that a flat, finite-sized element of this type was able to represent constant bending exactly. Implicit in the earlier discussion was the assumption that the stiffness matrix was formed by exact integration from the strain displacement relations. Due to the presence of the inverse jacobean, which represents terms with polynomial denominators, the strain variation within the element is not, in general, a simple polynomial function. (An exception is the rectangular plate element to be discussed further below.) Hence, no finite number of integration points in the ξ , η coordinates will give the exact stiffness.

So we must ask the question: What is the minimum integration grid to guarantee convergence of an arbitrary plate element? (A small enough shell element tends geometrically towards a plate element, so

except for effects related to integration in the normal direction ζ, the following remarks apply to shell elements.)

Consider an arbitrary quadrilateral plate element. We will look for the lowest order integration in the ξ, η coordinates that can integrate a constant function exactly, over the element. This integration scheme will then give a stiffness that will at least satisfy the constant strain states exactly, and hence the solution will converge to the correct solution as the mesh of elements is refined. This fundamental capability of the integration scheme to be adopted will be referred to often in the following sections.

The element to be examined consists of eight external nodes and one interior node. If the position of the interior node, instead of being arbitrary, is defined to be at the origin of the ξ, η coordinates defined by an eight nodal point expansion, then the coordinate transformations involving nine nodes and nine interpolation functions (V-18) (see Chapter V.1) reduces to the eight nodal point transformation (V-20).

To integrate a constant, say 1, over the element, we get, ignoring the ζ integration discussed earlier,

$$\iint_{\text{element}} dx\, dy = \int_{-1}^{+1}\int_{-1}^{+1} \det J\, d\xi\, d\eta$$

Now if we re-examine the relations (V-20) for p_i, we see that the coordinates x, y, z are functions of some or all of the following powers of ξ, η.

$$1,\ \eta,\ \eta^2,\ \xi,\ \xi\eta,\ \xi\eta^2,\ \xi^2,\ \xi^2\eta$$

so $\frac{\partial x}{\partial \xi}$, $\frac{\partial y}{\partial \xi}$, $\frac{\partial z}{\partial \xi}$ contain $1\ \ \eta\ \ \eta^2\ \ \xi\ \ \xi\eta$

and $\frac{\partial x}{\partial \eta}$, $\frac{\partial y}{\partial \eta}$, $\frac{\partial z}{\partial \eta}$ contain $1\ \ \eta\ \ \xi\ \ \xi\eta\ \ \xi^2$

Now the Jacobean

$$J = \begin{bmatrix} \frac{\partial x}{\partial \xi} & \frac{\partial y}{\partial \xi} & \frac{\partial z}{\partial \xi} \\ \frac{\partial x}{\partial \eta} & \frac{\partial y}{\partial \eta} & \frac{\partial z}{\partial \eta} \\ \frac{\partial x}{\partial \zeta} & \frac{\partial y}{\partial \zeta} & \frac{\partial z}{\partial \zeta} \end{bmatrix}$$

and for a plate with ζ in the same direction as z this becomes

$$J = \begin{bmatrix} \frac{\partial x}{\partial \xi} & \frac{\partial y}{\partial \xi} & 0 \\ \frac{\partial x}{\partial \eta} & \frac{\partial y}{\partial \eta} & 0 \\ 0 & 0 & const. \end{bmatrix}$$

So

$$det\ J = const. \times \left(\frac{\partial x}{\partial \xi} \frac{\partial y}{\partial \eta} - \frac{\partial x}{\partial \eta} \frac{\partial y}{\partial \xi} \right)$$

This is of order

$$(1 + \eta + \eta^2 + \xi + \xi\eta)(1 + \eta + \xi + \xi\eta + \xi^2)$$

$$= 1 + \eta + \eta^2 + \xi + \xi\eta + \xi\eta^2 + \xi^2 + \xi^2\eta + \xi^3 + \xi^3\eta + \eta^3 + \xi\eta^3$$

In order to integrate $\det J$ correctly, we see that we must integrate all the above terms exactly. We will adopt an integration scheme symmetric in ξ, η about the origin, hence any odd powers are automatically exactly integrated.

We are left with $1 + \eta^2 + \xi^2 + \xi^2\eta^2$ to be integrated.

Referring back to the discussion on Gaussian integration, in Chapter VI.1, we see that a two-point integration point is needed in each direction. So an absolute minimum integration grid is 2 x 2 points in the ξ, η directions.

We now know that the strain energy from nodal displacements corresponding to constant strain states will be correctly integrated, so the correct displacements are a possible solution to a problem that should result in constant strain.

However we must ask, is it possible that other displacements are possible solutions. This would mean that the stiffness formed from this low order integration would be singular. So we ask, is there a nodal displacement pattern that, using the minimum 2 x 2 integration grid, results in no computed strain energy? If there is, this set of nodal displacements will result in zero strain at the integration points.

To examine this question, we will consider a square plate element for simplicity, oriented as shown in Fig. VI.6. Deformation of the two types shown will result in no strains ϵ_{xx}, ϵ_{yy} at the integration points shown and when combined, will give no strain γ_{xy} either.

So a singular matrix would result, demonstrating the possibility of this mode of deformation occurring as a membrane or bending mode. So we will have to use a higher order integration grid for the in-plane direct strains ϵ_{xx}, ϵ_{yy}, so that neither of these two deformation modes is a zero energy mode. A 3 x 3 grid is sufficient to achieve this.

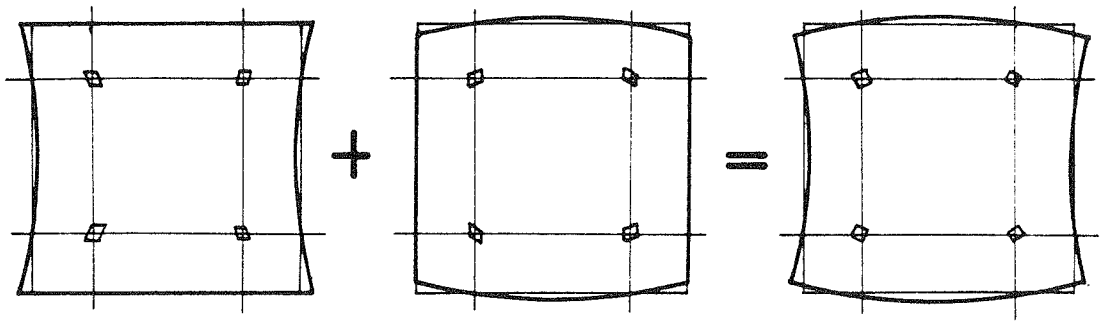

Fig VI.6 Zero Energy State for Membrane Action 8-node Element

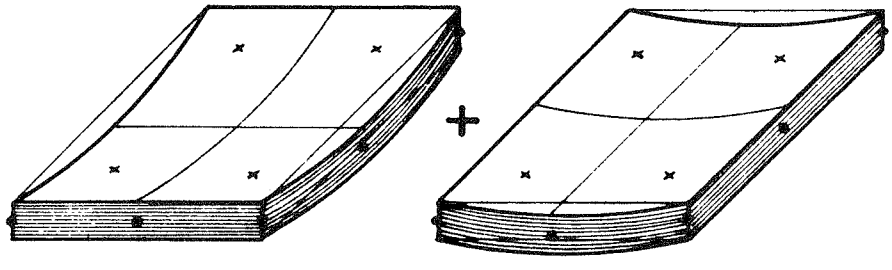

$w = -\frac{1}{3} y^2$ $\qquad$ $w = -\frac{1}{3} x^2$

$\frac{\partial w}{\partial y} = -\frac{2}{3\sqrt{3}}$ at int. pts. $\qquad$ $\frac{\partial w}{\partial x} = -\frac{2}{3\sqrt{3}}$ at int. pts

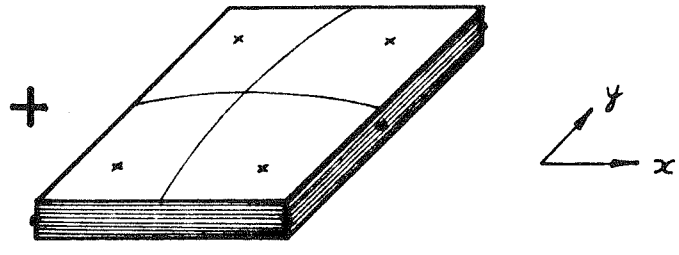

$$w = \tfrac{1}{2}(1-x^2)(1-y^2)$$

$$\frac{\partial w}{\partial y} = \frac{\partial w}{\partial x} = +\frac{2}{3\sqrt{3}} \quad \text{at int. pts.}$$

fig VI.7 Zero Energy State for Transverse Displacements. 8-node Element

A similar zero energy mode can occur with displacements normal to the surface also. The three types of displacements shown in Fig. VI.7, each resulting in transverse shear strains only, can be combined to give zero shear strain at the 2 x 2 grid points. Thus again the lowest acceptable symmetric integration grid is 3 x 3.

For completeness of this discussion we observe that a similar phenomenon occurs for the square linear displacement element (Fig. VI.8). In this case the determinant is formed by a product of linear functions

$$(1 + \xi)(1 + \eta).$$

So as one point integration is sufficient to integrate linear terms in ξ, η exactly, a one-point integration is sufficient to integrate a constant over the element. However, zero energy modes shown in Fig. VI.8 result from this one-point integration, and a 2 x 2 integration grid is the lowest symmetric integration grid to avoid singularities.

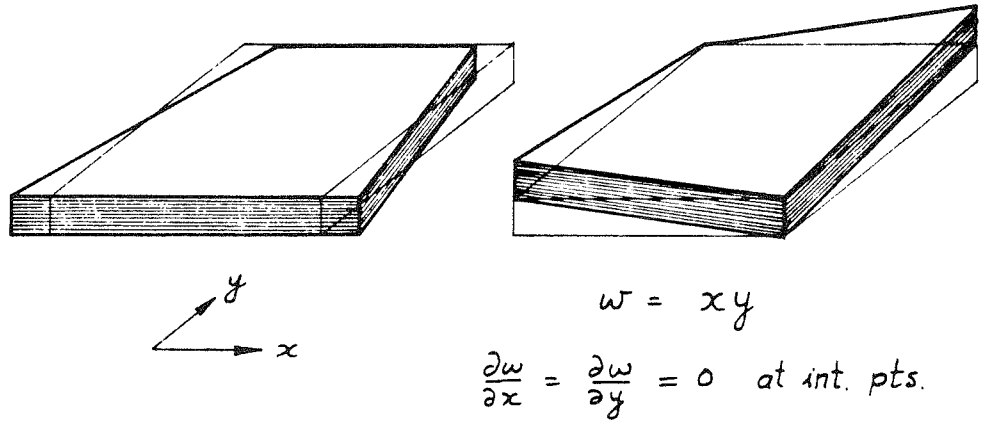

fig VI.8 Bending & Shear Modes for Linear Element

VI.3 MODIFIED INTEGRATION PROCEDURES

Having examined in Chapter V the characteristics, strengths and weaknesses of the Ahmad-Irons series of shell elements, and having discussed in Chapter VI.2 the requirements of the numerical integration grid to ensure convergence, we will now consider the choice of integration procedure to improve the efficiency of the solution. Since we are not altering the basic assumptions, the converged solution will be unaltered.

To examine this question, we will look at the bending and membrane effects separately, by discussing first the degenerate shell represented by a beam or arch, and secondly that represented by a flat plate with membrane stresses.

VI.3(a) Modified Integration for Arch or Beam Elements

The linear displacement arch element, a degenerate form of the linear displacement shell element is shown in Fig. V.17. This element is described by two nodes, each of which has two displacements u, v and a rotation θ as shown.

In the discussion of the Ahmad-Irons elements in Chapter V.4 we described the over-stiffness of a finite-sized element which results from the extraneous shear energy included. For this element the nodal displacements appropriate to constant moment are shown in Fig. V.18. Not only is the constant bending condition violated for a finite-sized element, but the transverse shear is able to vary linearly with x.

In a report in January 1969 (28), Doherty, Wilson and Taylor discussed this problem for the four nodal point Irons membrane element. They recognized that the "bending" mode was too stiff due to shear energy

and that a better element could be formed in which the shear energy was integrated by a one-point numerical integration at the center of the element, while maintaining the usual 2 x 2 integration on the stresses τ_{xx}, τ_{yy}. Consider the deformation modes shown in Fig. VI.9.

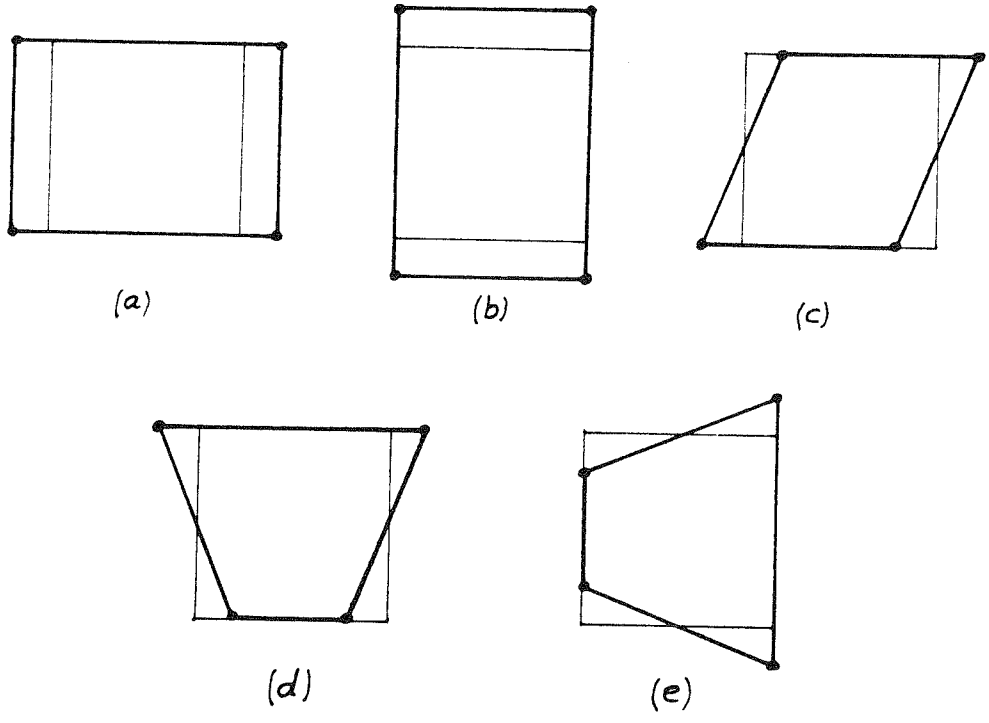

Fig. VI.9 Deformations of Linear Displacement Element (Membrane Strain)

We can see that in the two "bending" modes in this figure, (d), (e), the shear strains, while non-zero over most of the element, are zero at the center, and hence if a one-point integration is used, no shear energy results. This formulation is orientation-dependent and a local axis

system was recommended along which the strains are defined, to optimize the effect for all orientations of the element.

An equivalent process can be adopted for the arch or beam element, with only mid side nodes as shown (Fig. V.17). We note that the shear strain defined in local coordinates is zero at $\xi = 0$, for the constant bending mode (Fig. V.18). Therefore, since $\xi = 0$ is the position required for a one-point integration, if we adopt a one-point integration procedure for γ_{zx} in the ξ direction, we will get no extraneous shear energy for pure bending.

For the constant shear strain mode (Fig. VI.9(c)) the shear strain reproduced by the element is also constant in ξ and so again one-point integration is sufficient to give this deformation correctly.

Since the shear energy contribution to the bending mode is now zero, the "effective" deformation can be thought of as being the true bending deformation (Fig. VI.10).

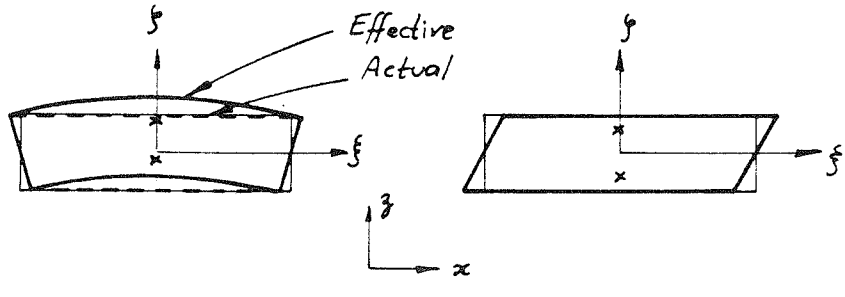

Fig. VI.10 Deformation Modes for Linear Element

We saw previously for the linear displacement shell element that a one-point integration in ξ was sufficient to guarantee convergence, and that the two-point integration was only needed to avoid the singularity due to the shearing mode of Fig. VI.8, which is not possible in the degenerate arch element. So a one-point integration in the ξ direction may be used for both ϵ_{xx} and γ_{zx} if desired.

This simple change in the integration procedure results in a dramatic change in the efficiency of the solution.

The integration in the "normal" direction is dictated by the thickness to radius of curvature ratio. As stated before a two-point integration gives satisfactory results for even quite severe examples.

For the reasons given in Chapter V.2, the quadratic displacement, rather than the linear displacement shell element will be used as a basic element in later work. The degenerate beam or arch element resulting is shown in Fig. VI.11.

This element suffers from a similar defect in transverse shear energy, as was pointed out in Chapter V.4. Although an initially flat element is able, due to its middle node, to represent a constant moment exactly, this is actually quite inefficient compared with a classical beam element which, with one less node, can reproduce linear moments exactly (admittedly without shear deformations). The shear strains developed by this element vary quadratically with x, an unnecessarily high order variation for a secondary effect.

Let us consider a beam element subjected to displacements appropriate to a beam with equal and opposite moments applied to each end (Fig. VI.11)

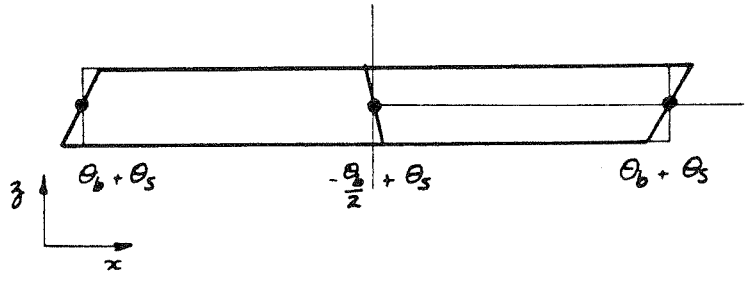

Fig. VI.11 Linear Moment Nodal Rotations

θ_b represents the rotations due to bending, and θ_s, the added rotations due to shear deflections.

We observe that, due to the quadratic variation of u with x, the in-plane strain varies linearly from end to end, reproducing correctly the in-plane strains for this condition.

However the transverse shear strain γ_{zx} varies as shown in Fig. VI.12

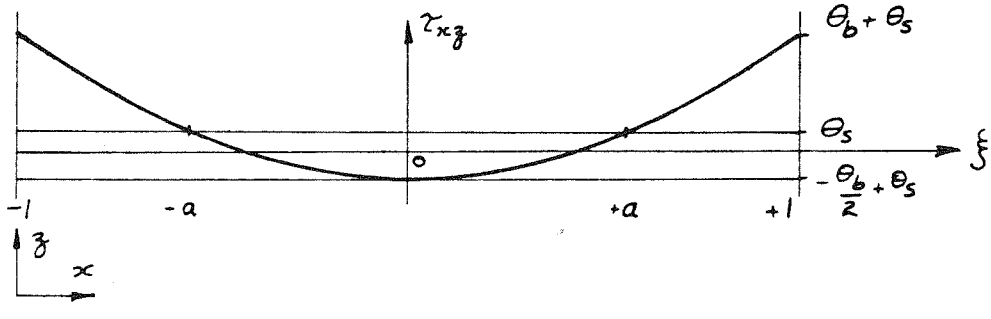

fig VI.12 Shear Strain Variation in Quadratic Element under Linear Moment Condition

We see that the shear strain is the correct value, θ_s , at only two points, ± a, as shown. The parabola representing shear strain is defined by

$$\gamma_{zx} = \left(-\frac{\theta_b}{2} + \theta_s \right) + \left(\frac{3\theta_b}{2} \right) \cdot \xi^2$$

We solve for a from

$$-\frac{\theta_b}{2} + \theta_s + \frac{3\theta_b}{2} a^2 = \theta_s$$

and get $$a = \pm\sqrt{\frac{1}{3}}$$

These are precisely the positions of the two-point integration scheme. If we integrate the shear strain energy at these points, the energy computed by the integration is that for a full linear moment (+ shear) so the element is now capable of representing this higher order bending mode.

We have already seen that a two-point integration is sufficient to guarantee convergence. The singularity problem of the shell deformation does not affect the arch, so we can adopt the two-point integration in the ξ direction for the shear strain γ_{zx} , to speed up convergence to the desired solution.

Again we will adopt a two-point integration in ζ .

The effect of the lower order integration procedure is to allow shear strain energy due only to the actual shear deformation of the beam, which effectively allows a deformation as shown in Fig. VI.13 to take place.

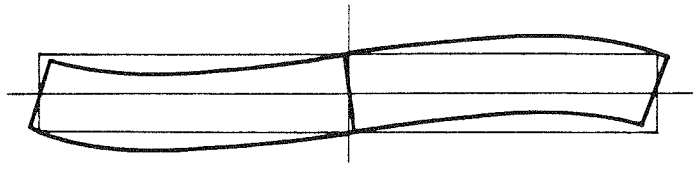

Fig. VI.13 Effective Deformation for Linear Moments

In Chapter V.4 we drew attention to another defect of the quadratic element that occurs when it is curved. The quadratic element is unable to reproduce the cubic variation with x (or ξ) of the displacement u, for the constant moment condition. See Fig. V.21

The correct expression for u (for a shallow arch) is

$$u = -\frac{2M}{3EI}\frac{\tau}{\ell^2}x^3 \qquad \text{(VI.6)}$$

while the best the finite element can do is the linear form

$$u = -\frac{2M}{3EI}\tau x \qquad \text{(VI.7)}$$

Which satisfies the nodal displacements at all nodes. The finite element does, however, give the correct expression for v, namely

$$v = \frac{M}{2EI}x^2 \qquad \text{(VI.8)}$$

Fig. VI.14 shows the relative displacements of two neighbouring points P_1, P_2 on the curved arch.

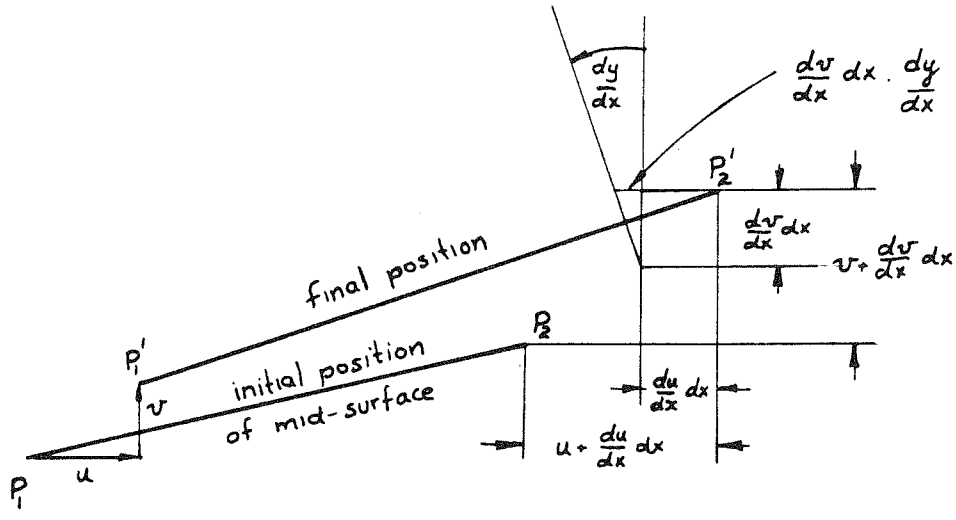

Fig. VI.14 Deflection of Element of Arch

From this diagram, we see that for flat arches, the in-plane strain at the mid-surface is

$$\epsilon_{\bar{x}\bar{x}} = \frac{du}{dx} + \frac{dv}{dx}\frac{dy}{dx} \qquad \text{(VI.9)}$$

Substituting the correct relation VI.6 (and VI.8) we see that the in-plane strain = 0 as it should be, but using VI.7 (and VI.8) for the finite element, we get a membrane strain of

$$\epsilon_{\bar{x}\bar{x}} = \frac{2M\tau}{EI}\left(-\frac{1}{3} + \frac{x^2}{\ell^2}\right)$$

As the size of the element decreases $\tau \longrightarrow 0$ and this error term $\longrightarrow 0$, confirming a less rigorous statement made in Chapter V.4. However, if a high order integration (greater than two points) is used

for the strain energy due to $\epsilon_{\bar{x}\bar{x}}$, we will get a contribution from this extraneous strain energy, resulting in a stiffness that is too high, and hence in rather slow convergence.

Again we seek to annul this effect by determining at what point the extraneous membrane strain vanishes.

This is at

$$\left(-\frac{1}{3} + \frac{x^2}{\ell^2} \right) = 0$$

or

$$\xi \left(= \frac{x}{\ell} \right) = \pm\sqrt{\frac{1}{3}}$$

These are again the two point integration positions, that were used to benefit the element integration previously.

So we see by integrating the in-plane local strain $\epsilon_{\bar{x}\bar{x}}$ also, at only two points in the ξ direction, we improve the element so that it will now be able to deform in a pure constant bending mode, exactly.

The algebra appropriate to greater initial curvature is much more involved than that described here, but the above improvement applies at least qualitatively for this condition.

So we see that maximum benefit is to be gained by using the two point integration in ξ for both strains $\epsilon_{\bar{x}\bar{x}}$ and $\gamma_{\bar{z}\bar{x}}$.

For completeness we should note that the other vital constant strain state that we must satisfy is the membrane state of deformation. This condition is satisfied exactly for any integration rule for $\epsilon_{\bar{x}\bar{x}}$ (greater than 1 of course). The exact arch displacements (for a shallow arch) are

$$u = \frac{M}{EI} x$$

$$v = \frac{M}{EI} \frac{r}{\ell^2} x^2$$

Both of these can be represented exactly by the finite element, and integrated exactly by any integration scheme, with greater than one integration point.

The preceding examination of bending and in-plane deformations of straight and curved beams leads us to draw a conclusion regarding the use of the Ahmad-Irons elements in axisymmetric problems. When the shell is axisymmetric, the problem can be reduced to a one-dimensional problem using the same basic assumptions described in Chapter V, sections 2, 3. (16) see Fig. VI.15. The most efficient element using quadratic displacement assumption will thus use an integration scheme involving only two points in the ξ direction, for both the in-plane strain $\epsilon_{\bar{x}\bar{x}}$ and the shear strain $\gamma_{\bar{z}\bar{x}}$.

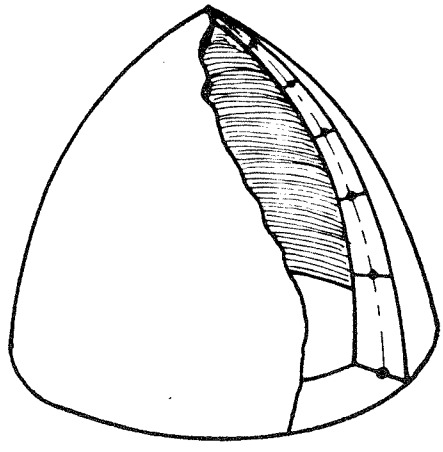

Fig. VI.15 Axisymmetrix Shell Element

VI.3(b) Modified Integration of Membrane Strains

The foregoing two sections have laid down;

1) certain minimum integration procedures for shell elements to guarantee convergence

2) desirable integration procedures for certain strain energy components for the degenerate arch element, to speed up convergence.

We will now look at one further facet of the integration method before attempting to set up a desirable integration scheme for general shell elements.

In most shells a considerable amount of energy (frequently the major amount) goes into membrane straining. It is desirable, therefore, that the shell elements behave as well as possible under these conditions.

We have referred to work by Doherty, Wilson and Taylor (28) who suggested that an improvement could be made to a four nodal point membrane element by integrating the shear energy with a one point scheme only. (2 x 2 integration is normally used and actually this is the minimum that will integrate all the terms that arise in integrating the shear energy in a rectangle.) This allows a lower energy for the sometimes important "bending" mode (Fig. VI.9(d), (e)). Johnson (29) and many others achieve this same result in a quadrilateral formed from four triangles, by using linear strain variation within the sub-elements.

This improvement is easy to include in the square linear shell element including bending, and is done similarly by using only one integration point for the in-plane shear strain. This is sufficient to guarantee convergence and does not introduce any singularities, so constitutes an acceptable and desirable improvement.

The success of the modified linear arch element integration and the similar quadratic arch element modification, leads us to suspect that an equivalent process may exist for the membrane shear integration of the nine nodal point quadratic displacement shell element. We would presume that a 2 x 2 integration for this membrane shear strain energy would be more accurate than a 3 x 3 integration (which is the minimum that will exactly integrate all terms of the shear energy for a rectangle .) This hypothesis is confirmed, numerically, by examples in Chapter VIII.

VI.3(c) An Improved Integration Scheme for Shell Elements

We will now summarize the findings to date:

1) There exists, for either the linear or quadratic displacement shell element discussed, a minimum integration in ξ, η that will integrate a constant strain state correctly and hence that will gurantee convergence.

2) The minimum integration grid is not sufficient to actually use, since a singular matrix results from this grid. We must therefore use a higher order integration for some strain components, at least,to get a non-singular matrix.

3) The higher order integration resulting from 2) is detrimental to efficiency if used on the transverse shear strains for either the linear or quadratic element, or if used on the membrane strains of the curved arch element, the integration resulting from 1) being superior.

4) The desirable membrane shear integration is that occurring in 1.

These are incompatible requirements, unless we break up the integration procedure so that each strain energy component is integrated over its own grid of integration points.

Re-examining the deformation modes of the nine-point element that cause the singularities in 2) (see Fig. VI.6) we observe that if we were to integrate ϵ_{xx} by a 2 x 3 grid and ϵ_{yy} by a 3 x 2 grid in ξ, η respectively, these deformations would now have non-zero strain energy, so that the resultant deformation would no longer represent a zero energy state. A similar conclusion can be made regarding the transverse shear deformation that causes a singularity (Fig. VI.7). If the transverse shear energy from γ_{zx} is integrated by a 2 x 3 grid and that from γ_{zy} by a 3 x 2 grid, the strains resulting from the three deformations shown in Fig. VI.7 no longer cancel, and the singularity is avoided.

We see that the lower order integration procedures suggested for ϵ_{xx} and γ_{zx} give just the same integration as our arch analysis suggested was desirable. The same of course holds for ϵ_{yy} and γ_{zy}.

Similar conclusions can be drawn for the rectangular linear displacement shell element. In each case the 3 x 2 integration grid is replaced by a 2 x 1 grid, and the 2 x 3 by a 1 x 2 grid.

If we denote the number of integration points in each direction needed to integrate a constant exactly, in an element of arbitrary shape, by n_c then we should integrate the following terms with the following grids:

term	grid	quadratic element	linear element
$\epsilon_{\bar{x}\bar{x}}\ \bar{E}_{11}\ \epsilon_{\bar{x}\bar{x}}$	$n_c \times (n_c + 1)$	2×3	1×2
$\epsilon_{\bar{y}\bar{y}}\ \bar{E}_{22}\ \epsilon_{\bar{y}\bar{y}}$	$(n_c + 1) \times n_c$	3×2	2×1
$\epsilon_{\bar{x}\bar{x}}\ \bar{E}_{12}\ \epsilon_{\bar{y}\bar{y}}$	$n_c \times n_c$	2×2	1×1
$\gamma_{\bar{x}\bar{y}}\ \bar{E}_{33}\ \gamma_{\bar{x}\bar{y}}$	$n_c \times n_c$	2×2	1×1
$\gamma_{\bar{y}\bar{z}}\ \bar{E}_{44}\ \gamma_{\bar{y}\bar{z}}$	$(n_c + 1) \times n_c$	3×2	2×1
$\gamma_{\bar{z}\bar{x}}\ \bar{E}_{55}\ \gamma_{\bar{z}\bar{x}}$	$n_c \times (n_c + 1)$	2×3	1×2

Table V.1

In establishing the rules for convergence, we were concerned with an arbitrary-shaped shell element, but in the subsequent discussion of desirable integration grids we discussed only arch elements which are in effect shell elements with a rectangular shape, and actual rectangular elements. If the element is non-rectangular, the foregoing integration grids will not, in general, lead to the higher order moment capability exactly, and the departure will be more pronounced as the element shape becomes "less rectangular." However, having satisfied the requirements of convergence for an arbitrarily shaped element, we need have no fear that the solution will not converge to the correct solution, but it may converge more slowly than a mesh of rectangles.

For a non-rectangular element there is, however, a situation that should be guarded against (at least in theory). If as the finite element mesh is refined, the element edges $\eta = 1$ and $\eta = -1$ do not approach parallel directions then a small error is introduced in the converged solution. This is because the direction of the axes along which the local strains are measured are defined as being along the axis locally and perpendicular to it. If the direction of this axis varies from integration point to integration point then the energy of a particular strain component will be slightly misrepresented. This does not occur when all strain energy components are integrated together, as in the usual isoparametric formulation, since, regardless of the directions chosen at an integration point the total strain energy is being correctly sampled.

This means that for highest accuracy, we should arrange our finite element mesh so that at least two sides of all elements are approximately parallel, skew boundaries being fitted by triangular elements.

To conclude this section we will briefly examine, for the simpler linear displacement shell element only, the effective displacements that the modified integration procedure produces. (See effective displacements for beams, Fig. VI.10, Fig VI.13). Whereas for the beam, a simple unique, higher order, bending deformation resulted, we now find that displacement incompatibilities occur, either within or between elements, for most nodal displacements. For the essential constant strain conditions, however, the compatibilities are restored, as required by Zienkiewicz' weakened compatibility requirement (see Chapter 1.3).

The first example (Fig. VI.16) shows an initially square element subjected to equal and opposite rotations of two nodes, as could occur in some bending problem. Referring to the previous table giving the integration scheme for a linear displacement element, we see that at the points at which γ_{xy}, γ_{yz}, γ_{zx}, and ϵ_{yy} are computed, these strains are all zero and the values of ϵ_{xx} at the two points at which ϵ_{xx} is computed indicate ϵ_{xx} varies linearly with z and y. Thus the effective displacement pattern is that for which $\gamma_{xy} = \gamma_{yz} = \gamma_{zx} = \epsilon_{yy} = 0$ and $\epsilon_{xx} = z\left(\frac{1-y}{2}\right)$.

The strain compatibility equations of the theory of elasticity (e.g. 30) require, among other relations:

$$\frac{\partial^2 \epsilon_{xx}}{\partial y \, \partial z} = \frac{\partial}{\partial x}\left(-\frac{\partial \epsilon_{yz}}{\partial x} + \frac{\partial \epsilon_{zx}}{\partial y} + \frac{\partial \epsilon_{xy}}{\partial z}\right)$$

This is violated, so the effective displacement pattern is not a compatible one.

The second example is that of two elements, as shown in Fig. VI.17 with equal and opposite in-plane displacements given to the two nodes as shown. Following the argument in Chapter VI.3(a) the effective displacement is as shown in the figure, separation occuring along the join of the two elements.

When nodal displacements appropriate to constant strain conditions are imposed, both these types of incompatibilities vanish.

It would appear at first that the use of the grid recommended for the quadratic element would lead to an increase in the time required to compute the element's stiffness, since it has 16 integration points instead of the 9 for the symmetric 3 x 3 scheme. However, the number

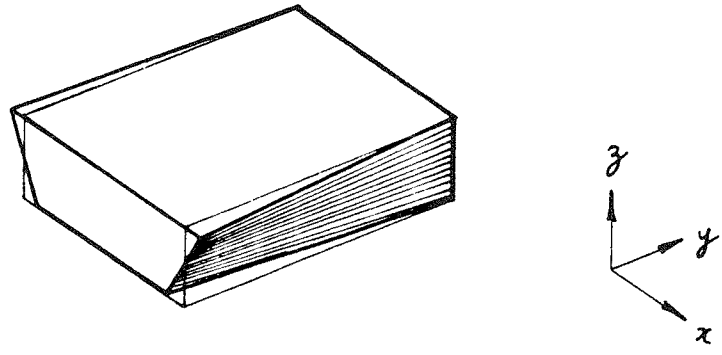

Fig. VI.16 Incompatible Displacements Within Element

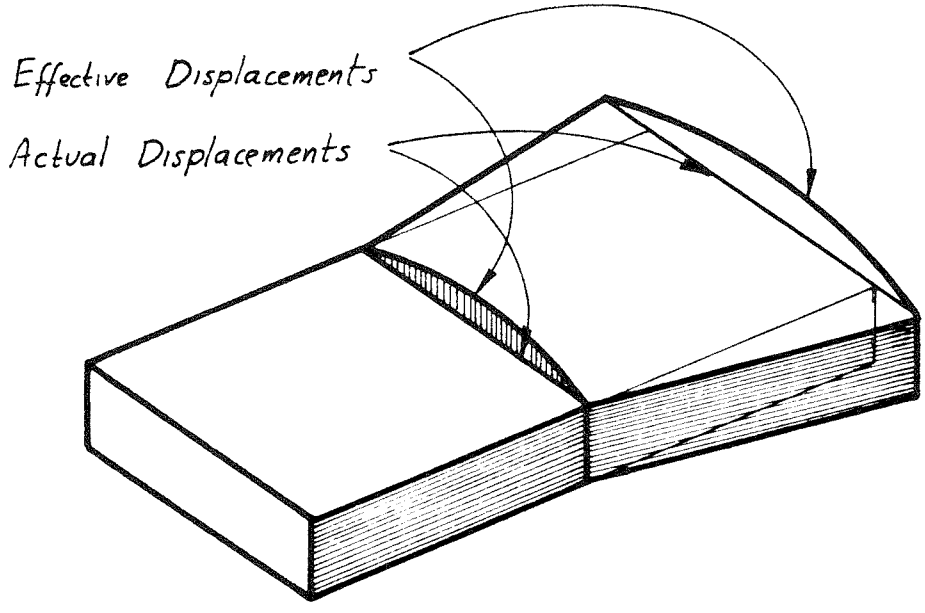

Fig. VI.17 Incompatible Displacements Between Elements

of strain components involved at each point is always only two or three, so the final $[\bar{T}]^T$ $[\bar{E}]$ $[\bar{T}]$ multiplication, which is the most time-consuming part, is reduced considerably, since less than half the columns and rows of the $[\bar{T}]$ matrix are now involved in the calculation at each point.

VI.4 DETAILS OF SHELL STIFFNESS, NODAL LOADS, ETC.

VI.4(a) Stiffness Matrix

The transformations involved in constructing the stiffness are given in some detail in Chapter V.3 for general shell elements, of the Ahmad-Irons type. Only those details not discussed there will be presented here.

The element chosen as the basic element is the nine nodal point quadratic displacement element Fig. VI.19.

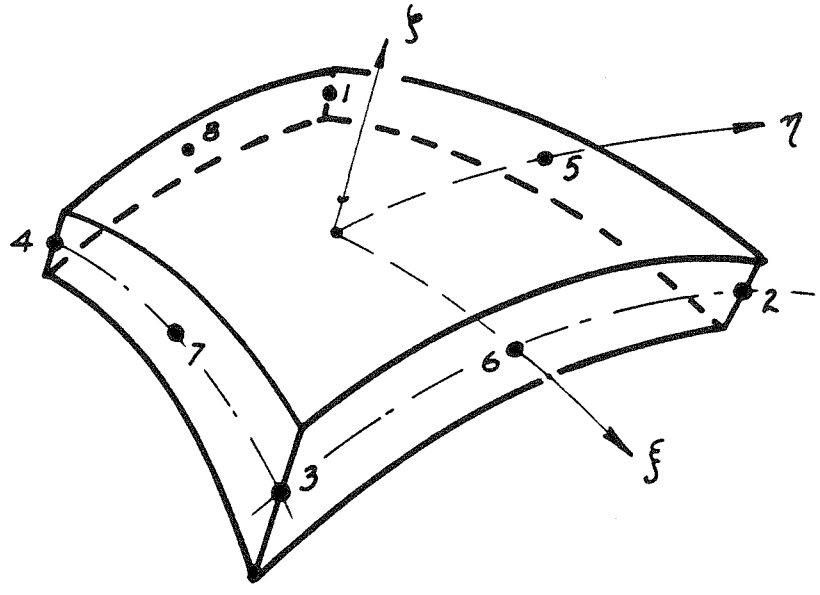

Fig. VI.19 Shell Element Adopted.

Only nodes 1 - 8 are referred to externally in the program, the coordinates of node 9 being generated internally. The position of node 9 is chosen to be the origin of the coordinates, defined by the eight external nodes.

$$\langle x\ y\ z\rangle = \langle p^r\rangle \left[\underset{\sim}{x}\ \underset{\sim}{y}\ \underset{\sim}{z}\right] + \zeta\langle p^r\rangle\left[\underset{\sim}{x}^*\ \underset{\sim}{y}^*\ \underset{\sim}{z}^*\right]$$

where $\langle p^r\rangle$ represents the <u>eight</u> interpolation functions given in Chapter V, equation V.20.

By substituting $\xi = \eta = \zeta = 0$ we get the mid-surface coordinate of node 9

$$\langle x_9\ y_9\ z_9\rangle = \langle p_{\xi=\eta=0}\rangle \left[\underset{\sim}{x}\ \underset{\sim}{y}\ \underset{\sim}{z}\right]$$

and we get the coordinate difference between $\zeta = 1$ and $\zeta = 0$ at node 9 similarly, from the second term of V.22

$$\langle x_9^*\ y_9^*\ z_9^*\rangle = \langle p_{\xi=\eta=0}\rangle \left[\underset{\sim}{x}^*\ \underset{\sim}{y}^*\ \underset{\sim}{z}^*\right]$$

From these two quantities, we can calculate for node 9 the nodal rotational axes $\hat{a}$ and $\hat{b}$ as in Chapter V.3. The displacement field is defined from the <u>nine</u> nodal displacements by equation V.26

$$\langle u\ v\ w\rangle = \langle p^r\rangle \left[\underset{\sim}{u}\ \underset{\sim}{v}\ \underset{\sim}{w}\right] - \tfrac{1}{2}\zeta\langle p^r\rangle \left[\underset{\sim}{t}\right]\left[\underset{\sim}{\alpha}\right]\left[\underset{\sim}{b}_1\ \underset{\sim}{b}_2\ \underset{\sim}{b}_3\right] + \tfrac{1}{2}\zeta\langle p^r\rangle \left[\underset{\sim}{t}\right]\left[\underset{\sim}{\beta}\right]\left[\underset{\sim}{a}_1\ \underset{\sim}{a}_2\ \underset{\sim}{a}_3\right]$$

We could use a completely new set of interpolation functions corresponding to nine nodes, (equation V.18) or, to simplify the computer programming, resort to a procedure similar to that described by Irons (13).

We will define the nodal "relative displacement"at node 9 by the difference between the actual displacement of node 9 and that, at node 9 due to displacements of the other 8 nodes. Then if we define $p_9 = (1-\xi^2)(1-\eta^2)$ and interpret u_9, v_9, w_9 as relative displacements, we can write the previous equation for displacements, using the first eight p_i identical to those for eight nodes, and p_9 as just described. This procedure preserves rigid body displacement and constant strain modes of deformation and results in an identical formulation to the usual nine node interpolation functions.

From this point on, the analysis proceeds exactly as described in Chapter V.3 and by use of the integration procedure developed in Chapter V.3(c) and listed in Table V.1 for quadratic elements, the 45 x 45 stiffness matrix is formed.

Since node 9 is internal to the element, the degrees of freedom associated with it are removed by static condensation, (see Chapter I.4) resulting in a 40 x 40 element stiffness matrix.

VI.4(b) Body Loads, Surface Loads

Nodal loads resulting from gravity and temperature will now be considered.

Gravity loads are calculated from a uniform density throughout each element, temperature loads from a temperature distribution T, uniform on each face of each element, and varying linearly through the thickness. The nodal loads associated with these conditions may be found by usual procedures, and only an outline is included here.

The vertical displacement w is given by

$$w = \langle p^T \rangle \{\underline{w}\} - \tfrac{1}{2}\zeta \langle (p\,t\,b_3)^T \rangle + \tfrac{1}{2}\zeta \langle (p\,t\,a_3)^T \rangle \{\underline{\beta}\}$$

So the element nodal loads from gravity are given by

$$\{\underline{R}\} = \iiint_{element} \rho g \begin{Bmatrix} \{p\} \\ -\tfrac{1}{2}\zeta \{p\,t\,b_3\} \\ \tfrac{1}{2}\zeta \{p\,t\,a_3\} \end{Bmatrix} dv$$

$$= \rho g \int_{-1}^{+1}\int_{-1}^{+1}\int_{-1}^{+1} \begin{Bmatrix} \{p\} \\ -\tfrac{1}{2}\zeta \{p\,t\,b_3\} \\ \tfrac{1}{2}\zeta \{p\,t\,a_3\} \end{Bmatrix} \det J \, d\xi\, d\eta\, d\zeta$$

If the temperature on the surfaces $\zeta = -1, +1$ are T_{-1} , T_{+1} then the temperature at any internal point is $T = T_{-1} + \frac{1+\zeta}{2}(T_{+1} - T_{-1})$

giving initial in-plane strains in local coordinates

$$\bar{\epsilon}_T = \alpha (T - T_{ref})$$

where T_{ref} is the zero-strain reference temperature and α is the coefficient of thermal expansion.

Then using equation V.34

$$\{\bar{\epsilon}\} = [\bar{T}]\{\underline{\tau}\}$$

So the nodal forces due to temperature become

$$\{\underline{R}\} = \iiint_{element} [\bar{T}^T][\bar{E}]\bar{\epsilon}_T \, dv$$

$$= \int_{-1}^{+1}\int_{-1}^{+1}\int_{-1}^{+1} [\bar{T}^T][\bar{E}]\,\alpha (T - T_{ref}) \det J \, d\xi\, d\eta\, d\zeta$$

Both the gravity and temperature load integrals are performed numerically.

The highest order term occurring in the gravity load integral results from $\xi^2\eta^2$ in $\{p\}$ and $\xi^2\eta^2$ in $\det J$. So to integrate this term exactly we will need a higher order integration than 2 x 2. Since we have already fixed the integration point grid for the stiffness, itself, we will use the same points for the body load integration also, to avoid having to use more integration points than necessary. We use the grid and weights shown in Fig. VI.4.

We could use the same integration for the loads due to temperature, but to economize on the stiffness formation time, we have not computed all strains at all points, so we will only use a 2 x 2 grid, where we do have these strains computed. To justify this, we again check that if the element is in a state of constant strain, the integral is exact. The energy integral

$$\langle \underset{\sim}{\tau}^T \rangle \iiint \left[\overline{T}^T\right]\left[\overline{E}\right]\{\bar{\epsilon}_r\}\, dv$$

$$\equiv \int_{-1}^{+1}\int_{-1}^{+1}\int_{-1}^{+1} \text{const} \times \det J \; d\xi\, d\eta\, d\zeta$$

since for constant strain $\langle \underset{\sim}{\tau}^T \rangle \left[\overline{T}^T\right] = \langle \bar{\epsilon}^T \rangle = \text{constant}.$

So once again, as a 2 x 2 grid integrates det J correctly, it will satisfy convergence requirements.

In addition to the loads discussed above, we wish to be able to apply surface loads due to a vertical uniform load on each element, and pressures either uniform, or due to water pressure, varying linearly with depth below some reference surface, as in the case of an arch dam.

To evaluate nodal loads for surface pressures we must determine the normal displacement of any point on the surface. Referring back to V.32 we see that we have the direction cosines of the normal in the last row of $\overline{J}$, so the normal deflection is given by

$$u_n = \langle u \; v \; w \rangle \begin{Bmatrix} \overline{J}_{31} \\ \overline{J}_{32} \\ \overline{J}_{33} \end{Bmatrix} \tag{VI.11}$$

Using equation V.26 we can set up the vector relating the normal displacement u_n with the nodal displacements $\{\tau\}$,

$$u_n = \langle S^T \rangle \{\tau\}$$

and after multiplying by the appropriate pressure, integrate over the surface area of the element.

$$\iint_{\text{area of element}} \{S\} \times \text{pressure} \; dA$$

This integration is performed in the coordinates ξ, η. Referring once more to Fig. V.2, the element of area

$$ds = \left| \hat{e}_1 \times \hat{e}_2 \right| = det_2 \times d\xi \, d\eta$$

where

$$det_2 = \sqrt{\left(\frac{\partial x}{\partial \xi}\frac{\partial y}{\partial \eta} - \frac{\partial x}{\partial \eta}\frac{\partial y}{\partial \xi}\right)^2 + \left(\frac{\partial x}{\partial \eta}\frac{\partial z}{\partial \xi} - \frac{\partial x}{\partial \xi}\frac{\partial z}{\partial \eta}\right)^2 + \left(\frac{\partial y}{\partial \xi}\frac{\partial z}{\partial \eta} - \frac{\partial y}{\partial \eta}\frac{\partial z}{\partial \xi}\right)^2}$$

Then the nodal loads, become

$$\int_{-1}^{+1}\int_{-1}^{+1} \{S\} \times \text{pressure} \times det_2 \; d\xi \, d\eta$$

The nodal loads due to vertical loading are computed similarly using $u_n = w$ instead of equation VI.11

Due to the quadratic terms, in both S , det_2 we would like to integrate this by a 3 x 3 grid on each surface, but this means 9 more integration points and it was decided to adopt the simpler 2 x 2 grid.

This is justifiable, since for a small element in a fine mesh, it isn't really important how the total force on the element is distributed, among the nodes, provided that this total element force is correct. The simplest mathematical proof that 2 x 2 is a sufficient grid goes back to considering the element as a full three dimensional element as in Fig. V.3 (An equivalent proof which is not quite as algebraically simple applies to the actual two dimensional element.)

We have $$u_n = \langle u \; v \; w \rangle \begin{Bmatrix} \overline{J}_{31} \\ \overline{J}_{32} \\ \overline{J}_{33} \end{Bmatrix}$$

$$= \langle p^T \rangle \left[\underline{u} \; \underline{v} \; \underline{w} \right] \begin{Bmatrix} \overline{J}_{31} \\ \overline{J}_{32} \\ \overline{J}_{33} \end{Bmatrix}$$

The (say) horizontal nodal forces in the x direction are

$$\int_{-1}^{+1}\int_{-1}^{+1} \{p\} \; \overline{J}_{31} \times \text{pressure} \times det_2 \; d\xi \, d\eta$$

Thus the total horizontal force =

$$\sum_i \int_{-1}^{+1}\int_{-1}^{+1} p_i \; \overline{J}_{31} \times \text{press.} \times det_2 \; d\xi \, d\eta$$

For a small enough element, we may consider the pressure and the term J_{31} as constant over the element, so the horizontal force becomes

$$= \text{press.} \times \overline{J}_{31} \int_{-1}^{+1}\int_{-1}^{+1} \sum_i p_i \; det_2 \; d\xi \, d\eta$$

$$= \text{press.} \times \overline{J}_{31} \int_{-1}^{+1}\int_{-1}^{+1} det_2 \; d\xi \, d\eta$$

since $\sum_i p_i = 1$ for any valid interpolation functions.

So the total of all nodal forces will be correct for a small element, provided we can integrate det_2 correctly, which is achieved by a 2 x 2 grid in ξ , η .

VI.4(c) Mass Matrix

The mass matrix, derived in a consistent way from the finite element method, contains terms in the same matrix locations as occur in the stiffness itself. However, common practice is to simplify this approach by using a diagonal matrix for the mass, representing a "lumped" mass at each node. Felippa (4) indicates that this, in fact, gives better results than the fully consistent mass, in many cases.

One way to achieve this diagonal matrix is to add to each diagonal element of the mass matrix, the elements of all columns in that row. This results in a mass distribution for each finite element, identical to that of the nodal forces resulting from body loads, and is given for a mass density ρ , by:

$$m_i = \iiint_{element} \rho p_i \, dv \qquad \text{for node } i$$

While satisfactory for many elements, this results in undesirable dynamic characteristics for this quadratic displacement element. When the mass is lumped in this manner, negative masses occur at the corner nodes, resulting in an indefinite mass matrix. To avoid this problem, (without simply dividing up the total mass of each element arbitrarily between the nodes, which takes no account of element shape, change of thickness etc.)

we can add linear combinations of the diagonal masses described first, in such a way as to produce positive values at all nodes. One formula for achieving this for corner (subscript c) and mid-side (subscript m) nodes is given by:

$$m_c^* = \frac{1}{8} m_c + \frac{7}{64} \left(\sum_{\substack{\text{adjacent} \\ \text{nodes}}} m_m \right)$$

$$m_m^* = \frac{25}{32} m_m + \frac{7}{16} \left(\sum_{\substack{\text{adjacent} \\ \text{nodes}}} m_c \right)$$

where m represents the nodal lumped mass from the body load distribution described above, and m* represents the new lumped masses. These modified lumped masses m* reflect changes in thickness of the shell, or non-rectangular geometry, as is desired, and, except perhaps for exceptional cases of strangely distorted elements, give positive definite nodal masses. The resulting distribution of the total mass M in a rectangular element is as shown in Fig. VI.20.

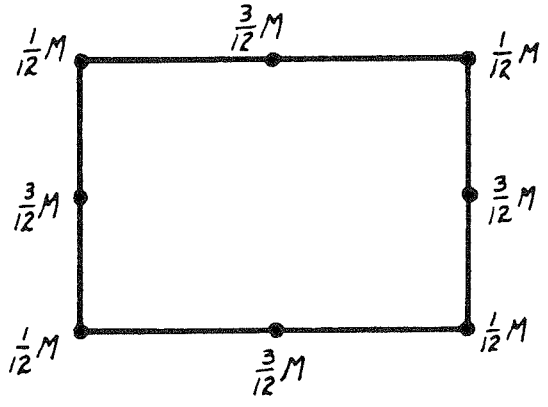

Fig. VI.20 Nodal Lumped Masses for Rectangle

Since we are primarily interested in thick shells, we will include both translational and rotational inertial effects by including the terms $\iiint P_i \rho \left(\zeta \frac{t_i}{2}\right)^2 dv$ associated with nodal rotations, and then distributing the nodal rotational "masses" in the same manner as the translational masses above.

The sum of the masses m^* of all corner and mid-side nodes, for each translational direction x, y, z is given by:

$$\sum m_c^* + \sum m_m^* = \frac{1}{8}\sum m_c + \frac{7}{64}\times 2 \sum m_m + \frac{25}{32}\sum P_m + \frac{7}{16}\times 2 \sum m_c$$

$$= \sum m_c + \sum m_m$$

which is equal to the sum of the nodal masses m_i.

This sum is given by:

$$\sum_i \iiint P_i \rho \, dv$$

$$= \iiint \sum P_i \rho \, dv$$

$$= \iiint \rho \, dv$$

= the total mass of the element. So for very small elements in a very fine mesh, the mass distribution will be represented correctly, and so convergence to the correct inertial behavior is assured. A similar proof applies for the rotational behavior.

Since the mass integration is of the same form as the body load integration, the same integration scheme is adopted.

VI.4(d) Stress Evaluation

For the unmodified Ahmad-Irons element we showed that the stress evaluation from the nodal displacements is of the form

$$\{\bar{\tau}\} = [\bar{E}][\bar{T}]\{\underset{\sim}{\tau}\}$$

In that situation, we could reasonably adopt any points within the element or on its inter-element boundaries, to find the stresses. Different investigators seem to favor different locations. However, when using the modified integration procedure we have definite optimum positions. If we examine the discussion of transverse shear integration for a quadratic displacement beam element, we recall that only at the points $\xi = \pm\sqrt{\frac{1}{3}}$ is the transverse shear due to a linear moment displacement, exact. (The same observation applies at $\xi = 0$ for the linear beam.) Similarly we find this position is the only point at which the in-plane strains are correct for a curved arch under constant moment.

So to get the best stresses we are to use these points. Since we have used $\xi, \eta = \pm\sqrt{\frac{1}{3}}$ for integration of the surface loads, we have evaluated the necessary stress-displacement transformations already, so these are, for a second reason, convenient points to evaluate stresses. So we will adopt the eight points $\xi = \pm 1$, $\xi, \eta = \pm\sqrt{\frac{1}{3}}$ in this shell program.

VI.4(e) Triangular Elements

To form triangular elements, the simplest way is to simply coelesce three nodes into one after forming the stiffness in the

usual way. If this is done as shown in Fig. VI.21, provided mid-side nodes are used, the ξ axes are parallel throughout the element and exact convergence is assured (see Chapter VI.3(c)).

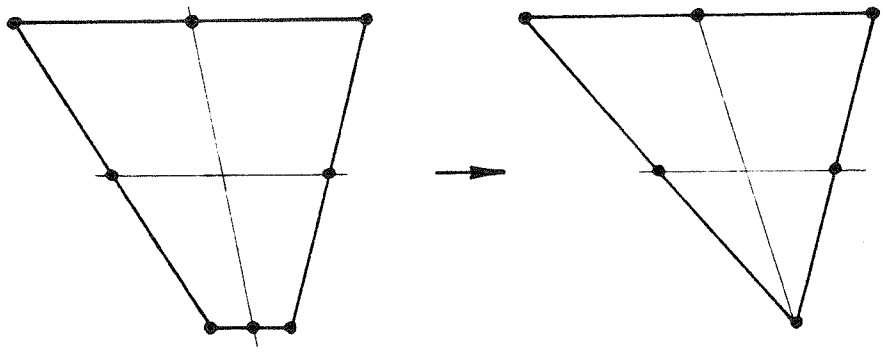

Fig. VI.21 Formation of Triangular Elements

VI.4(f) Connection to Three-Dimensional Elements

In order to connect these shell elements to three-dimensional elements the nodal displacements and rotations of the mid-surface nodes must be transformed to pure translational displacements of the nodes on the two shell surfaces adjacent to the mid-surface node (see Fig. VI.22).

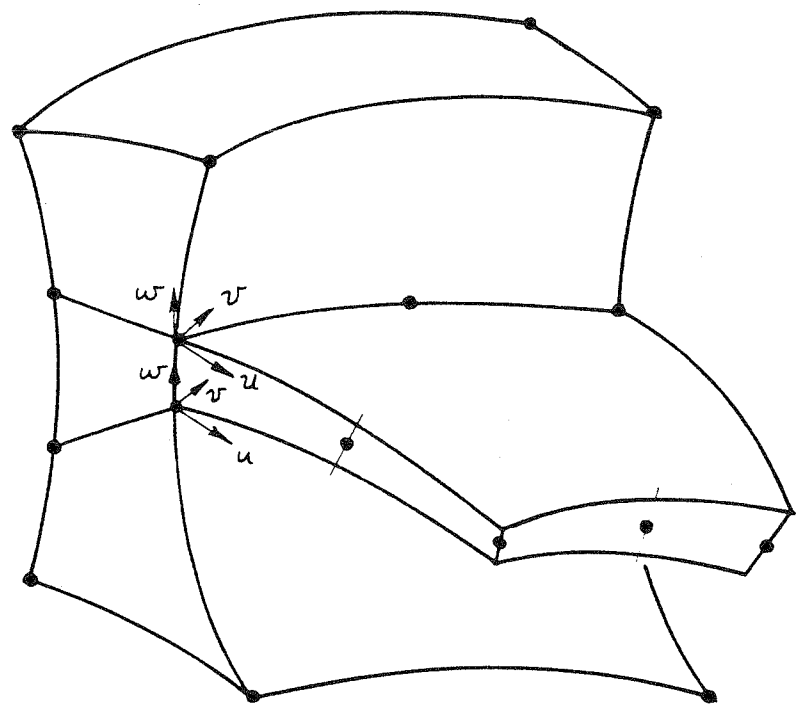

Fig. VI.22 Connection of Shell to 3-D Element

It can be easily verified that this transformation is given by:

$$\begin{Bmatrix} u \\ v \\ w \\ \alpha \\ \beta \end{Bmatrix} = \begin{vmatrix} \frac{1}{2} & & & \frac{1}{2} & & \\ & \frac{1}{2} & & & \frac{1}{2} & \\ & & \frac{1}{2} & & & \frac{1}{2} \\ -b_1/t & -b_2/t & -b_3/t & b_1/t & b_2/t & b_3/t \\ a_1/t & a_2/t & a_3/t & -a_1/t & -a_2/t & -a_3/t \end{vmatrix} \begin{Bmatrix} u_1 \\ v_1 \\ w_1 \\ u_2 \\ v_2 \\ w_2 \end{Bmatrix}$$

where u_1, v_1, w_1 are the displacements of the new node on the $\zeta = 1$ surface and u_2, v_2, w_2 are those on the $\zeta = -1$ surface. a_1, a_2 a_3, b_1, b_2 b_3 are the direction cosines of the vectors $\hat{a}$, $\hat{b}$ described in Chapter V.3.

Rewriting this transformation for node i as

$$\{u^i\} = [C^i]\begin{Bmatrix} u_1^i \\ u_2^i \end{Bmatrix}$$

we can express all the mid-surface node displacements and rotations in terms of both the unaltered shell node displacements and the connecting node displacements :

$$\begin{Bmatrix} u^1 \\ u^2 \\ \vdots \\ u^i \\ \vdots \\ u^n \end{Bmatrix} = \begin{bmatrix} I & & & & \\ & I & & & \\ & & \ddots & & \\ & & & C^i & \\ & & & & \ddots \\ & & & & & I \end{bmatrix} \begin{Bmatrix} u^1 \\ u^2 \\ \vdots \\ \begin{Bmatrix} u_1^i \\ u_2^i \end{Bmatrix} \\ \vdots \\ u^n \end{Bmatrix}$$

The element stiffness matrix, increased in size by one row and column for each connecting node so transformed becomes:

$$[K'] = \begin{bmatrix} I & & & & \\ & I & & & \\ & & \ddots & & \\ & & & C^{iT} & \\ & & & & \ddots \\ & & & & & I \end{bmatrix} [K] \begin{bmatrix} I & & & & \\ & I & & & \\ & & \ddots & & \\ & & & C^i & \\ & & & & \ddots \\ & & & & & I \end{bmatrix}$$

VII. PROGRAM SHELSOL

The concepts deseribed in Chapters V and VI were incorporated into a program called SHELSOL, for analyzing shells and three-dimensional solids. The program SHELSOL is based on a program called STRUCTURAL ANALYSIS PROGRAM, or SAP, developed by Edward L. Wilson and Lindsay R. Jones at the University of California, Berkeley. Modifications to SAP were made for more efficient handling of thick shells.

SHELSOL is a program for assembling the stiffnesses, nodal forces for any number of load cases, and nodal masses of shell or three-dimensional elements, and solving for displacements, stresses and dynamic mode shapes and frequencies if desired. The subroutines shown in Fig. VII.1 are called one after another by the control program SHELSOL. A brief description of the main characteristics of each subroutine will be given now.

For shells, INPUTNS reads, first, the coordinates of points adjacent to each shell node on each surface of the shell. For three-dimensional solids, this subroutine reads the coordinates of the nodes themselves. Next this subroutine reads an array called ID which specifies for each node whether each nodal degree of freedom is "free" or constrained to zero displacement. This array is subsequently modified to become an array giving the equation number for each degree of freedom for each node. Nodes for three-dimensional elements have three degrees of freedom and for shells have five, so this identifying array, ID, is referred to frequently for identifying terms in all matrices for the complete structure. Material properties of the various materials used, and details of water pressure loading, if any, are read at this stage.

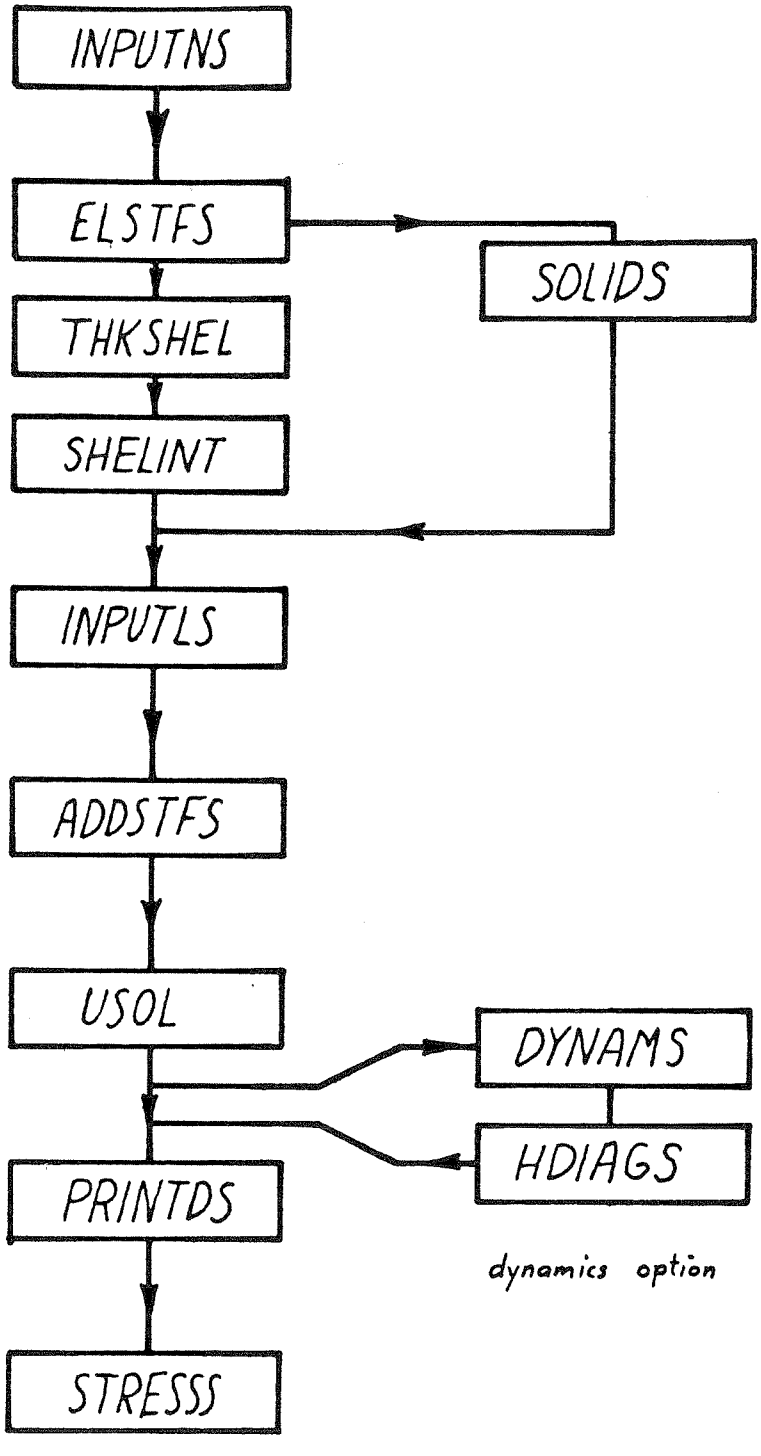

fig VII.1 Flow Chart

ELSTFS reads the node numbers for each element, and various details required for evaluating stiffnesses, masses and element loading, such as temperatures, surface pressures and vertical surface loading. Then by calling the stiffness subroutines THKSHEL or SOLID the stiffness and stress-displacement matrices for each element are formed. At the same time the mass vector and the load vector caused by internal loads, are formed. (Any combination of dead load, surface pressure and/or water pressure loading, surface loading in the vertical direction, and temperature can be added to any load case.) These are all placed on tape for later use. To provide flexibility of programming during development of the program, the integrations for THKSHEL are performed by a subroutine SHELINT called from THKSHEL. Two versions of SHELINT can be used. Version 1 is the unmodified Ahmad Irons symmetric integration, while Version 2 has the new modified integration scheme.

INPUTLS reads the externally applied nodal loads and adds them to the total nodal load vector, using the identifier array ID. Any number of load cases may be run at once.

ADDSTFS assembles the element stiffnesses into the full stiffness matrix, in blocks small enough to be stored in the available in-core memory, by running through the tape containing the element stiffnesses and picking out the desired terms for each block, by use of the array ID again. The element nodal loads and nodal masses are similarly assembled.

USOL is an equation solver which solves the full set of linear equations, two blocks at a time, making use of symmetry and recognizing zeroes within the bandwidth which is stored, to shorten the number of computations. Solutions for any number of load vectors can be found.

PRINTDS prints the displacements for each load case using the array ID to identify the results from USOL.

STRESSS computes stresses in the elements from the displacements from USOL for each load case, using the stress matrices computed under ELSTFS.

DYNAMS is a subroutine which can be called if mode shapes and frequencies of the structure are desired. To avoid finding eigenvalues and eigen vectors for the total number of degrees of freedom of the assembled structure, this subroutine uses only a limited number of constrained displacement patterns to form the eigenvectors. These displacement patterns are formed by applying loads to the structure in a manner selected by the user, and care must be taken to ensure that components of the vibration modes sought are included in one or more of these displacement patterns.

VIII. NUMERICAL RESULTS

A number of structures of differing types have been chosen to demonstrate the behavior of the THKSHEL element. The examples are designed to illustrate, firstly, the performance of the elements in special situations that emphasize certain characteristics and, secondly, their performance in more typical thin and thick shell situations.

The first set of examples is given to indicate the magnitude of the errors inherent in the basic kinematic and stress assumptions, in a situation of extreme thickness-to-curvature ratio.

The next set of examples illustrates the efficiency of the new element integration compared with the original symmetric integration scheme proposed by Ahmad and Irons, for both bending and in-plane displacements.

Finally, a number of examples are considered that represent typical (although simple) thin and thick shell structures. Comparisons of results obtained with the new element are made with the original Ahmad - Irons element and with solutions by other authors.

For simplicity, in the following section the unmodified Ahmad Irons element will be referred to as the A-I element and the new element presented here as THKSHEL.

VIII.1 Very Thick Ring

The thick ring shown in Fig. VIII.1 was analysed, subject to the three loading conditions given:

(a) Uniform body load directed radially outward

(b) Moment applied at one end

(c) Transverse shear applied at one end.

In each case, the surfaces perpendicular to the axis of the ring were free of stress.

The first two cases result in stresses that are constant around the ring, being the constant membrane and bending states, respectively. The third, case (c), includes both bending and membrane effects, as well as transverse shear.

A fine mesh of 20 elements in the circumferential direction was used in order to get a solution that includes insignificant errors due to discretization, and gives the best result which the underlying assumptions, used in both A-I or THKSHEL, can give.

The circumferential stresses across the beam at the lower end are shown in Fig. VIII.2. For comparison, the same stresses are shown for each case computed first by the simplest thin shell assumptions and secondly by the theory of elasticity, for a ring with plane stress assumptions, (39).

It is seen from the graphs of tangential stresses that even with the severe geometry used here the stress distribution is reasonably accurate, representing considerable improvement over thin shell approximations. Another analysis of a moderately thick shell is given later providing another comparison of thick shell behavior with the more accurate results from a three-dimensional finite element solution.

VIII.2 Membrane Behavior of Shell Elements

To compare the efficiency of the THKSHEL element with other shell elements for in-plane displacements a thin rectangular plate fixed at one end was loaded with a parabolically varying load in its own plane, as shown in Fig. VIII.4. This example has been used by Felippa (35) and Johnson (29) for the same purpose. The two surfaces of the plate are assumed stress free.

Two finite element meshes only were examined, the first being a single element representing the plate and the second being two elements across and eight along the cantilever, to give square elements. These two meshes (a) and (b) are shown in Fig. VIII.4.

Results are shown for both the A-I element and THKSHEL and a comparison is given with a thin shell quadrilateral element used by Johnson (29). To give a meaningful comparison in this and subsequent examples, it is noted that a mesh of quadrilaterals with only corner nodes requires approximately the same amount of work to solve the equations as a mesh twice as coarse formed with quadrilaterals including mid-side nodes. For proof, see the brief digression below. Therefore in this and subsequent examples, when comparisons are made with a certain $r \times n$ mesh, say, a mesh of $2r \times 2n$ is used for the four node elements.

Digression to prove statement of comparison mesh fineness.

Consider a square plate to be solved by

(a) Elements with mid side and corner nodes

(2) Elements with only corner nodes

We divide the plate into two different meshes as shown in Fig. VIII.3, which represent the same amount of work to solve the equations when used with the two different element types. If the number of elements is "large", we get the following:

Element Type	Corner, Mid-Side Nodes	Corner Nodes
Ext. degrees of freedom/element	40	20
No. of elements along each side	m	c
Total number of nodes	$3m^2$	c^2
Total degrees of freedom "n"	$5 \times 3m^2$	$5 \times c^2$
½ bandwidth "b"	$5 \times 3m$	$5 \times c$
Solution time (= ½ nb^2)	½ x $15m^2$ x 15^2 m^2	½ x $5\,c^2$ x $25\,c^2$

equating $\frac{1}{2} \times 5^3 \times 27\ m^4 = \frac{1}{2} \times 5^3 \times c^4$

we see

$$c = 2.25\ m$$

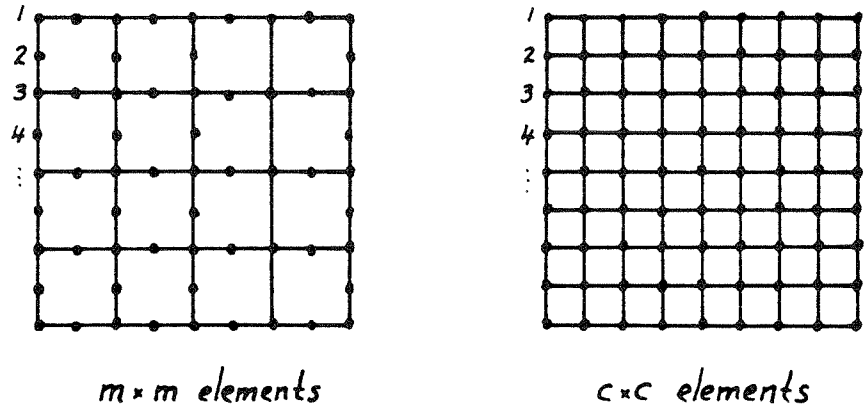

Fig. VIII.3 Mesh Comparisons

Thus to make an approximate comparison with elements without mid-side nodes, we can use a mesh twice as fine as the original mesh.

Given in Table VIII.1 are the tip deflections for the two discretizations, and the longitudinal stress at the points where the stresses are evaluated by the subroutine. Each is compared with the theoretical solution for the beam, given by Felippa.

It is seen that in this example both the A-I and THKSHEL elements are more efficient than the elements used by Johnson and the improvement shown by THKSHEL relative to A-I is considerable.

So we can feel confident of good membrane behavior of the new element THKSHEL.

TABLE VIII.1

Mesh	Element	Tip Deflection	Stress at P
a	A-I	.3028	29.165
a	THKSHEL	.3476	36.427
beam theory		.3558	36.429
b	A-I	.3553	45.603
b	THKSHEL	.3554	45.657
beam theory		.3558	45.654
c	Johnson	.3497	58.37
beam theory		.3558	60.00

VIII.3 Plate-Bending Behavior of Shell Elements

To examine the bending behavior of the new element, THKSHEL, the square, simply supported thin plate shown in Fig. VIII.5 was analysed, loaded by a concentrated central load. Using conditions of symmetry, only a quarter of the plate was analysed. Three different meshes were used, as shown in Fig. VIII.5.

For comparison, the results given by Clough and Tocher (1) for the triangular thin plate element HCT, and results given by Clough and Felippa (4) for the quadrilateral element Q 19 are included, using a mesh twice as fine, for the reason described in the last example.

The numerical results are shown in Fig. VIII.6 and VIII.7. The first shows the convergence of the central displacement to the solution given by thin plate theory (36) for the different elements. The second gives the convergence of displacements along a line of symmetry as the mesh is refined.

The two plots show remarkable bending behavior of the element THKSHEL. Dramatically improved from the parent A-I element, the central deflection is actually more accurate than the highly efficient Q-19 element in this particular example, converging from above.

We are thus assured of good bending behavior for the element THKSHEL.

To examine the behavior of shell elements of non-rectangular geometry, the same plate-bending problem was analysed again, using non-rectangular elements with both straight and curved sides. The three examples are shown in Fig. VIII.8. The first, (mesh (a)) is highly distorted from the optimum rectangular shaped elements. The second and third examples (meshes (b), (c)) are about as non-rectangular as may be needed in more typical finite element applications.

Fig. VIII.8 shows the displacements along the line of symmetry for each of the meshes, using THKSHEL.

It is seen from the graph, that the two straight-sided elements give significantly poorer results than the rectangular grid, with approximately 5% error being introduced in each case. The much distorted curved element mesh (a) gives a very poor solution, matched only by the incredibly bad solution for A-I with this geometry.

It can be inferred from these examples that, as we have said before, it is desirable to use rectangular elements, wherever possible, especially at regions of high change of stress. Again it should be stressed that meshes containing elements whose two edges $\eta = 1$ and $\eta = -1$ are not parallel or do not converge towards parallelism will not converge to the exact solution. However the small errors introduced may, in a particular example, be quite acceptable.

The last set of plate-bending examples is to determine quantitatively, what defines a structurally thin plate. That is, at what thickness-to-span ratio do shear effects start to modify the deflections due to bending significantly. The same simply supported plate, as previously examined, was loaded, this time with a uniform load to avoid the problems of the singularity in the shear stresses at the center. Four different thickness were considered, varying from a thickness-to-span ratio of 1/2000 to a ratio of 1/2, (at which, incidentally, the various kinematic assumptions are probably unacceptable). The loading was increased with the thickness, to give an identical bending deflection for each example.

The total deflection at the center, and the bending stress τ_{xx} at the center are given for each thickness in Figs. VIII.9, VIII.10.

Since for this example the loading increases as the cube of the thickness, and the shear area as only the first power, the shear deflection (added onto the bending, approximately) varies approximately with the thickness squared. This is very small compared with the bending deflection until the thickness to span ratio is about 1/20, then increases rapidly quickly dominating the bending effects. As a rule of thumb this example would indicate that the use of a thick shell element would be indicated for thickness to span ratios between about 1/40 and 1/5, the larger ratio being simply an estimate of when the shell assumptions used become invalid.

VIII.4 Thin Cylindrical Shell Roof

To examine the effectiveness of the THKSHEL element for analyzing thin shells, the first example chosen was cylindrical shell cited by Johnson, (29). The geometry, material properties and loading

are given in Fig. VIII.11. The shell is supported on diaphragms as shown, that allow no displacements in their own plane, but offer no resistance to displacements perpendicular to it.

Only a quarter of the shell was actually analyzed, by using symmetric boundary conditions along the two orthogonal planes of symmetry. The three different finite element meshes used are shown in Fig. VIII.11.

Displacements of the shell in the vertical direction at the mid-span section are shown in Fig. VIII.12 and Fig. VIII.13. The reference curve is that used by Johnson. Fig. VIII.14 an Fig. VIII.15 show the longitudinal force per unit length and moment per unit length across the same section for the finest mesh, Mesh (c). These values were computed from the stresses in the adjacent elements using interpolation with these stresses and the identical values on the opposite side of the line of symmetry.

The graphs show that this thin shell is well modelled by the 4 x 4 mesh, Mesh (c), yielding moments and forces accurate enough for design purposes. The improvement shown in both stresses and deflections by the improved integration technique used in THKSHEL is very significant. The solution is of comparable accuracy to that obtained by Johnson using an 8 x 12 mesh.

VIII.5 Thin Hyperbolic Paraboloid Shell

The next structure to be examined is the thin hyperbolic paraboloid or hypar shell as shown in Fig. VIII.16. This structure has its boundaries rigidly held against both displacements and moments, and develops high moments as a result.

The structure possesses rotational symmetry about two perpendicular axes and thus can be analysed by considering only a quarter of the full shell. The loading due to dead weight is anti-symmetric for this type of symmetry and leads to the anti-symmetric boundary conditions shown.

Three meshes were used, as shown in Fig. VIII.16. Vertical displacements and moments Mxx along the OX axis are shown in Figs. VIII.17, 18, 19. The moments on the axis were found by interpolation about the axis of symmetry, using the stresses on the adjacent elements. The results are compared with those given by Chetty and Tottenham (32).

This problem containing high moment gradients converged rather slowly, with THKSHEL again providing much better solutions, for all meshes, than A-I.

VIII.6 Arch Dam Number One

A thick shell in the form of an arch dam of simple geometry was next analyzed. This dam is a segment of a thick cylinder and is number one of the series of arch dams proposed for study by the institution of Engineers. This is the simplest of the series, consisting of a thick cylinder of uniform thickness, in a rigid valley. The dam is loaded by water pressure with the water level at the crest of the dam. Details of the geometry are given in Ref. 37.

Using a symmetrical half of the dam, three finite element meshes were considered, as shown in Figs. VIII.20, 21. In each case there are triangular or quadrilateral elements associated with the sloping edge. As was pointed out in Chapter V, the terms of the stiffness matrix of triangular elements, formed by coalescing three nodes, depend on the orientation of the element numbering. To determine how sensitive the

solution was to this orientation the three different orientations were tried, using THKSHEL and Mesh (b). To see whether the solution was sensitive to the theoretically incorrect use of distorted quadrilaterals (see Chapter VI.3(c)) a fourth run was made using THKSHEL with an extra corner node added to the sloping side of the triangular elements. Since the most accurate definition of the stiffness results when the $\eta = 1$ edge is parallel to the $\eta = -1$ edge, trapezoidal elements, when used, were defined with the local element nodal numbering rotated through 90° as indicated in the figures.

For purposes of comparison, the same basic three meshes were used for analyses using A-I elements. Although any shaped triangles or quadrilaterals converge correctly as the mesh is refined, since the triangles were so distorted it was decided to re-run Mesh (b) using a quadrilateral definition of the triangles using an extra corner node on the sloping side, as was done for THKSHEL above. To increase the accuracy (not necessarily the efficiency) of the stiffness matrix for these elements, a higher order (4 x 4) integration rule was used.

Comparisons of the various runs on Mesh (b) using different methods of defining the triangular elements, as described above, resulted in virtually no difference in the solutions for either A-I or THKSHEL elements. These results are not shown here, for almost all points would fall on top of the points shown on the accompanying graphs, to the accuracy plotted.

Graphs of normal displacements on the centerline and along the 80 m. level are given in Figs. VIII.22, 23 for both A-I and THKSHEL elements. Also shown are the same displacements, as determined by Zienkiewicz using a full three dimensional finite element analysis (14), and by Otter using dynamic relaxation and thick shell assumptions, (33).

Fig. VIII.25 shows the vertical stresses on the water face at the center line of the dam found by interpolation with the symmetrically equal stresses, as outlined in the previous example. Fig. VIII.26 compares the converged result with the results of Otter and Zienkiewicz. The graphs show that the solution by THKSHEL elements converged more rapidly than the A-I solution, once more. The converged solution differs slightly from the three dimensional solution by Zienkiewicz lying closer to the thick shell solution of Otter. However, for this structure these differences are not significant for purposes of design.

VIII.7 Arch Dam No. 5

A second arch dam of a more realistic geometry than the previous one was examined under water pressure loading. This dam is number five in the Institution of Civil Engineers' series of arch dams. It is of variable thickness and curvature, the ratio of thickness to radius of curvature varying from that typical of geometrically thin shells, at the crest ($t/R = 1/30$), to a very thick shell at the base, ($t/R = 1/3$). The geometry and material properties are given in Ref. (37). The cross section of the dam is shown in Fig. VIII.27 along with horizontal cross sections at the base and crest of the dam. Meshes similar to those shown in Fig. VIII.24 (b), (c) were adopted.

Zienkiewicz (14) examined the same dam using loading resulting from pore pressure within the dam varying linearly from the full water pressure on the water face, to zero on the air face. This is equivalent to a radial body force distribution. To approximate this loading, the results shown for THKSHEL are the mean of applying the water pressure on the water and air faces.

Fig. VIII.28 shows the radial displacement at the centerline of the dam for the three-dimensional solution by Zienkiewicz and for solutions by THKSHEL using 1, 9 and 32 elements, the latter two being graphically indistinguishable. An interesting comparison is made between the solutions from one THKSHEL element and one cubic A-I element (34)

Fig. VIII.29 shows the vertical stresses on the water face at the dam's centerline. In this graph, the discrepancy between the 9 and 32 element solutions by THKSHEL is more significant. The 32 element THKSHEL solution is somewhat different from the 32 element three-dimensional solution. This is due largely to the great thickness at the base of the dam. A further analysis using 3 integration points in the "normal" direction gave virtually identical results, confirming an earlier statement that two-point integration in the normal direction is satisfactory up to the point where the shell assumptions themselves are invalid. It is seen, that with the extreme thickness over the most highly stressed part of the shell the stresses are reaching the limit of acceptability for design purposes.

VIII.8 Dynamic Analyses

VIII.8(a) Simply Supported Plate

To examine the dynamic response of THKSHEL elements, the first example chosen was a square, simply supported plate as in Chapter VIII.3. A mesh identical to Mesh (b) was used, with alternately symmetric and anti-symmetric boundary conditions at the lines of symmetry. Various thicknesses of the plate were chosen, ranging from a thickness to span ratio of 1/2000 to approximately 1/6.

The frequencies of vibration (normalized by division by $\pi^2\sqrt{\frac{D}{m}} \times \frac{1}{20^2}$ where D is the flexural plate stiffness and m is the mass per unit area) for each thickness are shown in Fig. VIII.30.

As expected, the higher frequencies suffer more than the lower frequencies from discretization errors, resulting in frequencies below the theoretical frequencies. As the plate thickness is increased, the frequencies decrease, the higher frequencies being most affected. This is because the higher frequencies have shorter distances between the lines of zero displacement and hence the effective thickness to span ratio is greater than for the lower frequency vibrations. The reduction in frequency is due to both the reduced stiffness as a result of increasing shear deflection, and the increased inertia due to rotational effects.

Considering the high accuracy in bending of square elements, the results for the higher modes are disappointing. Apparently, the rather arbitrary way in which the mass was lumped at the nodes is not completely satisfactory. It does of course converge to the correct solution as the mesh is refined.

VIII.8(b) Cooling Tower

Fig. VIII.32 shows an axisymmetric concrete cooling tower, constructed in Czechoslovakia. The geometry of this shell was approximated by the dimensions given in Table VIII.2. The boundary conditions at the base prevent translational movement, but allow rotations about both tangential axes. It was desired to determine the lowest frequency of vibration that is symmetrical about each of two perpendicular planes of symmetry. For this mode of vibration, a quarter of the tower may be analysed, with symmetric boundary conditions along the vertical sections.

Two meshes were used, as shown in Fig. VIII.31. Fig. VIII.32 shows the radial displacements of the shell (plotted from the undisplaced position) for this mode of vibration. Also shown are the same displacements calculated by Chang Hua Yeh (graduate student, U.C. Berkeley) using thin shell quadrilateral elements. (In the circumferential direction, the radial displacement of the converged solution varies with the angle, θ, according to sin 4θ. Also shown are the frequencies of vibration for each of the above analyses. A convergence study by Chang Hua Yeh using the thin shell elements in the same structure with slightly different boundary conditions indicated that the 8 x 9 mesh appeared to give the frequency correct to about ± 0.2.

This indicates that again the convergence of dynamic analyses, using THKSHEL, is rather slow. This again appears to be the result of the poor mass distribution within each element.

TABLE VIII.2

Z	Radius	Thickness
624.6	935.0	31.0
581.0	930.0	5.12
300.0	915.0	"
0.0	905.5	"
-300.0	915.0	"
-600.0	930.0	"
-900.0	968.0	"
-1200.0	1013.0	"
-1500.0	1066.0	"
-1800.0	1130.0	5.12
-2100.0	1200.0	5.22
-2400.0	1280.0	5.63
-2700.0	1360.0	7.80
-3024.0	1452.0	21.60

VIII.8(c) Arch Dam Number Five

The same dam examined previously was analysed to determine the first six modes of vibration. Mesh (c) was used and fifty different displacement modes were used to construct the six vibration modes. The dam was assumed empty. Symmetric and antisymmetric boundary conditions at the center line were used to determine symmetric and antisymmetric modes.

Figs VIII.33, 34 show representative displacements for each of the modes. The frequencies of vibration are shown in Table VIII.3. Also shown in the Table are results given by Ermutlu (37). Almost no correlation between the two sets of results exists. It is believed that the discrepancy is due to the use of a poor finite element model by Ermutlu. He uses one layer of constant strain tetrahedra through the thickness of the dam to model the dam. This produces a structure that is very stiff in bending regardless how fine the mesh is. With a shell so stiff in bending, the bending that should occur in the low modes of vibration is prevented and a deflection consisting largely of in-plane deformations occurs. The "antisymmetric" modes shown by Ermutlu depart considerably from exact antisymmetry, indicating either serious round off error or more likely erroneous programming.

		ω_1	ω_2	ω_3	ω_4	ω_5	ω_6
THKSHEL	freq. c.p.s.	2.08	2.28	3.01	3.58	4.40	4.59
	sym. or anti-sym.	a	s	s	a	s	s
ERMUTLU	freq. c.p.s.	3.27	4.16	6.18	6.83	7.25	–
	sym. or anti-sym.	s	approx. a	s	approx a	s	

TABLE VIII.3 Arch Dam No. 5 Frequencies

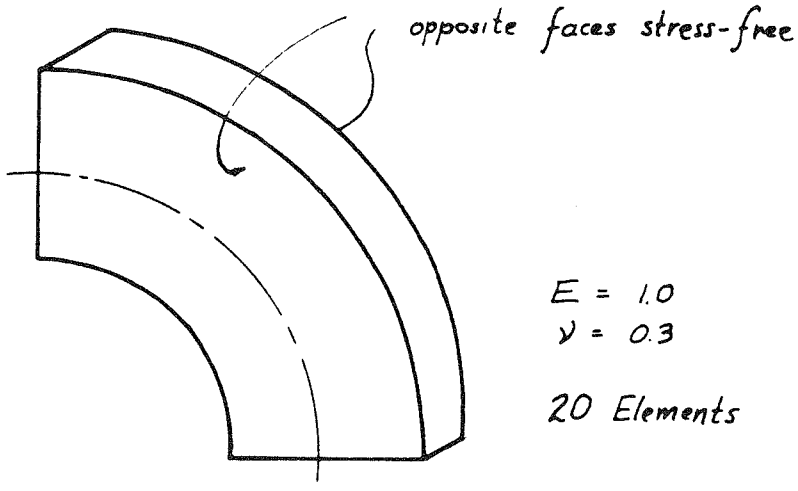

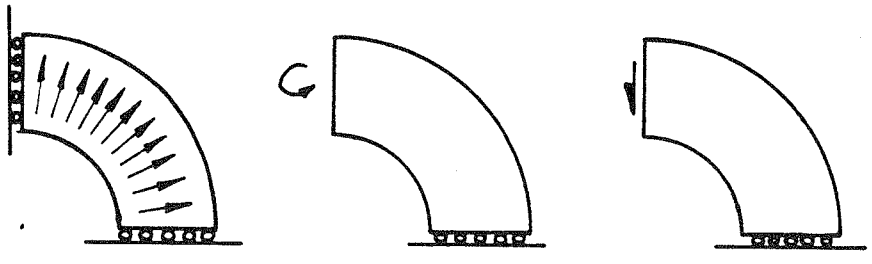

fig VIII.1 Thick Ring

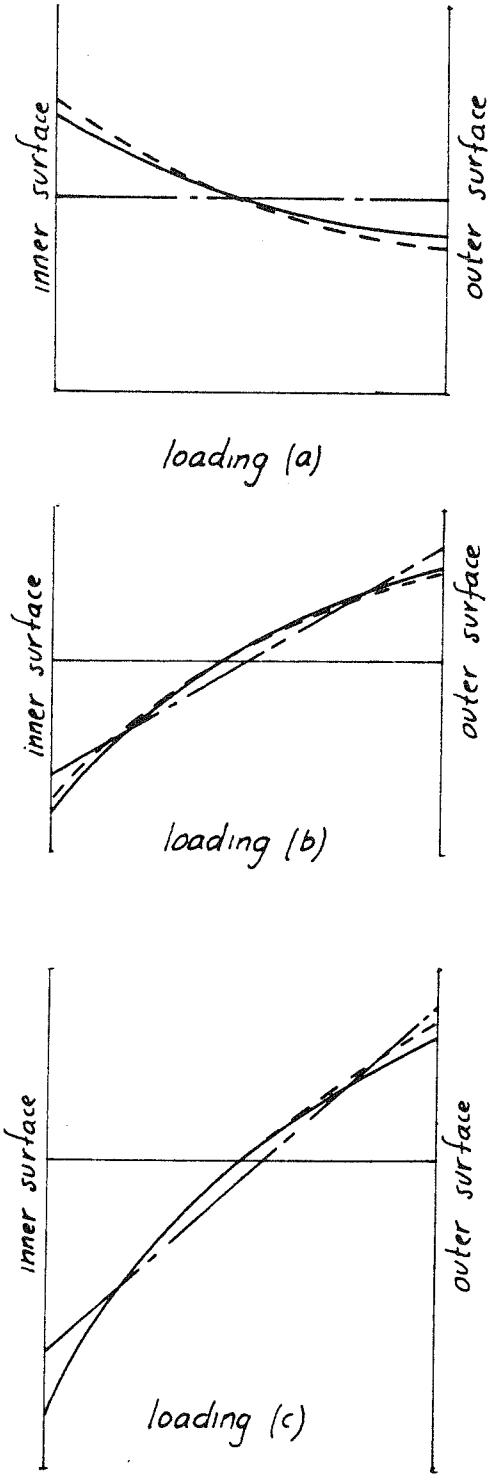

fig VIII.2 Circumferential Stresses across Thick Ring

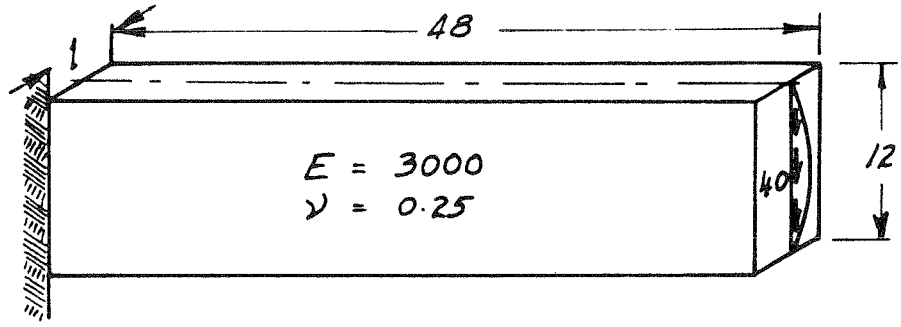

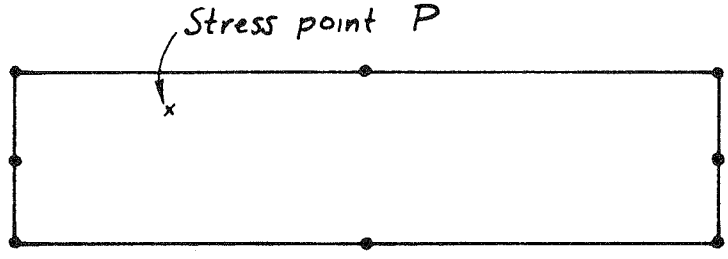

Mesh (a)

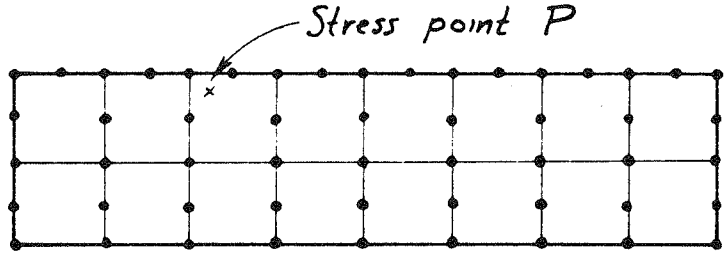

Mesh (b)

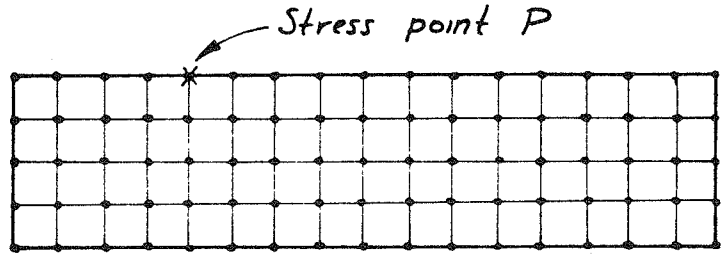

Mesh (c)

fig VIII.4 Membrane Deformation Example

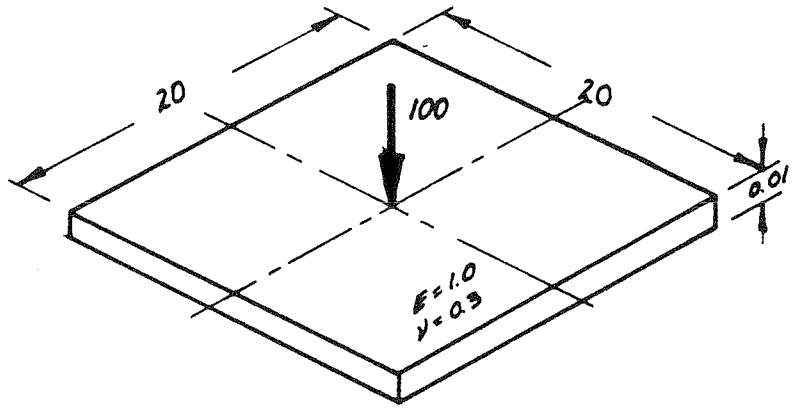

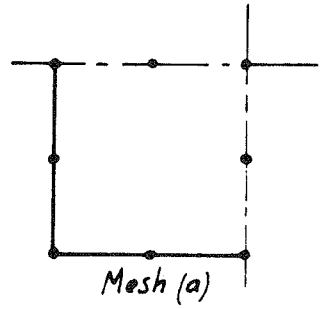

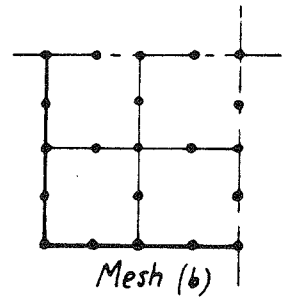

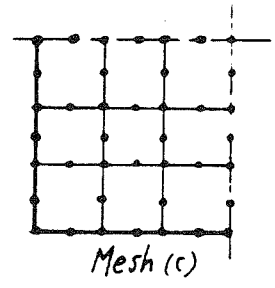

fig VIII.5 Plate Bending Example

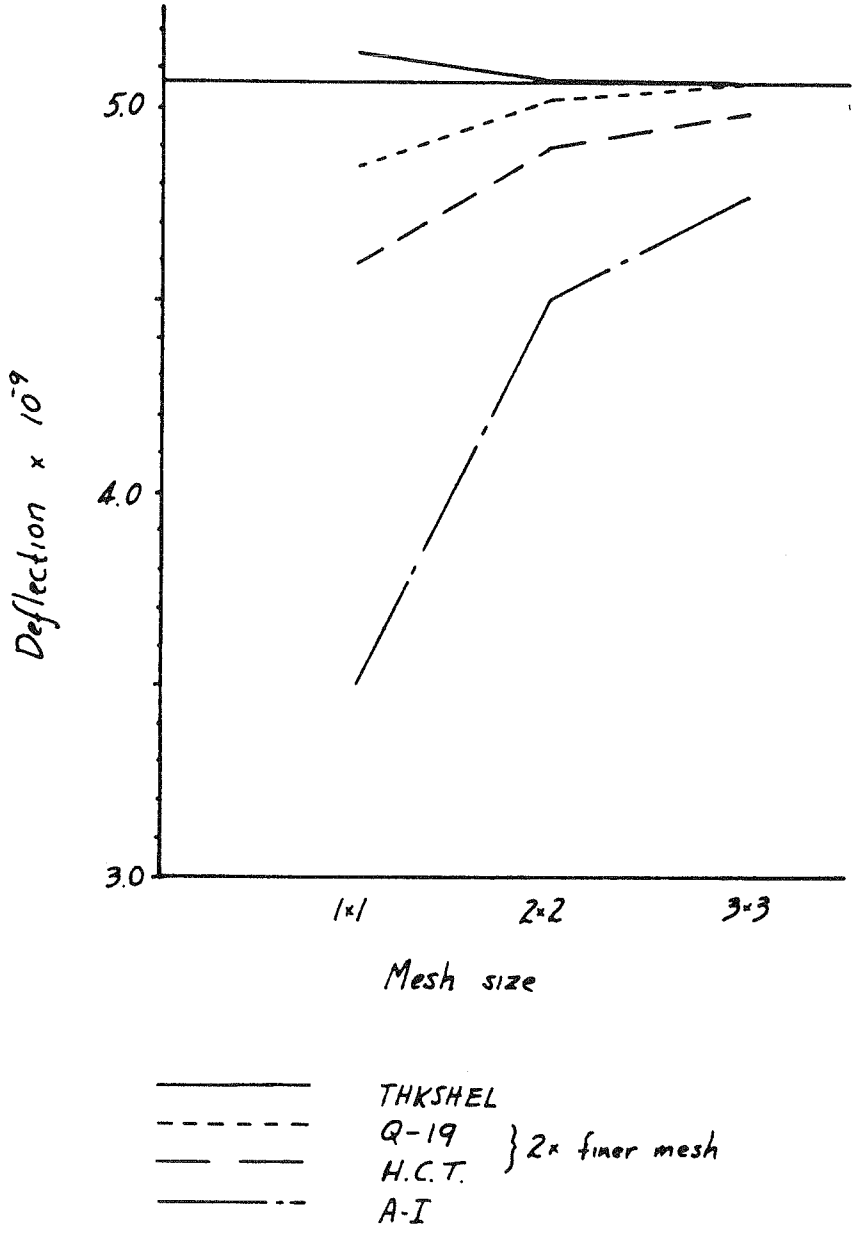

fig VIII.6 Plate Bending

Convergence of Central Displacement

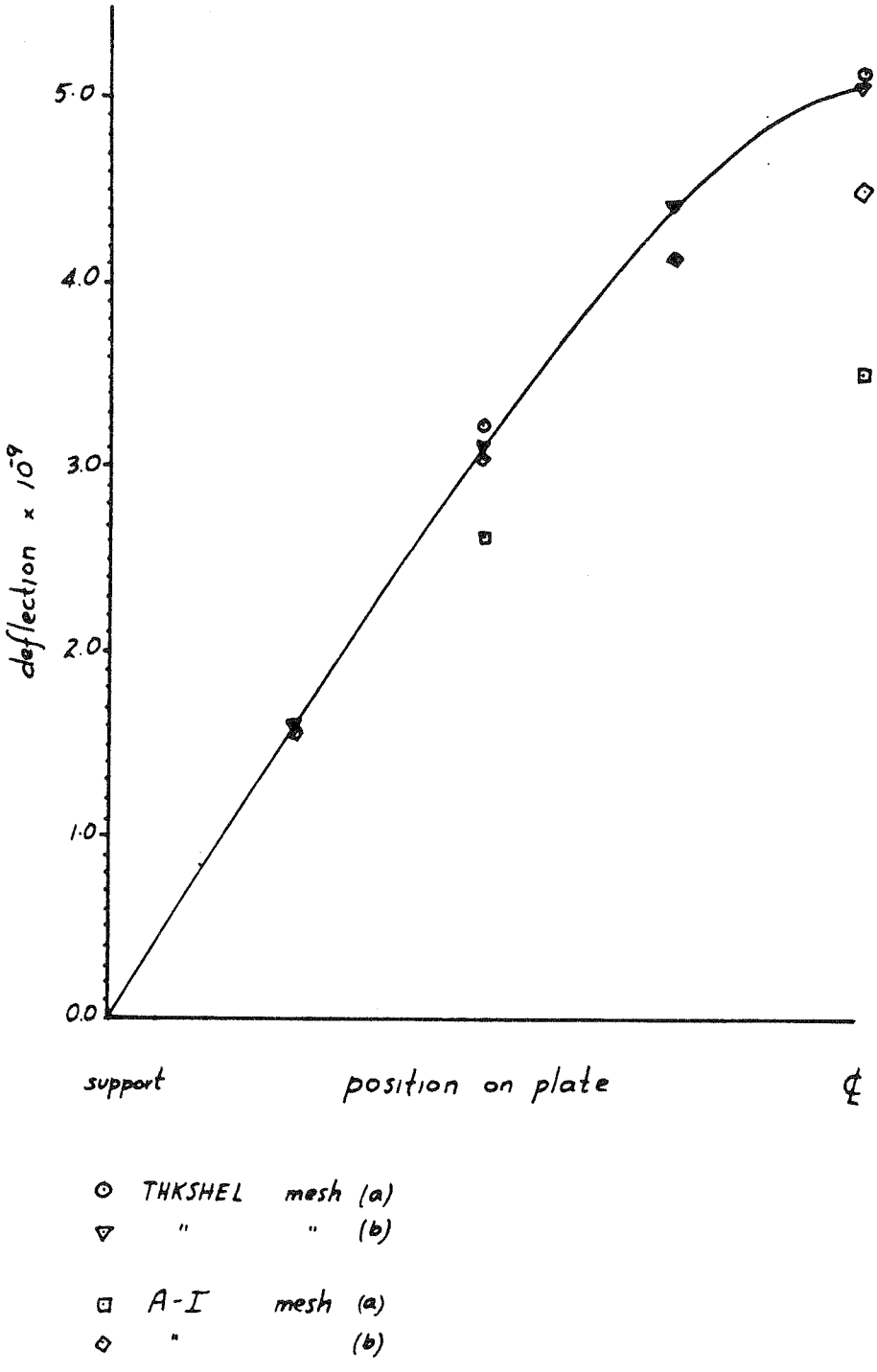

fig VIII.7 Plate Bending

Displacements on Centerline of Plate

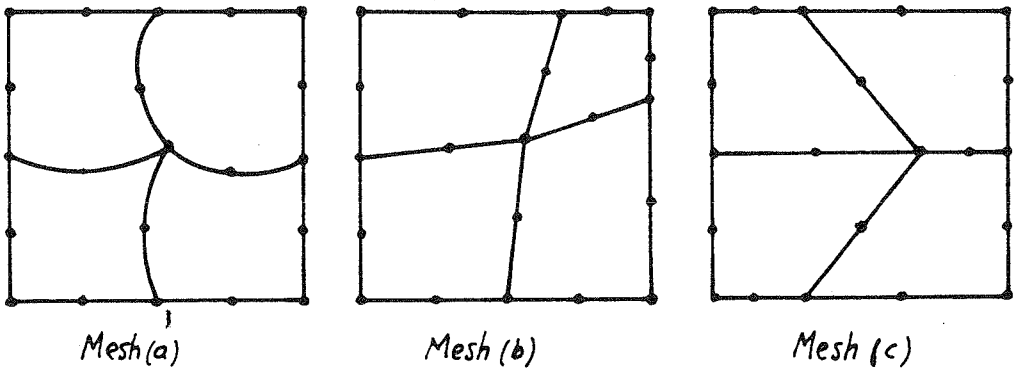

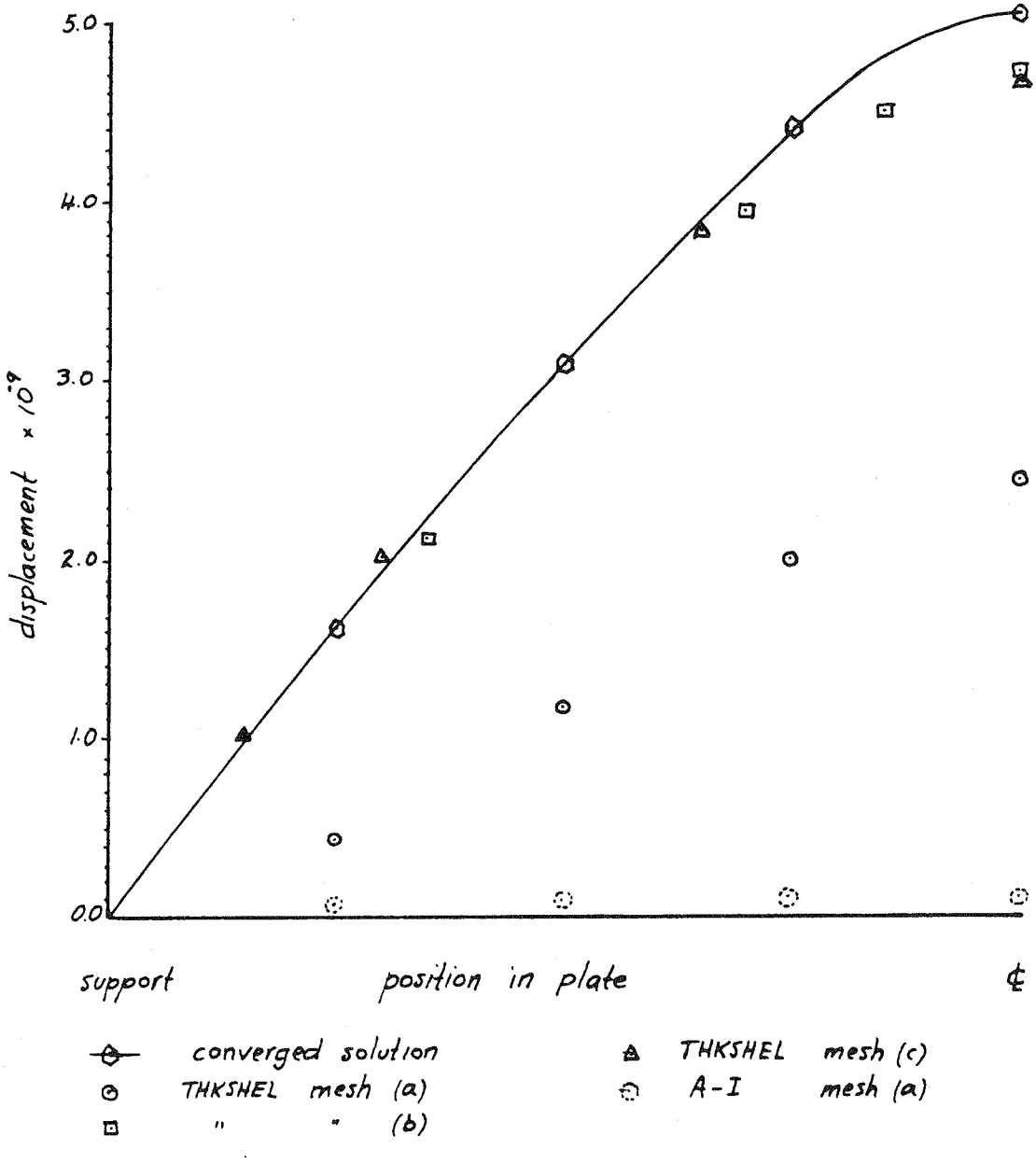

fig VIII.8 Plate Bending Non-rectangular Elements

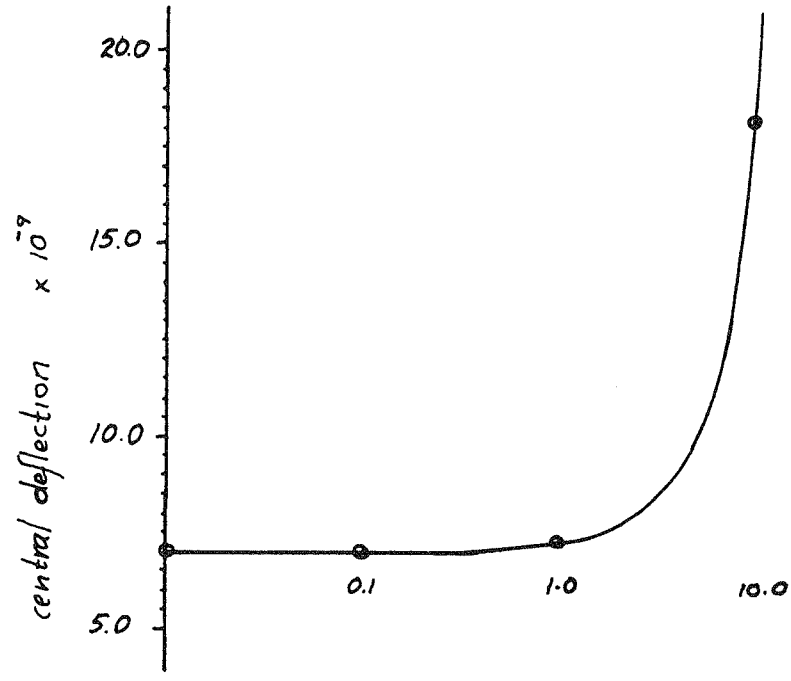

fig VIII.9 Plate Bending, Uniform Load
Effect of Thickness on Central Displacement

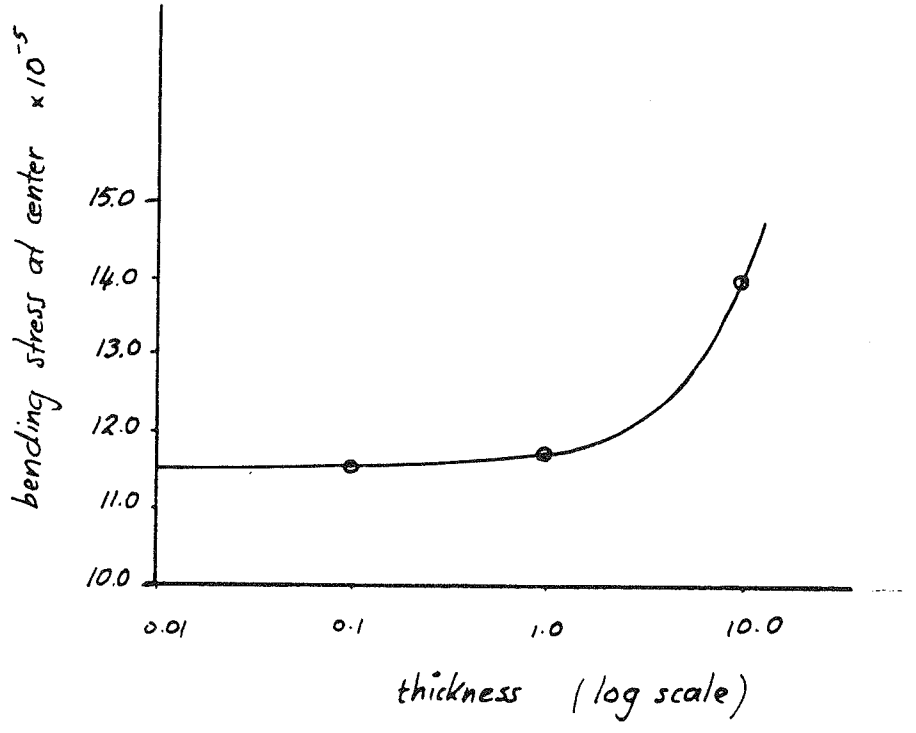

fig VIII.10 Plate Bending, Uniform Load
Effect of Thickness on Bending Stress

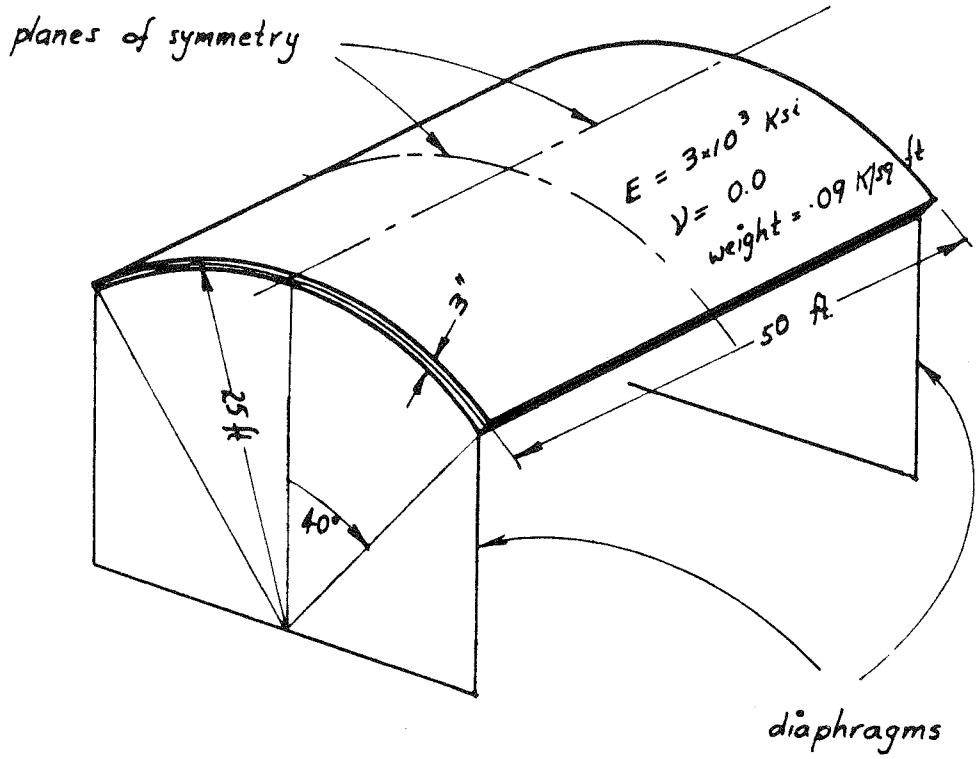

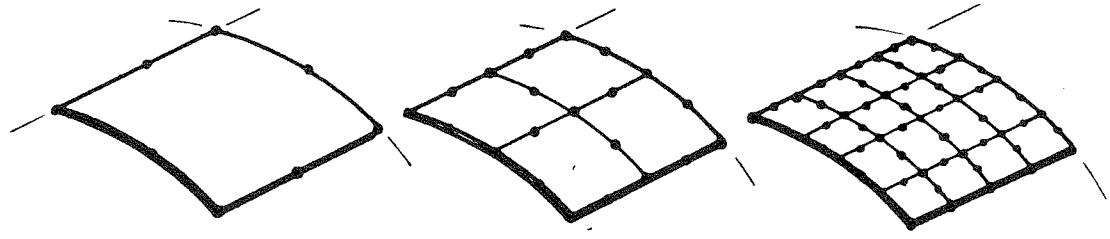

Mesh (a) Mesh (b) Mesh (c)

fig VIII.11 Thin Cylindrical Shell Roof

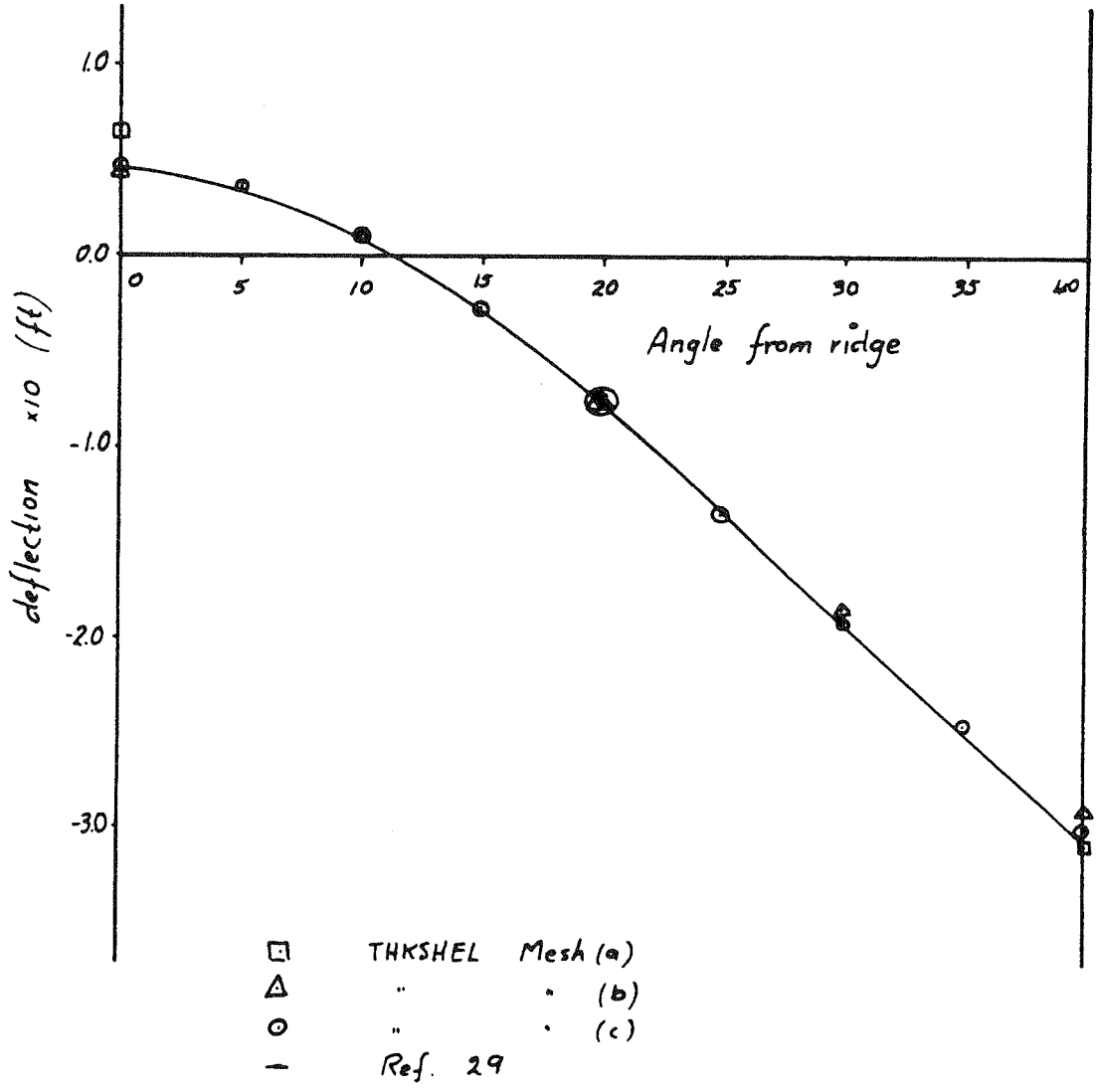

fig VIII.12 Thin Cylindrical Shell Deflection at Mid-span. THKSHEL

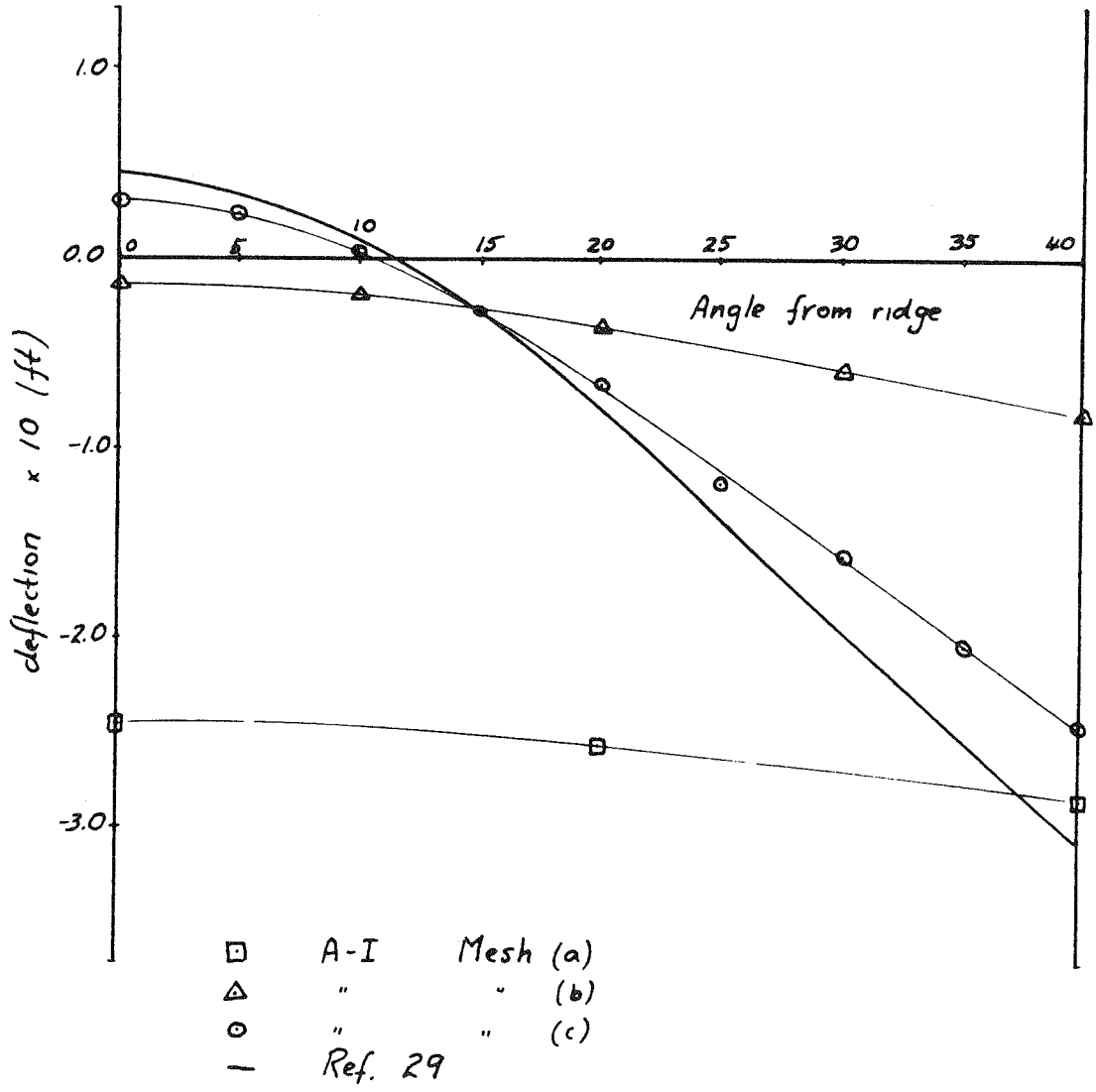

fig VIII.13 Thin Cylindrical Shell Deflection at Mid-span. A-I

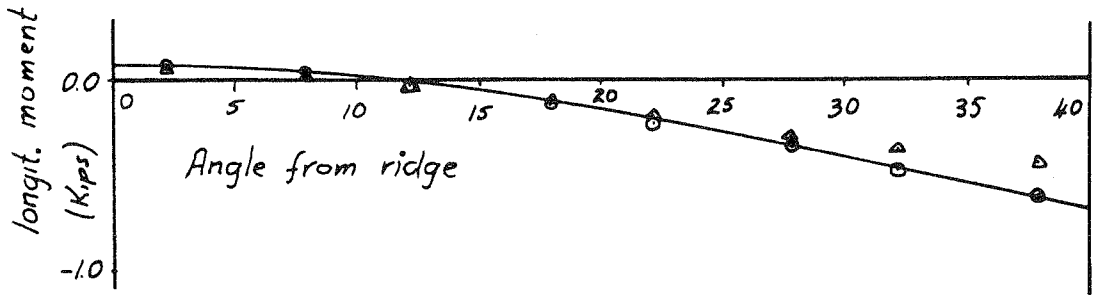

fig VIII.15 Thin Cylindrical Shell Longit. Moments at Mid-span. Mesh(c)

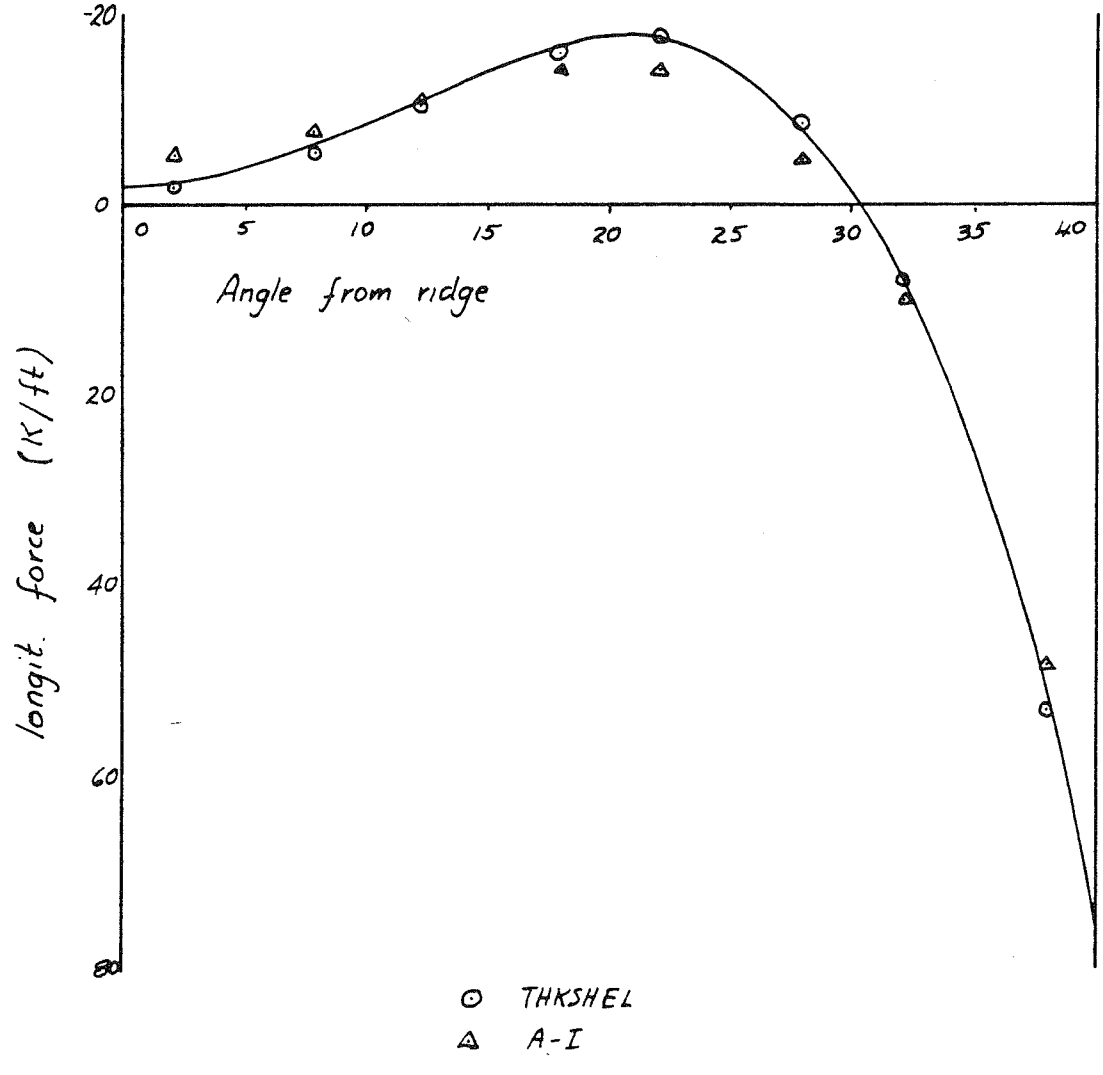

fig VIII.14 Thin Cylindrical Shell Longit. Force at Mid-span. Mesh(c)

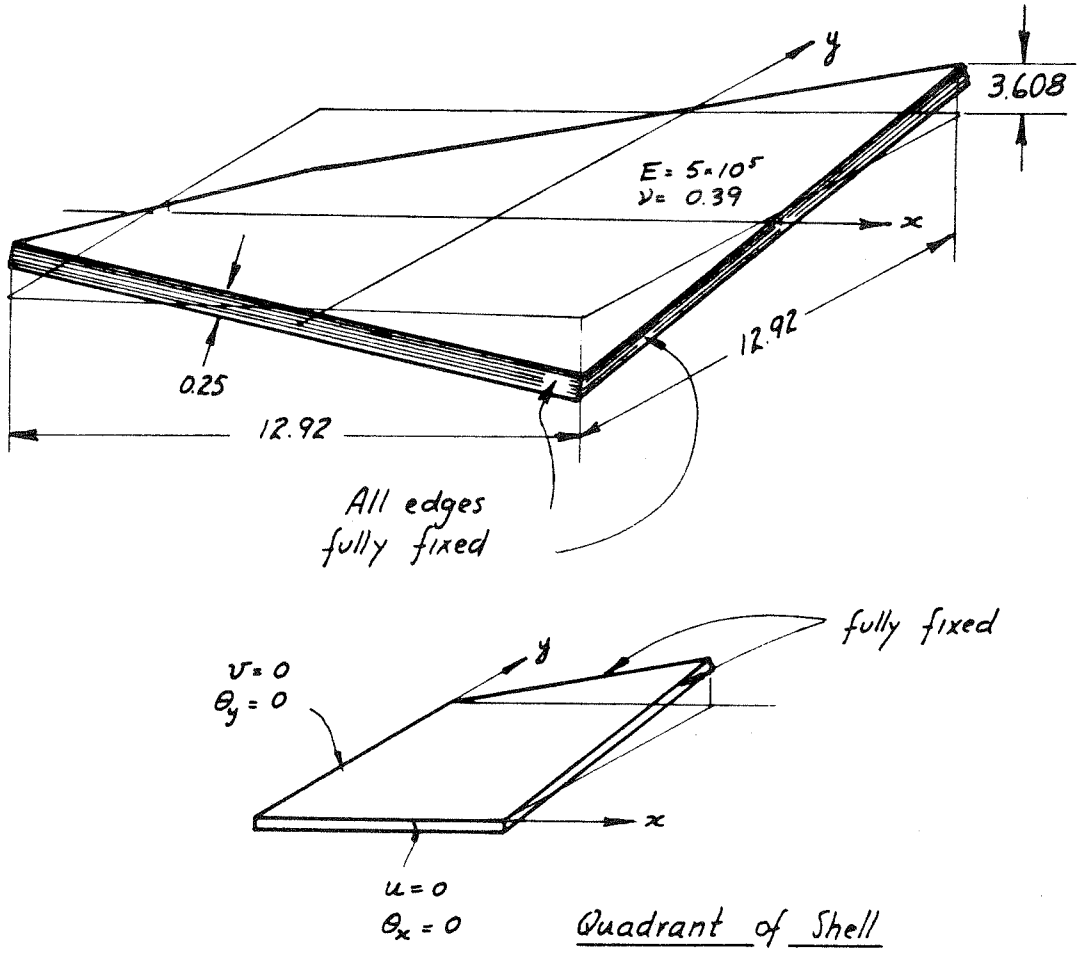

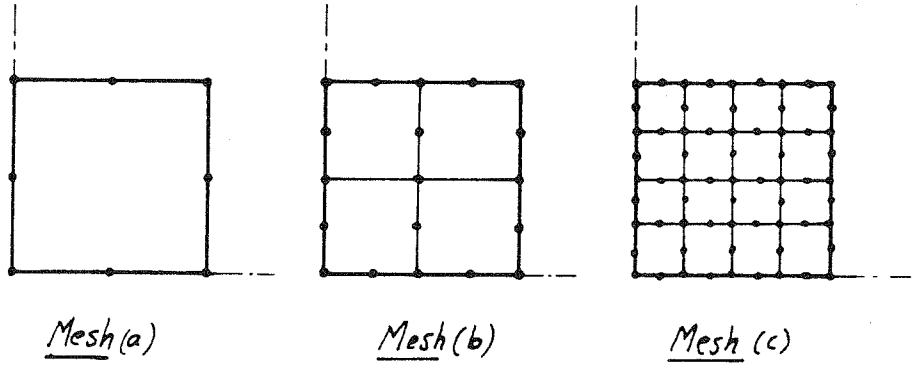

fig VIII.16 Hypar Shell

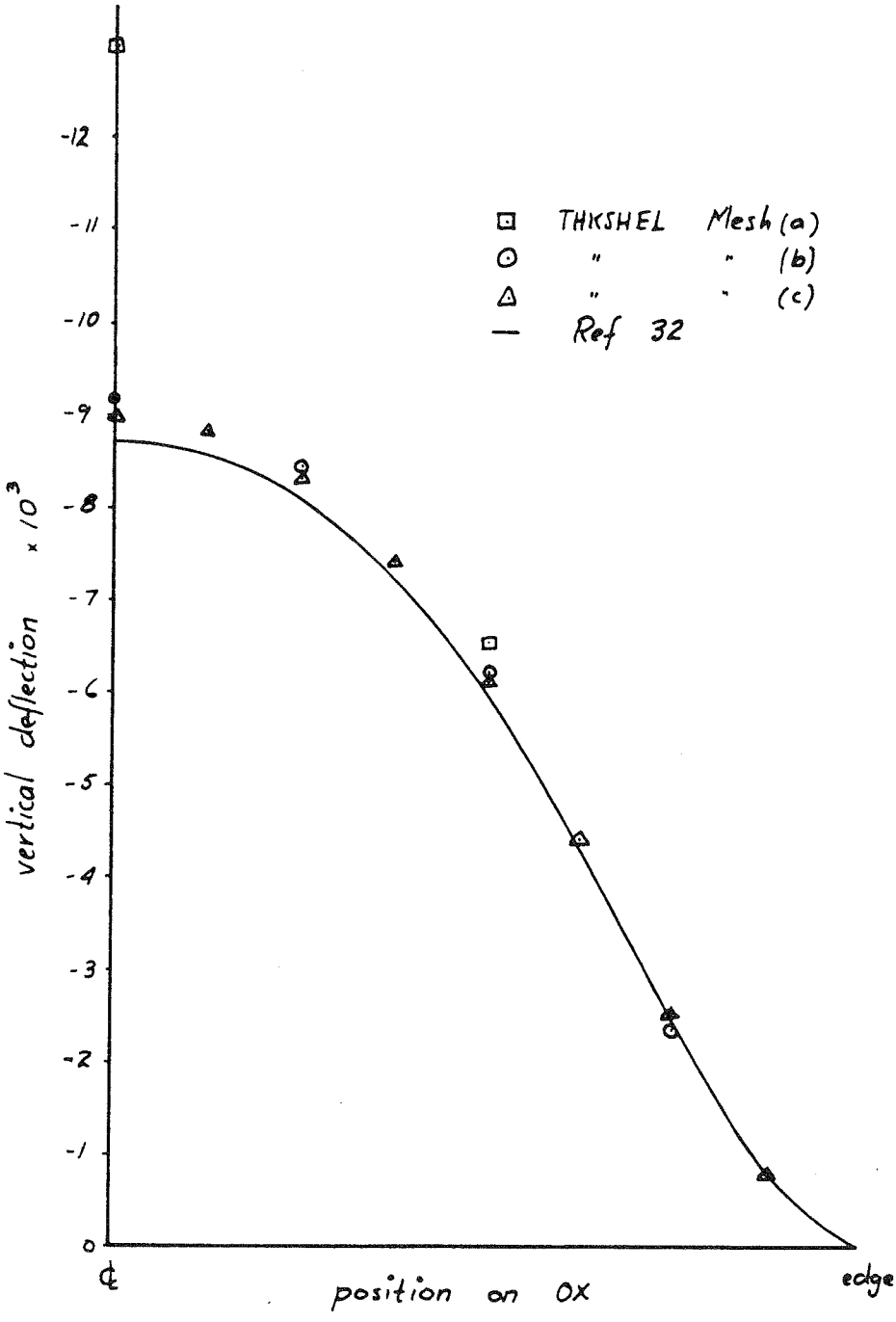

fig VIII.17 Hypar Shell

Vertical Deflections on OX. THKSHEL

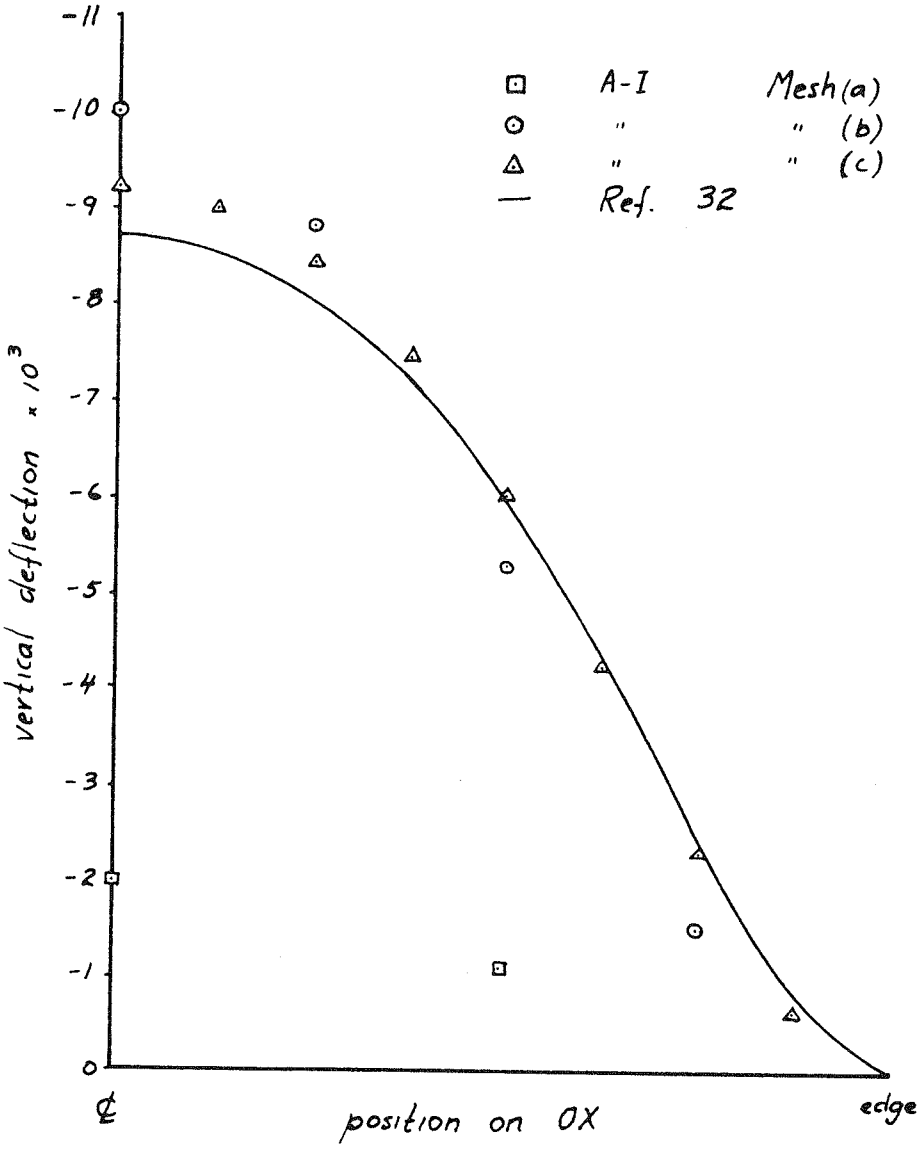

fig VIII.18 Hypar Shell

Vertical Deflections on OX A-I

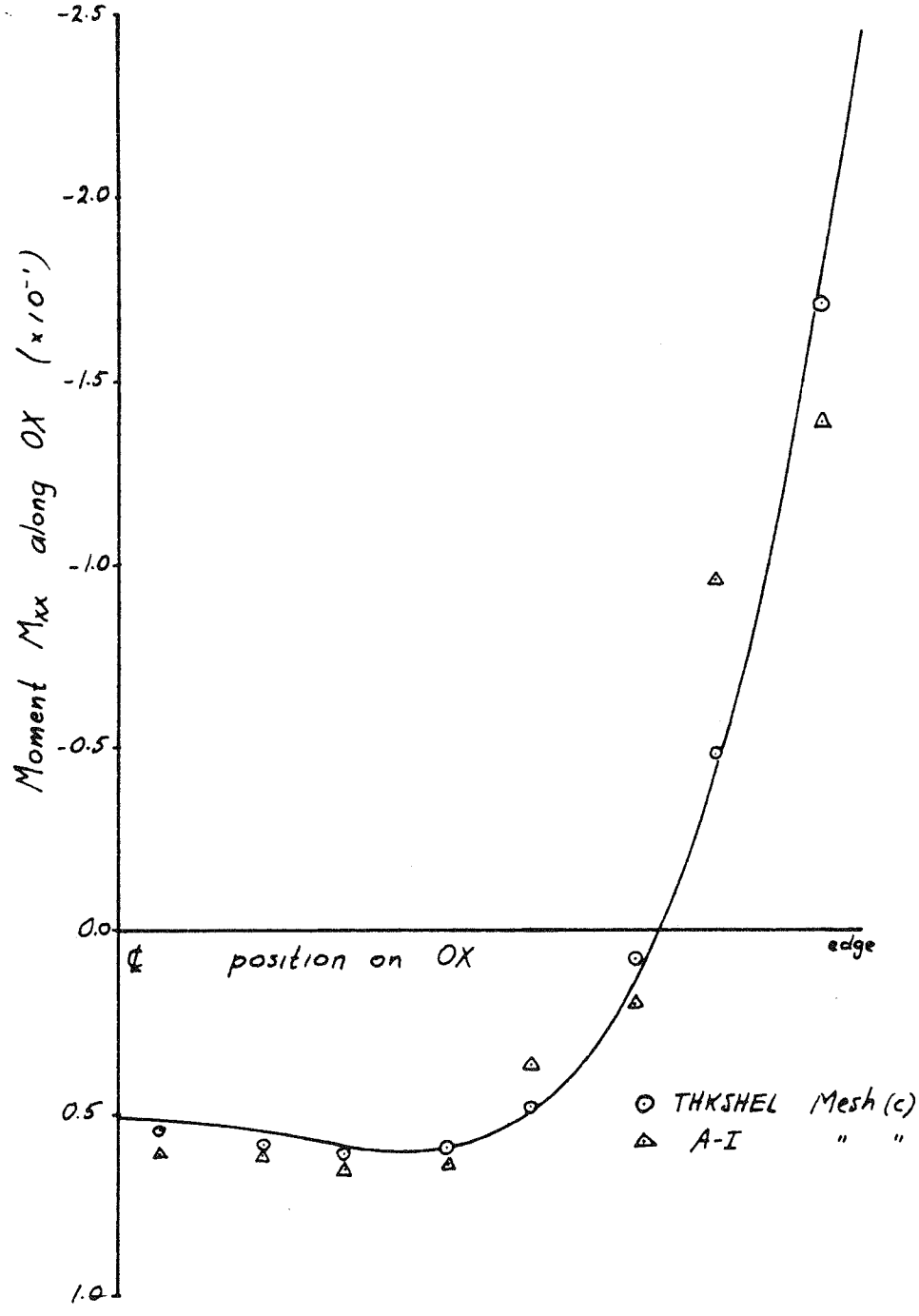

fig VIII.19 Hypar Shell

Moment M_{xx} along OX Mesh (c)

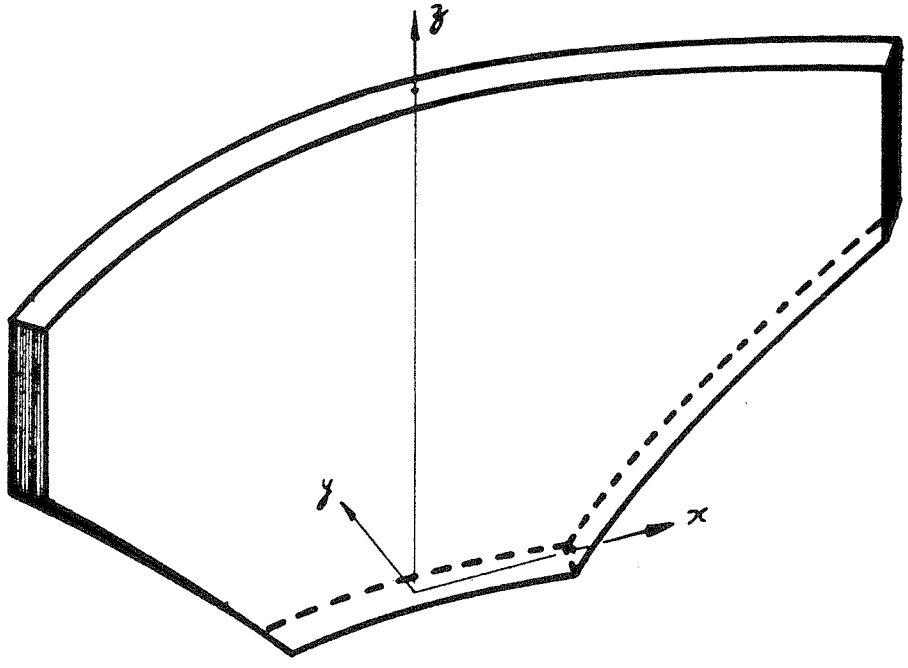

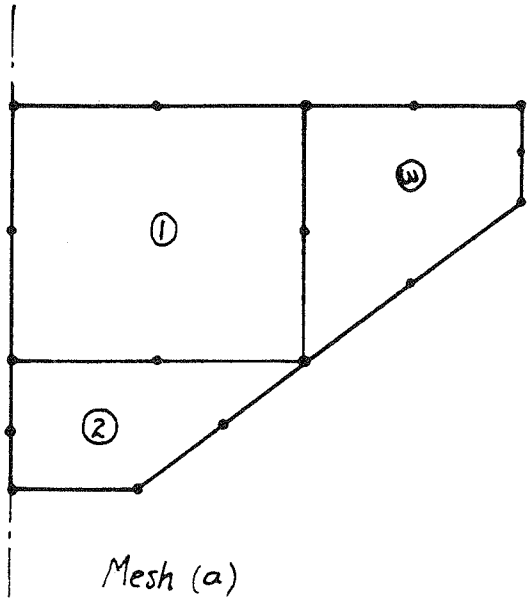

fig VIII.20 Arch Dam Number 1

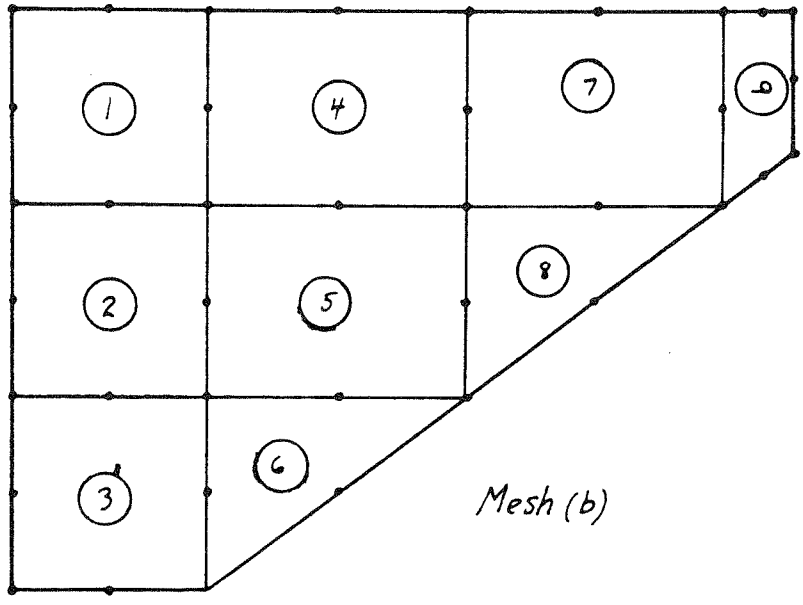

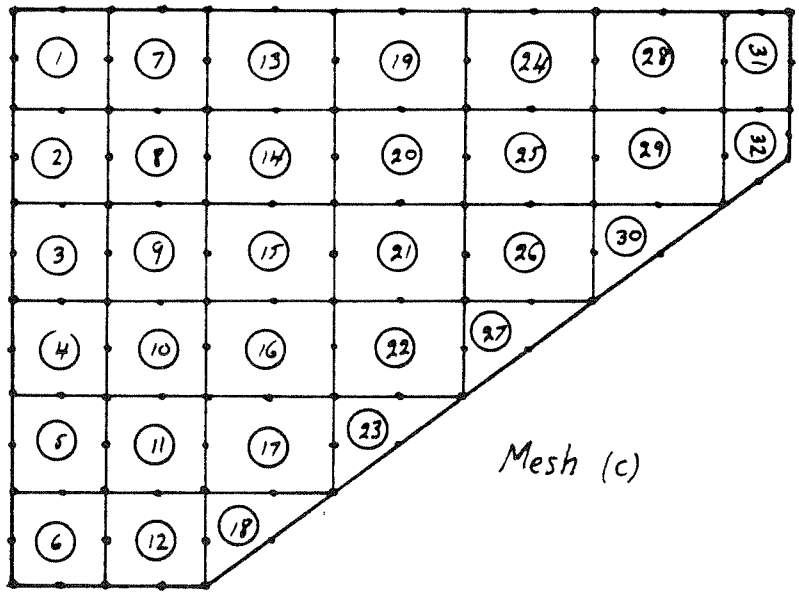

fig VIII.21 Arch Dam Number 1

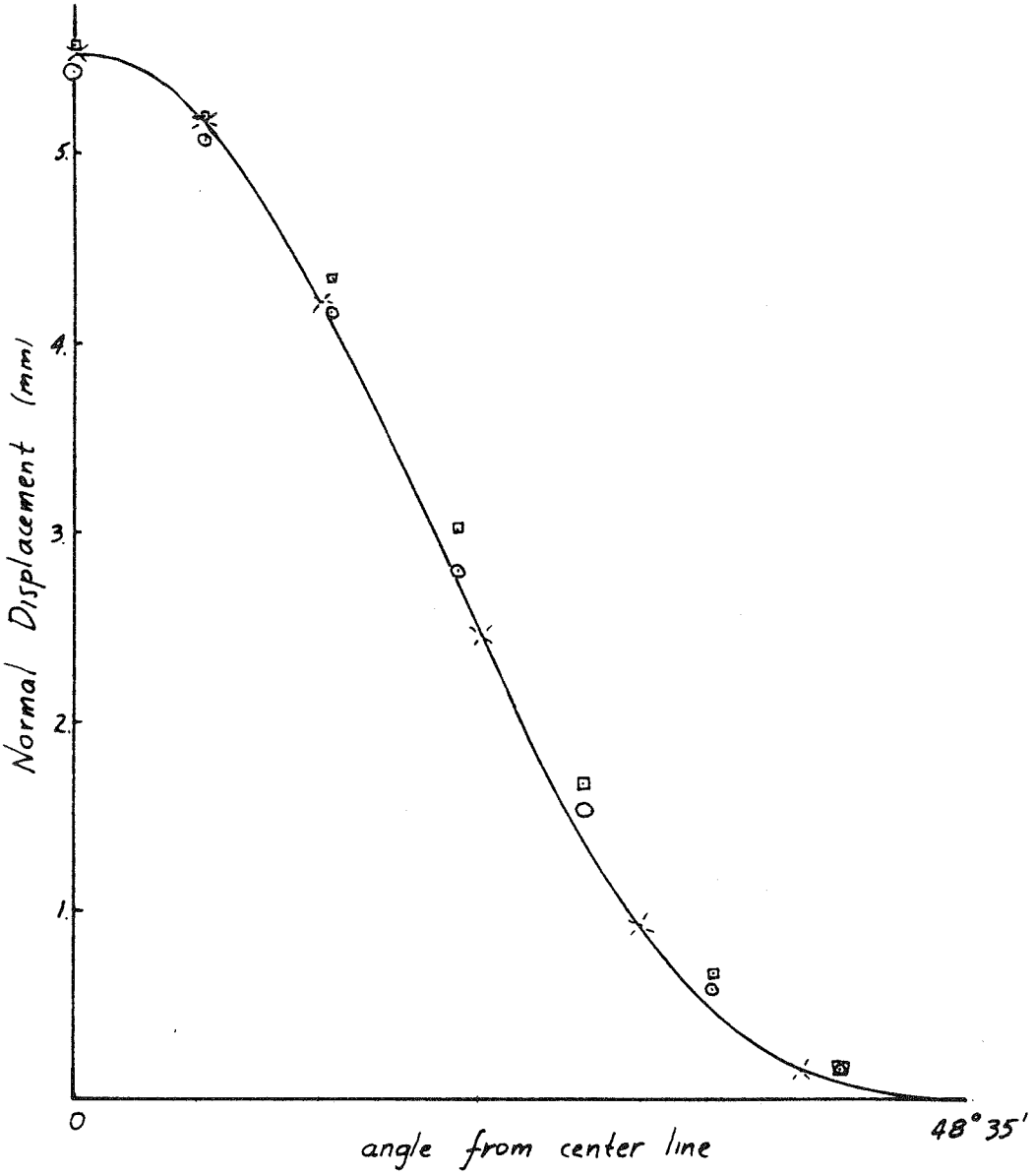

fig VIII.22 Arch Dam Number 1

Normal Displacements along 80m. level

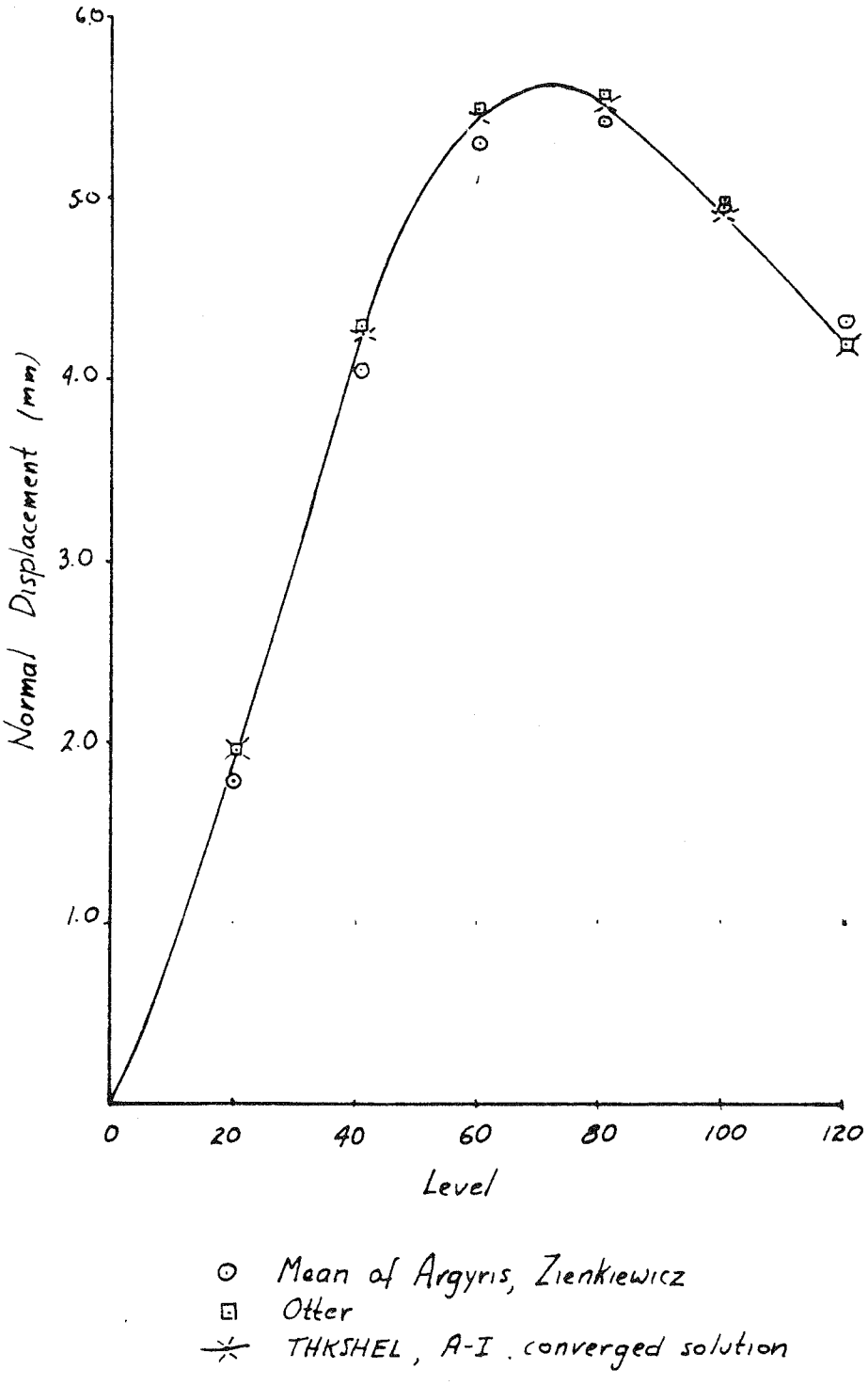

fig VIII.23 Arch Dam Number 1

Normal Displacements at Centerline

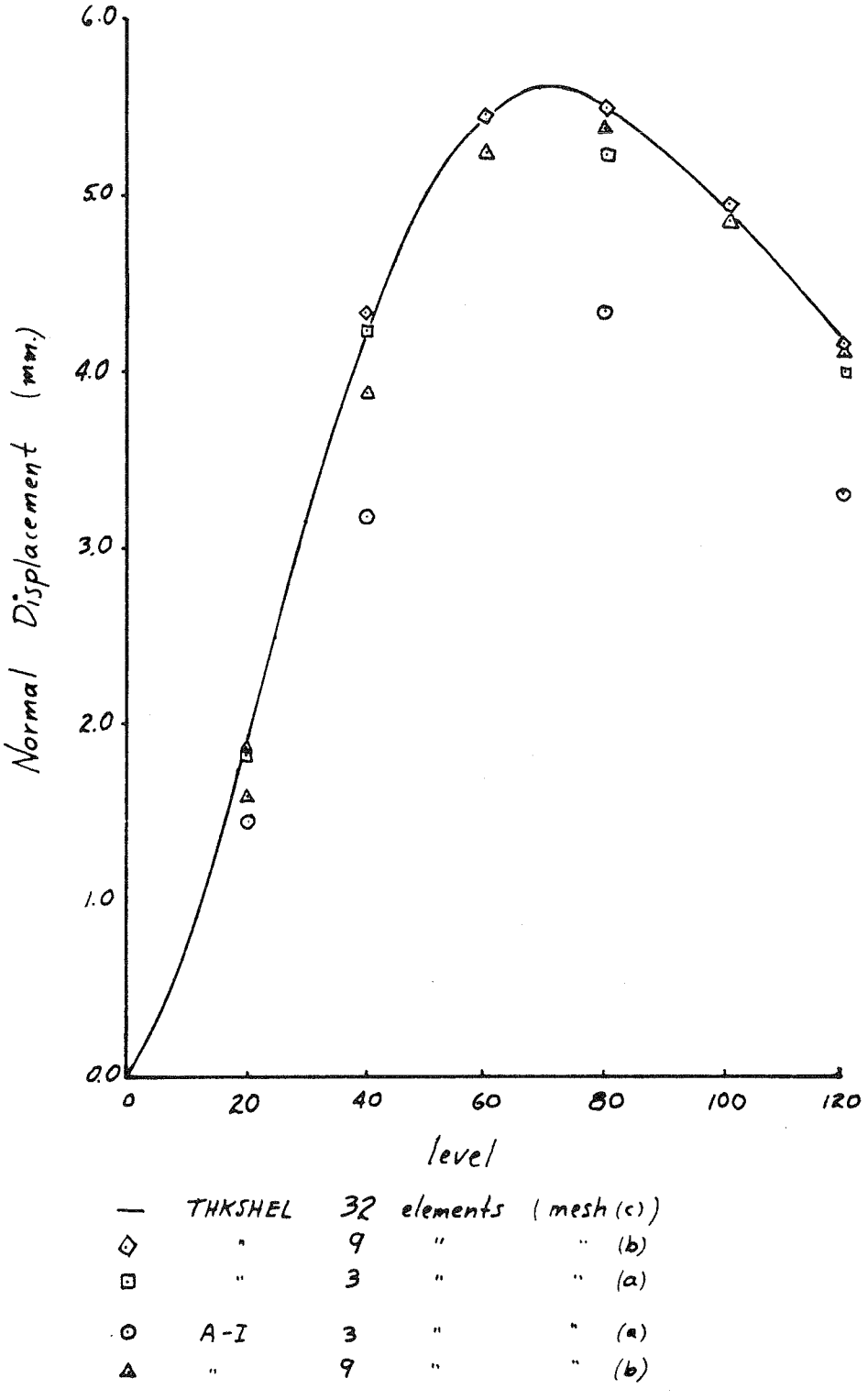

fig VIII.24 Arch Dam Number 1

Normal Displacements at Centerline. Convergence.

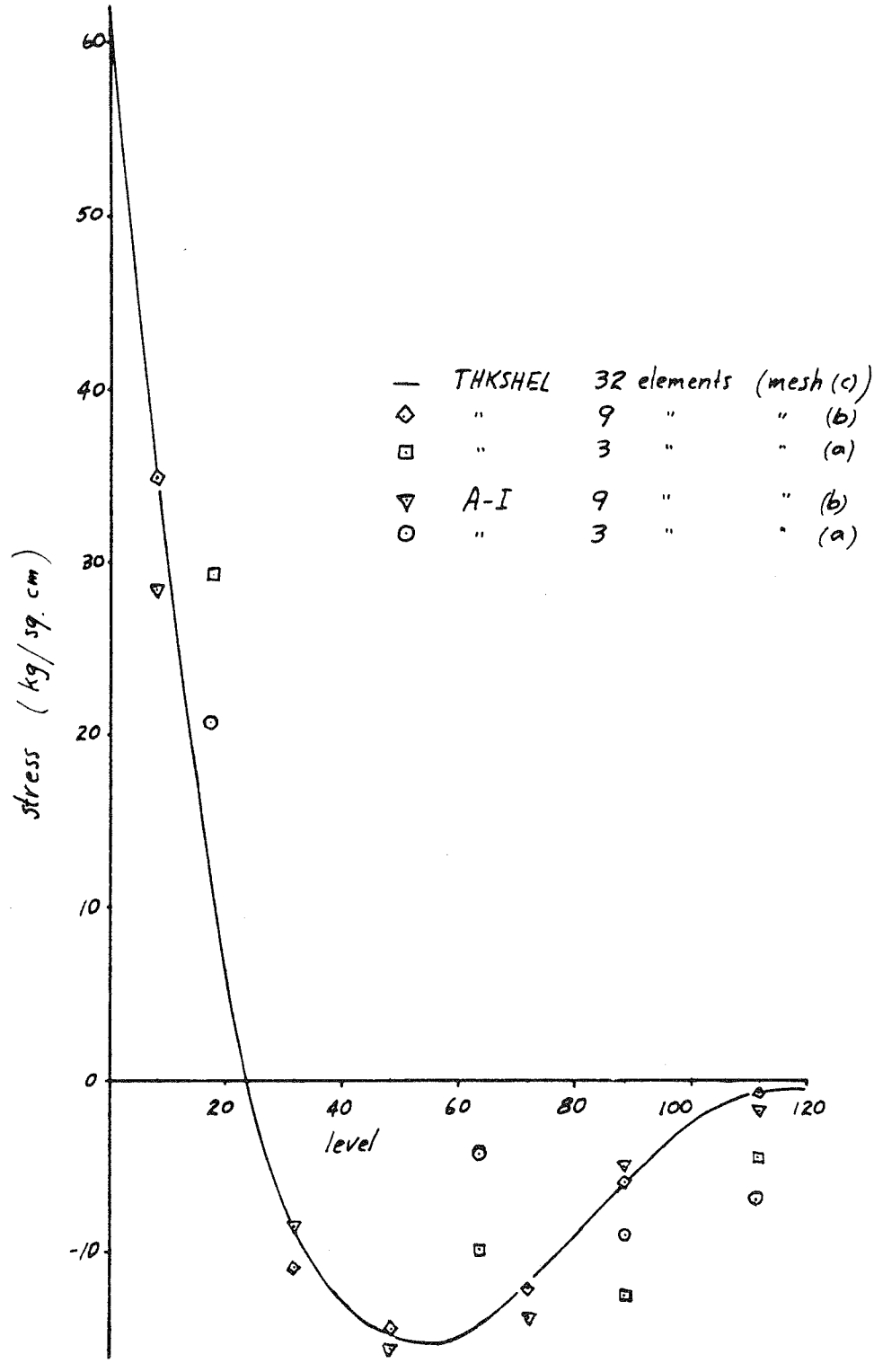

fig VIII.25 Arch Dam Number 1

Convergence of Vertical Stresses on Centerline. Water Face.

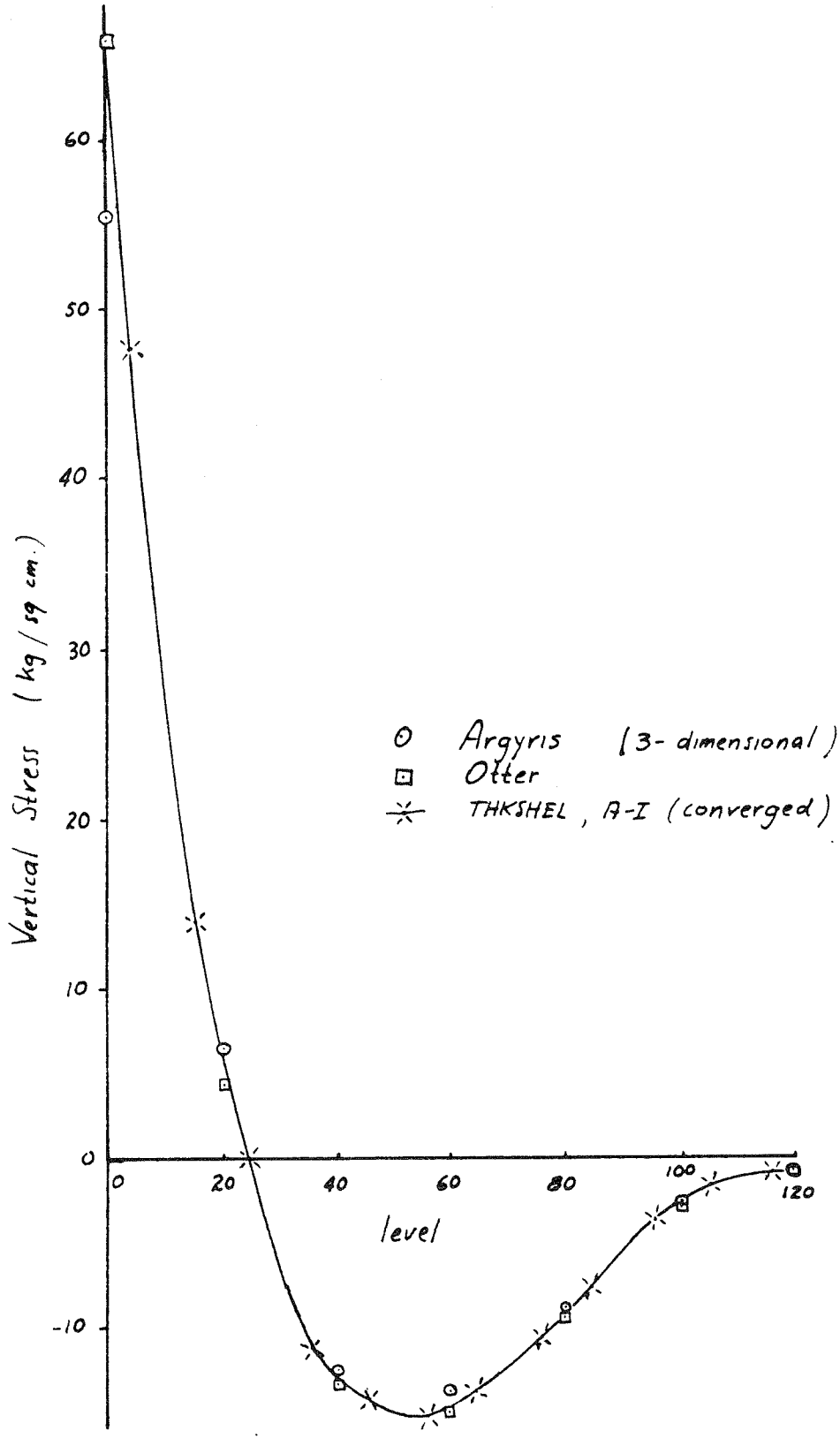

fig VIII.26 Arch Dam Number 1

Vertical Stresses on Centerline. Water Face.

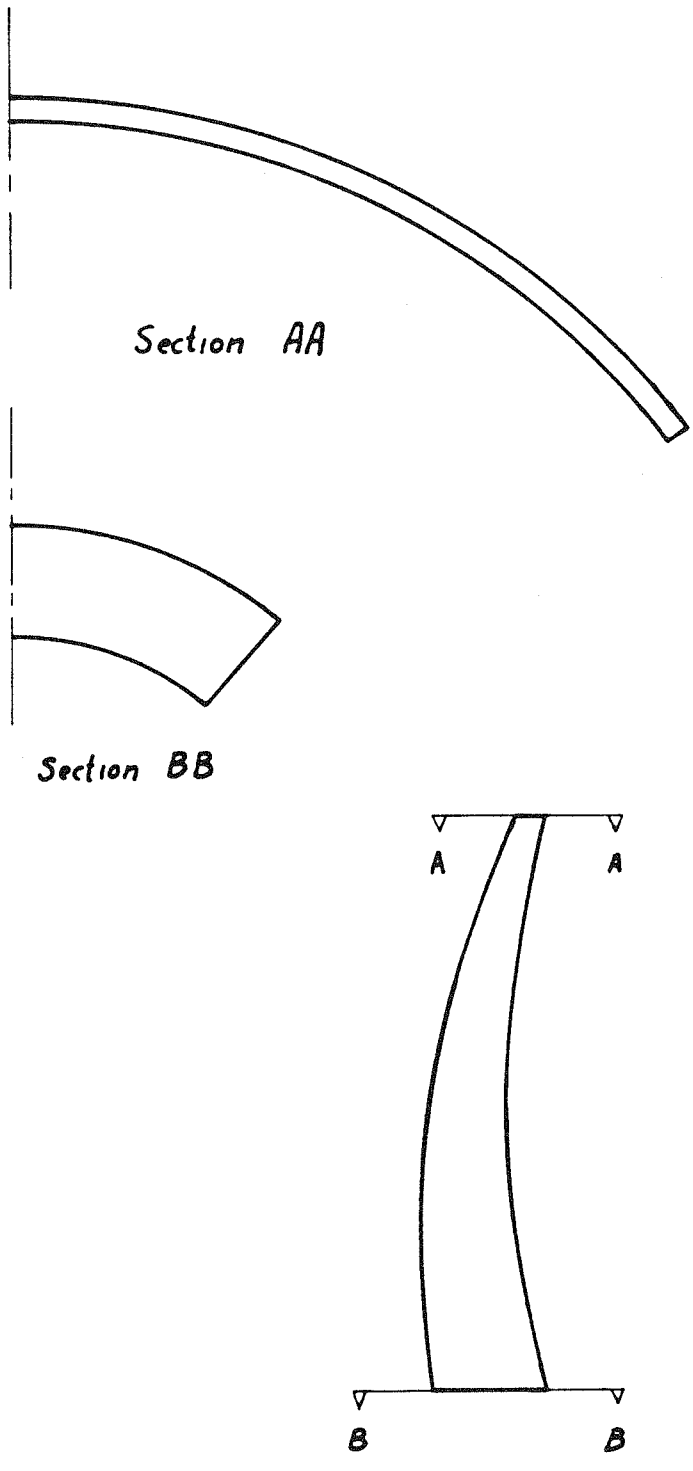

fig VIII.27 Arch Dam Number 5

Cross Sections

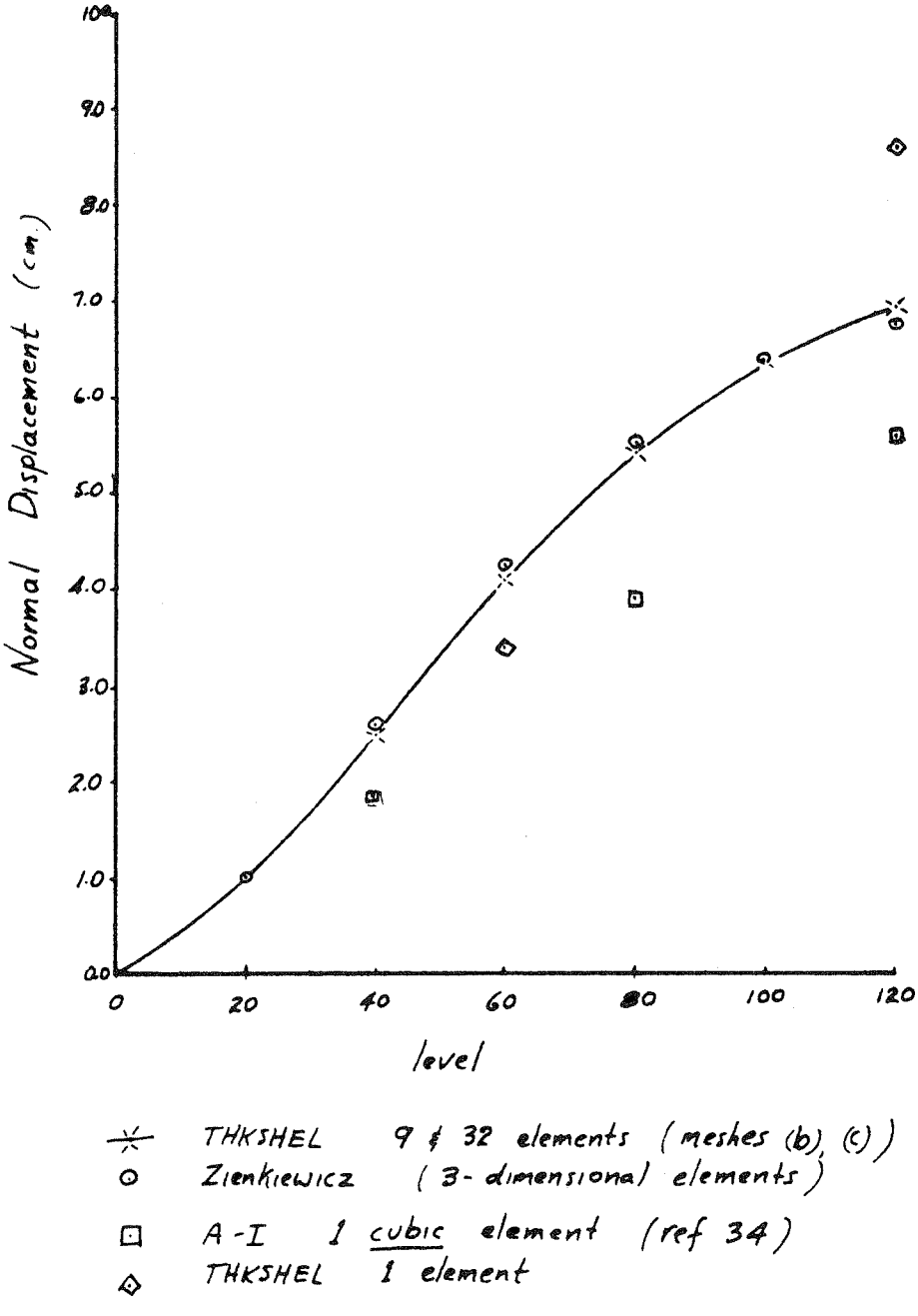

fig VIII.28 Arch Dam Number 5

Radial Displacements on Centerline

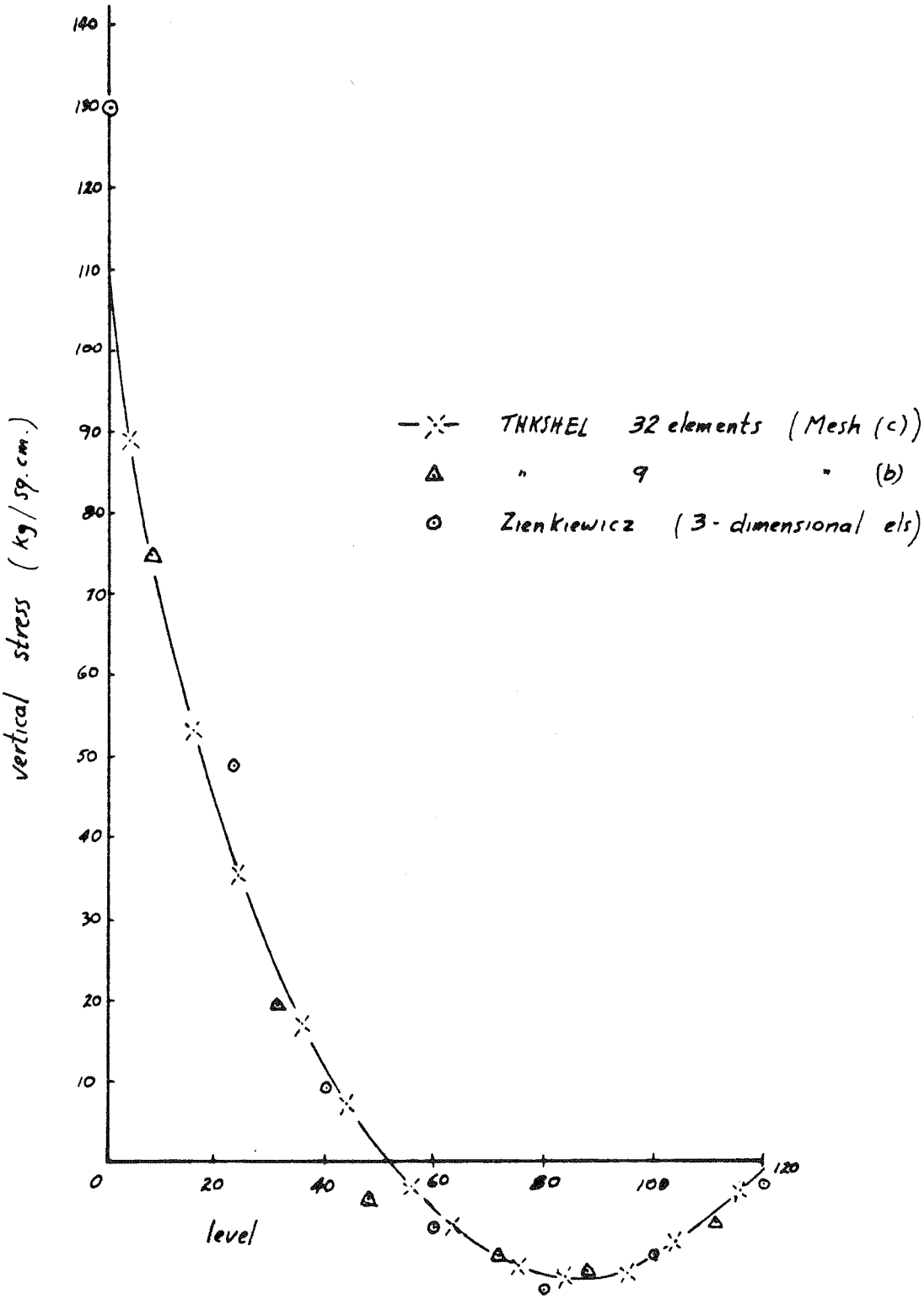

fig VIII.29 Arch Dam Number 5

Vertical Stresses on Centerline. Water Face.

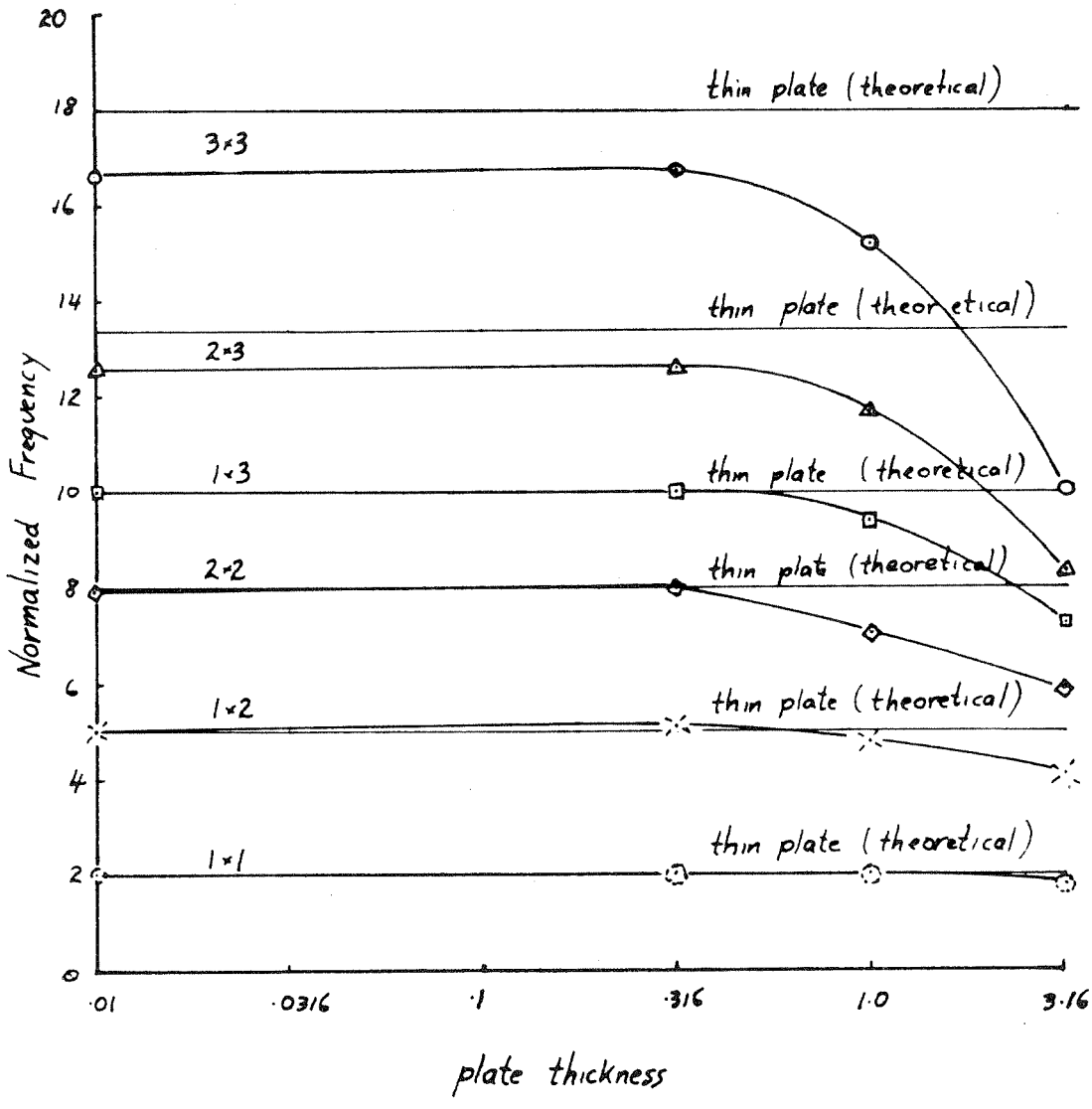

fig VIII.30 Plate Vibration

Effect of Thickness on Normalized Frequencies

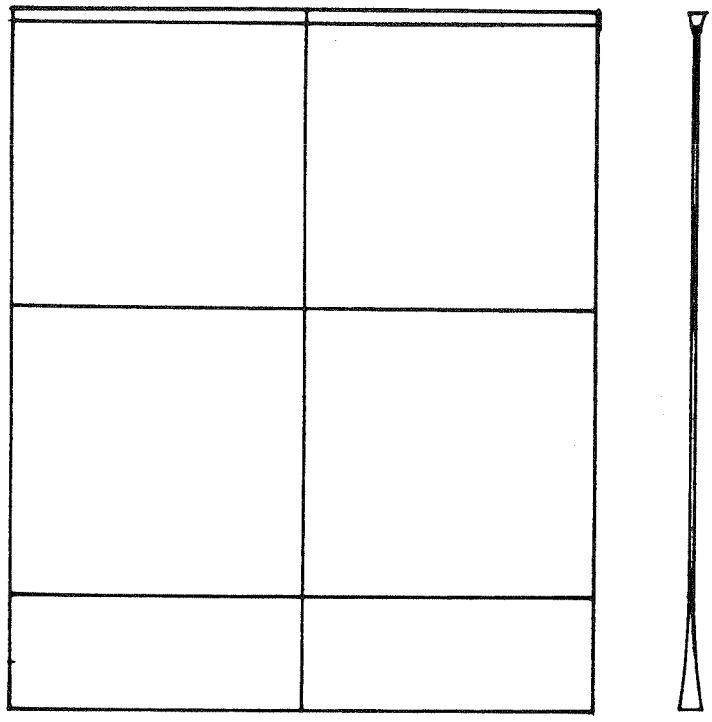

Mesh (a)

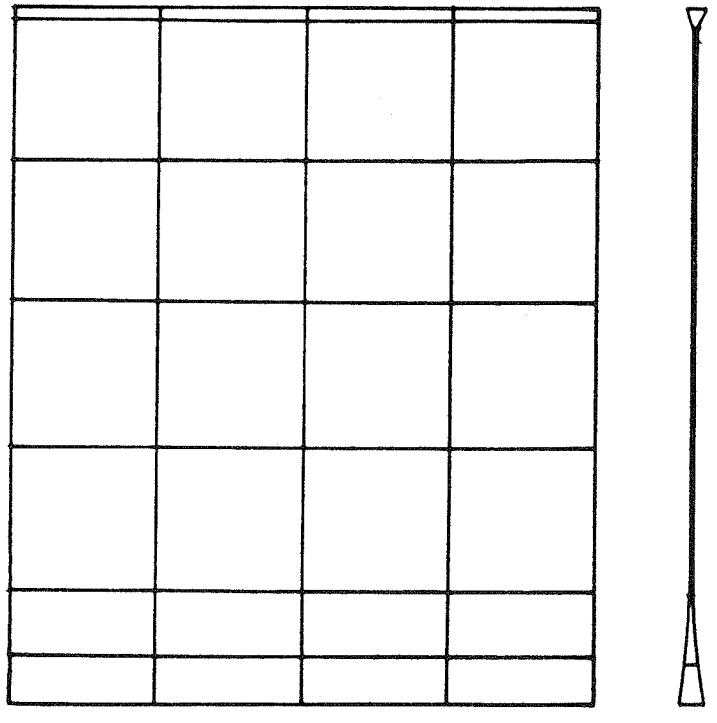

Mesh (b)

fig VIII.31 Cooling Tower Meshes

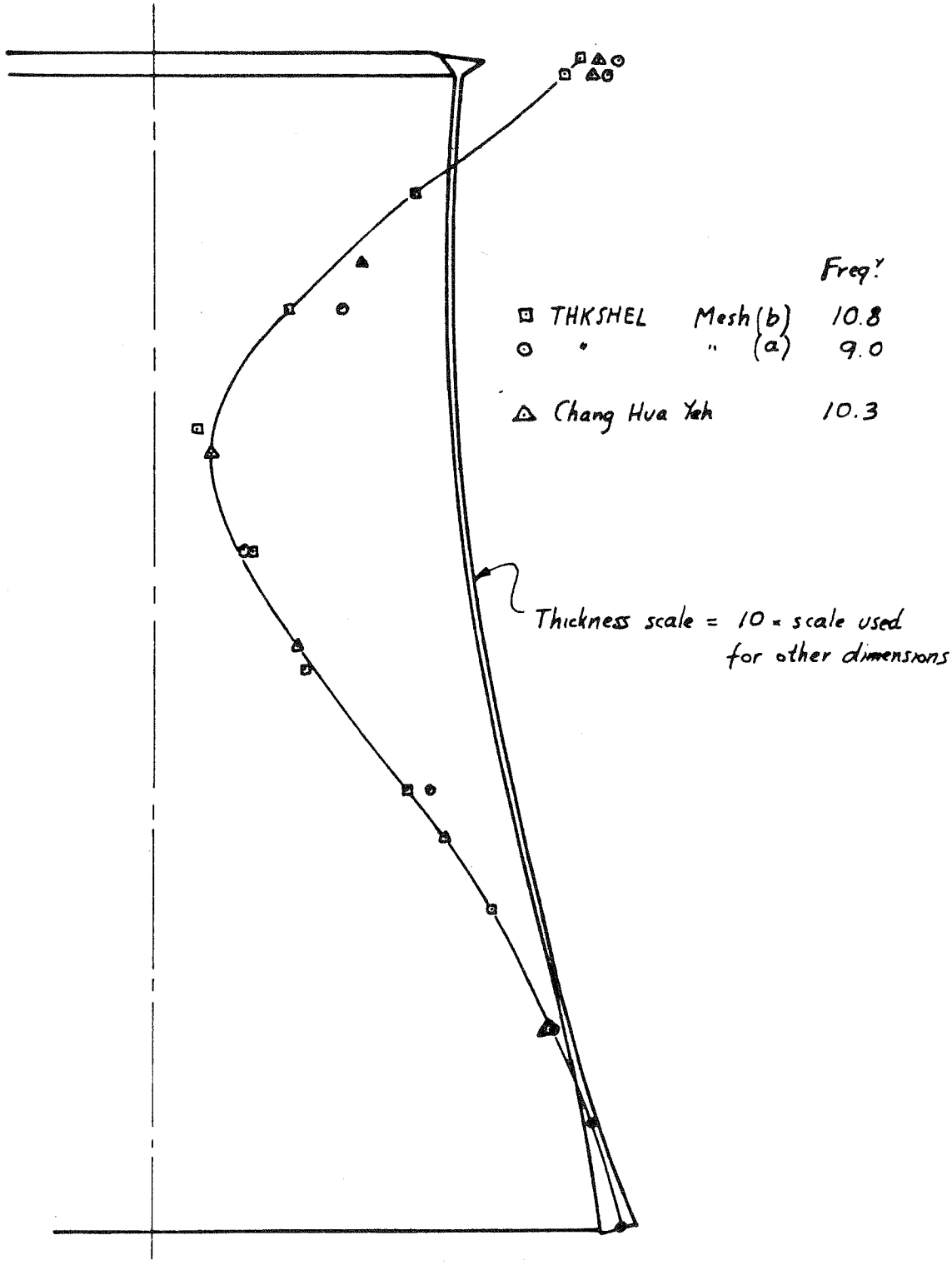

fig VIII.32 Cooling Tower Vibration

Horiz. Displacements. (Measured from Original Position)

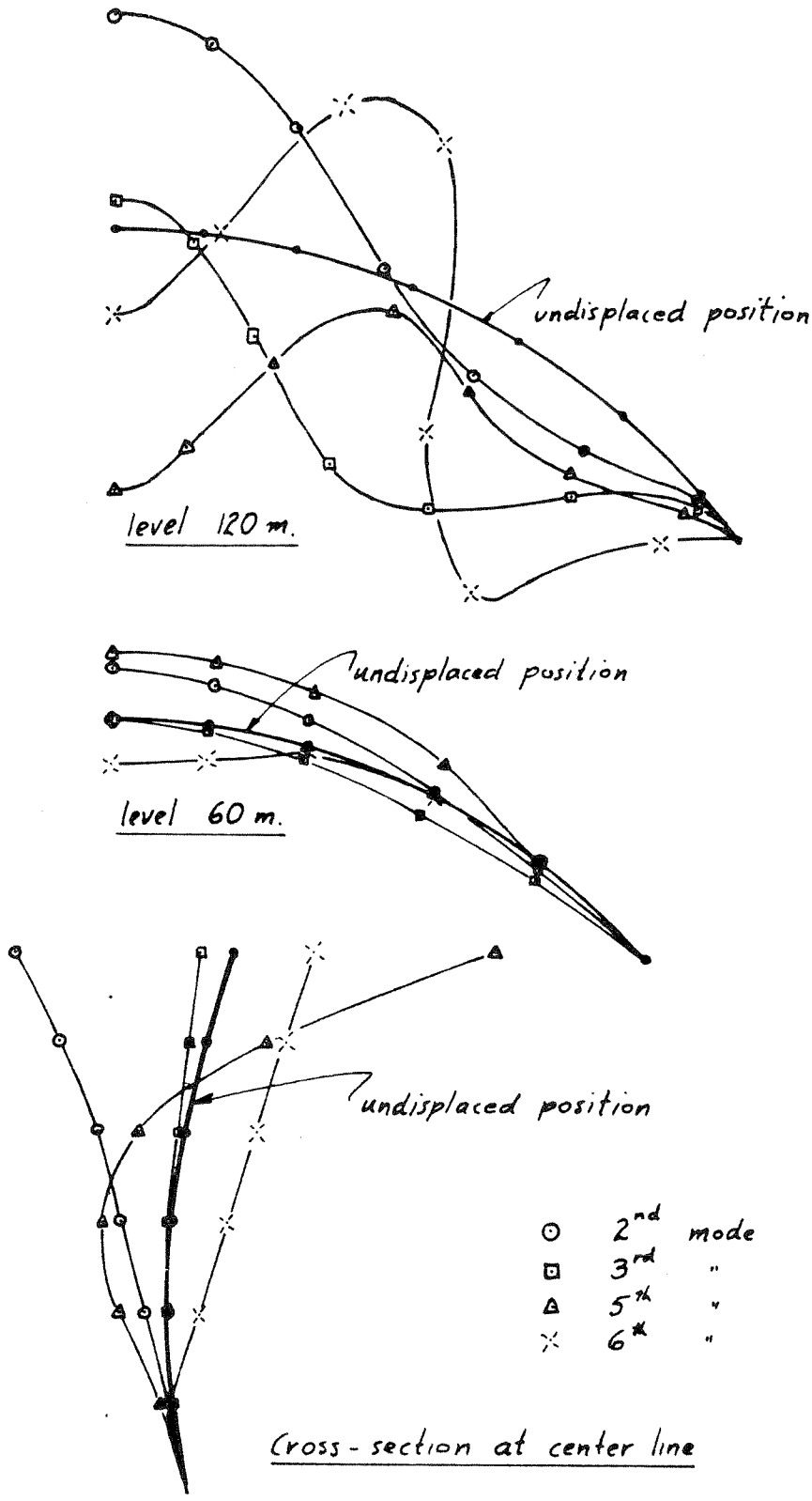

fig VIII.33 Arch Dam Number 5. Vibration Symmetric Modes (Horiz. Dsps.)

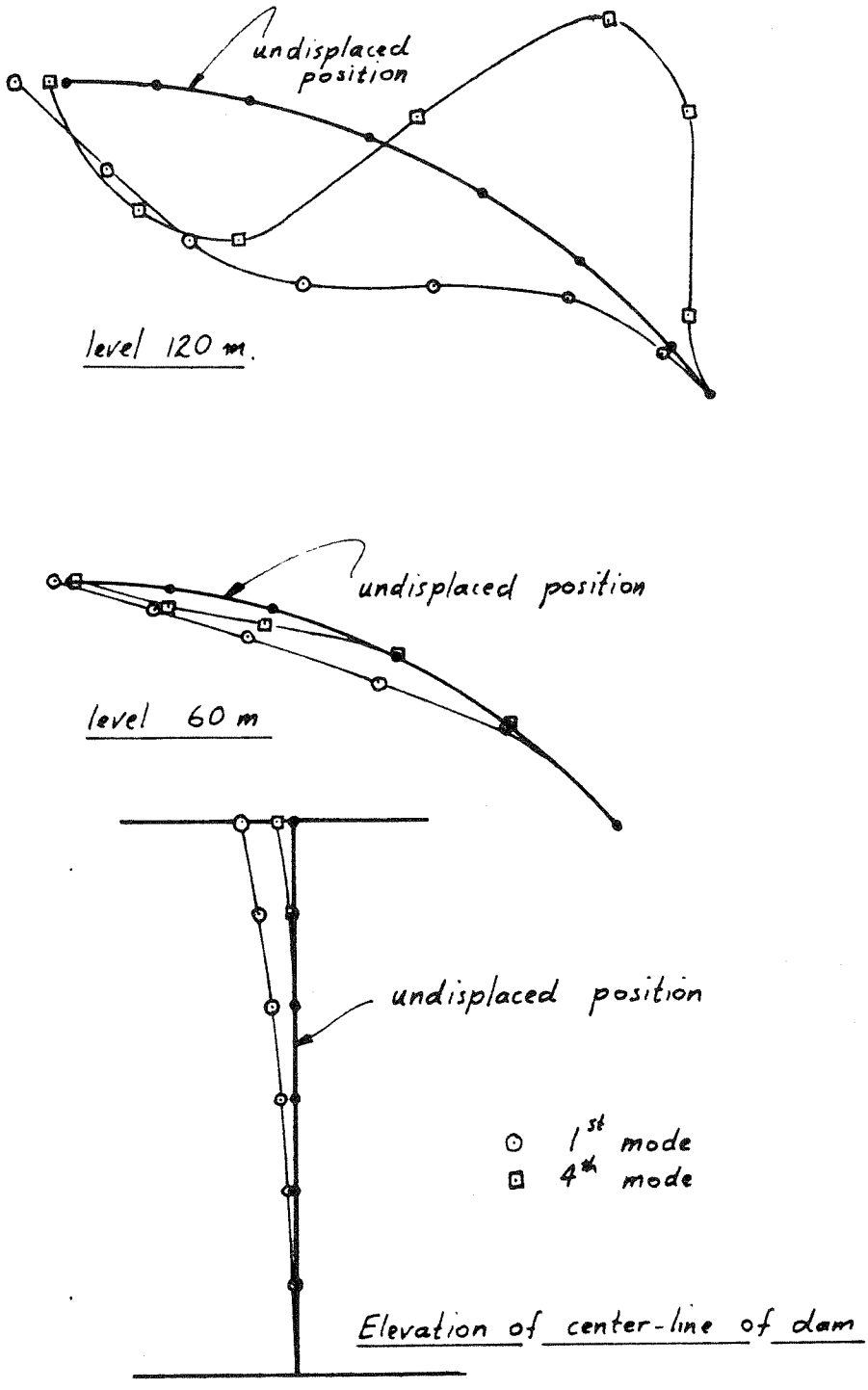

fig VIII.34 Arch Dam Number 5. Vibration Anti-symmetric Modes (Horiz. Disps)

IX. CONCLUSIONS AND RECOMMENDATIONS FOR FURTHER RESEARCH

The shell element THKSHEL has been shown to be applicable to a wide range of shell problems. The kinematic and geometric assumptions used in the formulation ensure that the element will accurately represent situations where the curvature of the shell is significant, and where the transverse shear stresses are large enough that shear deflections must be considered. At the same time, the important class of shells, thin enough that these can effects can be ignored, is also efficiently represented by the same element. Accuracy, comparable with thin-shell finite elements currently in use, was attained, when the element mesh finenesses were such as to give the same equation-solving time in each case. It is therefore a particularly suitable element for use when parts of a shell could be represented by thin shell elements, but parts could not, due to large thickness, excess curvature or high transverse shears. Similarly, since high frequency modes of vibration can cause high transverse shear stresses in shells and plates, which could otherwise be solved satisfactorily for the static situation using thin-shell elements, THKSHEL provides a useful element to represent either situation.

Since the efficiency decreases as the shape of the elements departs from rectangularity, it is undesirable to divide the shell into a mesh containing many elements whose shape is markedly "non-rectangular". Small errors are introduced also, even into the converged solution, if the $\eta = 1$ and the $\eta = -1$ edges do not converge towards parallelism as the mesh is refined. However, in most structural applications, these

situations can be readily avoided. If necessary, the mesh can follow the geodesic lines of the shell's mid-surface, for then the elements will automatically converge to small rectangular elements.

Perhaps one of the greatest advantages of this type of shell element (common to all shell elements derived from three-dimensional elements) is the small amount of expertise in shell theory that is required to understand the behavior of the element. A curved shell element, involving virtually any level of desired mechanical behavior can be formulated without any knowledge of the intricasies of the coordinate geometry of curved surfaces (necessary to even the simplest closed-form method of solution). Only a basic knowledge of the three-dimensional field equations of elasticity and of the transformation of strains from global to local coordinate systems, is required. This knowledge is needed for three-dimensional elements also, so the two and three dimensional analyses are unified into one general method of analysis. This is most desirable from the point of view of both teaching and learning the analysis of shells by the finite element method.

An apparent weakness of the THKSHEL element, as formulated, is that the accuracy of the mass matrix seems to be much inferior to that of the stiffness matrix. To overcome the difficulties presented by the indefinite mass matrix when usual lumping procedures were used, a highly arbitrary lumping procedure was adopted. Significant errors were introduced in the dynamic problems presented in Chapter VIII. Probably the best way of improving the dynamic performance is to introduce the full consistent mass matrix. Using the Rayleigh-Ritz technique for vibrations, the dynamics subroutines take only a small proportion of the

total time of solution. So, although using the full mass matrix will approximately double the computer time for the dynamics section, it will not appreciable affect the total solution time.

It is noted here also, that in situations that can arise in arch dams (e.g. Number 5) the limit of "moderately" thick shell behavior may be reached and loss of accuracy compared with the three-dimensional solution may occur.

To conclude this Chapter, some suggestions for possible future research arising from this work are made. As pointed out above, a more thorough examination of the role of the mass matrix should be made, and either a more accurate lumped mass distribution should be used, or perhaps the full consistent mass matrix.

As noted in Chapter VI, the integration developed for beams and arches is directly applicable to axisymmetric shell problems. It would be interesting to see whether the axisymmetric THKSHEL element is more efficient than elements at present in use.

Although not brought out strongly in the preceding Chapters, the integration procedure adopted is the minimum integration that can be used without introducing singular stiffness matrices. It is hypothesized that a isoparametric three-dimensional element, based on integrating each strain component over its minimum integration grid, will be far more efficient than the full integration, and will of course converge correctly if the minimum integration requirements are met.

No great difficulties arise in using other than the isotropic constitutive relation adopted here. For example an orthotropic relation could be used for a reinforced concrete shell. Since transverse shear

is automatically included, a constitutive relation arising from sandwich construction could be easily derived for sandwich shells, the transverse shear modulus being that of the core material, the in-plane moduli being derived easily from the face materials and dimensions.

X. REFERENCES

1. Clough, R.W., Tocher, J.L., "Finite Element Stiffness Matrix for Analysis of Plate Bending," Proc. of Conf. on Matrix Methods in Structural Mechanics, Wright-Patterson A.F.B. Ohio, 1965.

2. Melosh, R. "A Flat Triangular Shell Element Stiffness Matrix," Proc. Conf. on Matrix Methods in Structural Mechanics, Wright Patterson A.F.B. Ohio, 1965.

3. Bazeley, G.P., Cheung, Y.K., Irons, R.M. and Zienkiewicz, O.C. "Triangular Elements in Plate Bending Conforming and Non Conforming Solutions," Proc. of Conf. on Matrix Methods in Structural Mechanics, Wright Patterson A.F.B. Ohio, 1965.

4. Clough, R.W., Felippa, C.A., "A Refined Quadrilateral Element for Analysis of Plate Bending," Proc. of 2nd Conf. on Matrix Methods in Structural Mechanics, Wright Patterson A.F.B. Ohio, 1968

5. Herrmann, L.R., "A Bending Analysis for Plates," Proc. of Conf. on Matrix Methods in Structural Mechanics, Wright Patterson A.F.B. Ohio, 1965.

6. Fraejis de Veubecke, B.F., "Displacement and Equilibrium Models in the Finite Element Method," Stress Analysis, John Wiley & Sons.

7. Herrmann, L.R., "Finite Element Bending Analysis of Plates," Journal of Engineering Mechanics Division A.S.C.E. October, 1967.

8. Pian, T.H.H., "Element Stiffness Matrices for Boundary Compatibility or for Prescribed Boundary Stress," Proc. of Conf. on Matrix Methods in Struct. Mech. Wright Patterson A.F.B. Ohio, 1965.

9. Dungar, R., Severn, R.T., and Taylor, P.R., "Vibration of Plate and Shell Structures Using Triangular Finite Elements," Journal of Strain Analysis, Vol. 2, No. 1, January, 1967.

10. Stricklin, J.A., Haisler, W.E., Tisdale, P.R., and Gunderson, R. "A Rapidly Converging Triangular Plate Element," Journal of AIAA, Vol. 7, No. 1, January, 1969.

11. Utku, S., "Stiffness Matrices for Thin Triangular Elements of Non-Zero Gaussian Curvature," AIAA Journal, Vol. 5, No. 9, September, 1967.

12. Bogner, F.K., Fox, R.L. and Schmit, I.A., "A Cylindrical Shell Discrete Element," AIAA Journal, Vol. 5, No. 4, April 1967.

13. Irons, B.M., "Numerical Integration applied to the Finite Element Method," Conference on the Use of Digital Computers in Structural Engineering. University of Newcastle, July 1966.

14. Ergatoudis, J., Irons, B.M. and Zienkiewicz, O.C., "Three-Dimensional Analysis of Arch Dams and Their Foundations," Symposium on Arch Dams, Inst of Civil Eng. London, March, 1968.

15. Argyris, J.H., Redshaw, S.C., "Three Dimensional Analysis of Two Arch Dams by a Finite Element Method," Symposium on Arch Dams, Inst. of Civil Engineers, London, March, 1968.

16. Ahmad, S., Irons, B.M. and Zienkiewicz, O.C., "Curved Thick Shell and Membrane Elements with Particular Reference to Axisymmetric Problems," Proc. of 2nd Conf. on Methods in Struct. Mech. Wright Patterson A.F.B. Ohio, 1968.

17. Wempner, G.A., Oden, J.T. and Kross, D.A., "Finite Element Analysis of Thin Shells," Journal of Eng. Mech. Div. Proc. ASCE December, 1968.

18. Ergatoudis, J., Irons, B.M. and Zienkiewicz, O.C., "Curved Isoparametric Quadrilateral Elements for Finite Element Analysis," Int. Journal of Solids and Structures, Vol. 4, pp 31-42, 1968.

19. Fraejis de Veubecke, B.F.," An Equilibrium Model for Plate Bending," Int. Journal of Solids and Structures, Vol. 4, No. 2, 1968.

20. Fraejis de Veubecke, B.F., "Bending and Stretching of Plates Special Models for Upper and Lower Bounds," Proc. of Conf. on Matrix Methods in Structural Mechanics, Wright Patterson A.F.B. Ohio, 1965.

21. Reissner, E., "On a Variational Theorem in Elasticity," Journal of Math. and Physics, Vol. XXIX No. 2, July, 1950.

22. de Arantes e Oliveira, E.R., "Mathematical Foundations of [illegible] Finite Element Method," Lab. Nacional de Engenharia Civil, Lisb[illegible] 1967.

23. Irons, B.M., Draper, K.J., "Inadequacy of Nodal Connections in a Stiffness Solution for Plate Bending," AIAA Journal, Vol. 3, p. 965 1965.

24. Argyris, J.H., "Continua and Discontinua," Proc. of Conference on Matrix Methods in Structural Mech. Wright Patterson A.F.B. Ohio, 1965.

25. Zienkiewicz, O.C., "The Finite Element Method in Structural and Continuum Mechanics," McGraw-Hill Ltd. London, 1967.

26. Prziemienki, J.S., "Theory of Matrix Structural Analysis," McGraw Hill.

27. Popov, E.G., "Introduction to Mechanics of Solids," Prentice Hall

28. Doherty, W.P., Wilson, E.L. and Taylor, R.L., "Stress Analysis of Axisymmetric Solids Utilizing Higher Order Quadrilateral Finite Elements," Report No. 69-3, SESM Dept. of Civil Engineering, University of California, Berkeley, 1969.

29. Johnson, C.P., "The Analysis of Thin Shells by a Finite Element Procedure," Report No. 67-22, SESM Dept. of Civil Engineering University of California, Berkeley, 1967.

30. Sokolnikoff, I.S., "Mathematical Theory of Elasticity," McGraw Hill 2nd Edition (equations 10.10.)

31. Willam, K., "Finite Element Analysis of Cellular Structures," Doctoral Dissertation, University of California, Berkeley, 1969.

32. Chetty, S.M.K., Tottenham, H., "Indian Concrete Journal," July, 1964.

33. Otter, J.R.H., et al., "Dynamic Relaxation," Proc. Instn. Civ. Engrs. 1966. 35. December, 633-656.

34. Ahmad, S., "Arch Dams," Instn. Civ. Engrs. Proceedings of Symposium, 1968, 102-104.

35. Felippa, C.A., "Refined Finite Element Analysis of Linear and Nonlinear Two-Dimensional Structures," Report No. 66-22 SESM Dept. of Civil Engineering, University of California, Berkeley.

36. Timoshenko, S.P., Woinowsky-Krieger, S., "Theory of Plates and Shells," McGraw Hill.

37. Arch Dams, Instn. Civil Enginrs. Proc. of Symposium 1968.

38. Dunham, R., Ph.D. Dissertation, Dept. of Civil Engrg. University of California, Berkeley.

39. Timoshenko, S., Goodier, J.N., "Theory of Elasticity," McGraw Hill.

40. Howland, R.C.J., "Trans. Royel Soc.," London, Series A., 221 p. 265. 1921.